


8-1-2015

The Optimization of Concrete Mixtures for Use in Highway Applications

Mohamadreza Moini

University of Wisconsin-Milwaukee

Follow this and additional works at: <https://dc.uwm.edu/etd>

 Part of the [Civil Engineering Commons](#), and the [Materials Science and Engineering Commons](#)

Recommended Citation

Moini, Mohamadreza, "The Optimization of Concrete Mixtures for Use in Highway Applications" (2015). *Theses and Dissertations*. 976.

<https://dc.uwm.edu/etd/976>

This Thesis is brought to you for free and open access by UWM Digital Commons. It has been accepted for inclusion in Theses and Dissertations by an authorized administrator of UWM Digital Commons. For more information, please contact open-access@uwm.edu.

THE OPTIMIZATION OF CONCRETE MIXTURES FOR USE IN HIGHWAY
APPLICATIONS

by

Mohamadreza Moini

A Thesis Submitted in
Partial Fulfillment of the
Requirements for the Degree of

Masters of Science
in Engineering

at

The University of Wisconsin-Milwaukee

August 2015

ABSTRACT

THE OPTIMIZATION OF CONCRETE MIXTURES FOR USE IN HIGHWAY
APPLICATIONS

by

Mohamadreza Moini

The University of Wisconsin-Milwaukee, 2015
Under the Supervision of Professor Konstantin Sobolev

Portland cement concrete is most used commodity in the world after water. Major part of civil and transportation infrastructure including bridges, roadway pavements, dams, and buildings is made of concrete. In addition to this, concrete durability is often of major concerns. In 2013 American Society of Civil Engineers (ASCE) estimated that an annual investment of \$170 billion on roads and \$20.5 billion for bridges is needed on an annual basis to substantially improve the condition of infrastructure. Same article reports that one-third of America's major roads are in poor or mediocre condition [1]. However, portland cement production is recognized with approximately one cubic meter of carbon dioxide emission. Indeed, the proper and systematic design of concrete mixtures for highway applications is essential as concrete pavements represent up to 60% of interstate highway systems with heavier traffic loads. Combined principles of material science and engineering can provide adequate methods and tools to facilitate the concrete design and improve the existing specifications. In the same manner, the durability must be addressed in the design and enhancement of long-term performance. Concrete used for highway

pavement applications has low cement content and can be placed at low slump. However, further reduction of cement content (e.g., versus current specifications of Wisconsin Department of Transportation to 315-338 kg/m³ (530-570 lb/yd³) for mainstream concrete pavements and 335 kg/m³ (565 lb/yd³) for bridge substructure and superstructures) requires delicate design of the mixture to maintain the expected workability, overall performance, and long-term durability in the field. The design includes, but not limited to optimization of aggregates, supplementary cementitious materials (SCMs), chemical and air-entraining admixtures. This research investigated various theoretical and experimental methods of aggregate optimization applicable for the reduction of cement content. Conducted research enabled further reduction of cement contents to 250 kg/m³ (420 lb/yd³) as required for the design of sustainable concrete pavements. This research demonstrated that aggregate packing can be used in multiple ways as a tool to optimize the aggregates assemblies and achieve the optimal particle size distribution of aggregate blends. The SCMs, and air-entraining admixtures were selected to comply with existing WisDOT performance requirements and chemical admixtures were selected using the separate optimization study excluded from this thesis. The performance of different concrete mixtures was evaluated for fresh properties, strength development, and compressive and flexural strength ranging from 1 to 360 days. The methods and tools discussed in this research are applicable, but not limited to concrete pavement applications.

The current concrete proportioning standards such as ACI 211 or current WisDOT roadway standard specifications (Part 5: Structures, Section 501: Concrete) for concrete have limited or no recommendations, methods or guidelines on aggregate optimization,

the use of ternary aggregate blends (e.g., such as those used in asphalt industry), the optimization of SCMs (e.g., class F and C fly ash, slag, metakaolin, silica fume), modern superplasticizers (such as polycarboxylate ether, PCE) and air-entraining admixtures. This research has demonstrated that the optimization of concrete mixture proportions can be achieved by the use and proper selection of optimal aggregate blends and result in 12% to 35% reduction of cement content and also more than 50% enhancement of performance. To prove the proposed concrete proportioning method the following steps were performed:

- The experimental aggregate packing was investigated using northern and southern source of aggregates from Wisconsin;
- The theoretical aggregate packing models were utilized and results were compared with experiments;
- Multiple aggregate optimization methods (e.g., optimal grading, coarseness chart) were studied and compared to aggregate packing results and performance of experimented concrete mixtures;
- Optimal aggregate blends were selected and used for concrete mixtures;
- The optimal dosage of admixtures were selected for three types of plasticizing and superplasticizing admixtures based on a separately conducted study;
- The SCM dosages were selected based on current WisDOT specifications;
- The optimal air-entraining admixture dosage was investigated based on performance of preliminary concrete mixtures;

- Finally, optimal concrete mixtures were tested for fresh properties, compressive strength development, modulus of rupture, at early ages (1day) and ultimate ages (360 days).
- Durability performance indicators for optimal concrete mixtures were also tested for resistance of concrete to rapid chloride permeability (RCP) at 30 days and 90 days and resistance to rapid freezing and thawing at 56 days.

© Copyright by Mohamadreza Moini, 2015
All Rights Reserved

Dedicated to :

My Parents

TABLE OF CONTENTS

1. INTRODUCTION	1
2. LITERATURE REVIEW	10
2.1. CONCRETE OPTIMIZATION	10
2.2. AGGREGATE OPTIMIZATION	11
2.2.1 Theories of Particle Packing.....	11
2.2.1.1. Discrete Models	13
2.2.1.2. Continuous Models	30
2.2.1.3. Discrete Element Models (DEM)	34
2.2.2 Coarseness Chart	38
3. MATERIALS AND METHODS	40
3.1. MATERIALS	40
3.1.1. Portland Cements.....	40
3.1.2. Fly Ash	42
3.1.3. Blast Furnace Slag.....	43
3.1.4. Chemical Admixtures	44
3.1.5. Aggregates	44
3.2. EXPERIMENTAL PROGRAM AND TEST METHODS	47
3.2.1. Experimental Testing Methods for Packing Density.....	48
3.2.2. Preparation, Mixing, and Curing	50
3.2.3. Slump.....	50
3.2.4. Density of Fresh Concrete	50
3.2.5. Air Content of Fresh Concrete.....	51
3.2.6. Temperature.....	51
3.2.7. Compressive Strength.....	52
3.2.8. Flexural Strength (Modulus of Rupture)	52
3.2.9. Chloride Permeability.....	53

3.2.10. Freeze Thaw Durability	55
4. RESULTS AND DISCUSSION.....	57
4.1. AGGREGATES OPTIMIZATION.....	57
4.1.1. Experimental Packing of Aggregates	57
4.1.2. Proposed Packing Simulation Model	58
4.1.3. Packing Simulation.....	60
4.1.4. Concrete Mixtures	68
4.1.5. Gradation Techniques - Particle Size Distribution (PSD) Curve	68
4.1.6. Coarseness Chart	70
4.1.7. Evaluation of Concrete Mixtures.....	73
4.1.8. Modeling vs. Experimental Packing.....	77
4.2. MIXTURE OPTIMIZATION	86
4.2.1. Preliminary Admixture Optimization.....	86
4.2.2. Optimized Mixture Evaluation	102
4.2.3. Optimized Mixture: Fresh Properties	103
4.2.4. Optimized Mixture: Hardened Properties.....	105
4.2.5. Optimized Mixtures: Strength Development.....	115
4.2.6. Optimized Mixture: Durability.....	121
5. CONCLUSIONS	128
6. FUTURE RESEARCH.....	133
REFERENCES	134

LIST OF FIGURES

Figure 1. Packing of two monosized particle classes [20].	15
Figure 2. The interaction effects between the aggregates [51].	16
Figure 3. The ternary diagram and isodensity lines calculated for cement, sand, and coarse aggregate blends [21].	22
Figure 4. Ternary diagram with isodensity lines and equal sand to coarse aggregate ratio [21].	23
Figure 5. Ideal distribution curves developed by Fuller, Andreassen, and Funk and Dinger [20].	33
Figure 6. The DEM generating unrealistic random distribution of particles [95].	35
Figure 7. The DEM (dynamic) generating stable loose packing structure of particles [95].	36
Figure 8. The 2D (sequential packing model) and 3D visualization of the algorithm [37].	37
Figure 9. Coarseness chart of aggregate mixtures [18].	39
Figure 10. Sieve analysis of southern aggregates (C1,F1,I1)	47
Figure 11. Sieve analysis of northern aggregates (C2,F2,I2)	47
Figure 12. VB apparatus used for experimental packing test	49
Figure 13. Air meter used for air test	51
Figure 14. The output of packing algorithm: a) representation of Apollonian Random Packing with LIP separation b) 3D visualization and c) the associated PSD the output of packing algorithm	60
Figure 15. The experimental packing degree of Southern aggregate a) compacted vs. loose; b) the effect of fine aggregates; c) ternary diagrams d) compacted packing	62

Figure 16. The experimental packing degree of Northern aggregates a) compacted vs. loose; b) the effect of fine aggregates; c) ternary diagrams d) compacted packing	63
Figure 17. The PSD corresponding to a) the best fit to experimental blends and b) 3D packing simulation and	64
Figure 18. The PSD of experimental southern aggregate blends.....	70
Figure 19. The PSD of experimental northern aggregate blends.....	70
Figure 20. Coarseness chart of Southern aggregate mixtures [18, 105]	72
Figure 21. Coarseness chart of Northern aggregate mixtures [18, 105]	73
Figure 22. The correlation between the compressive strength and packing degree of Southern aggregates	77
Figure 23. The correlation between the compressive strength and packing degree of Northern aggregates	77
Figure 24. Toufar and Aim model versus packing degree of binary blends (C1 and F1)	80
Figure 25. Toufar and Aim model versus packing degree of binary blends (I1 and F1)..	81
Figure 26. Toufar and Aim model versus packing degree of binary blends (C1 and I1) .	81
Figure 27. Toufar and Aim model versus packing degree of binary blends (C2 and F2)	82
Figure 28. Toufar and Aim model versus packing degree of binary blends (I2 and F2)..	83
Figure 29. Toufar and Aim model versus packing degree of binary blends (C2 and I2) .	83
Figure 30. a) Southern 3D Toufar b) Northern 3D Toufar	84
Figure 31. The relationship between air content and fresh density of tested final mixtures	102
Figure 32. The relationship between the compressive strength and modulus of rupture	115

Figure 33. Strength development of the concrete produced at W/CM of 0.42 and 279 kg/m ³ [470 lb/yd ³] cementitious materials content	116
Figure 34. Strength development of the concrete produced at W/CM of 0.37 and 279 kg/m ³ [470 lb/yd ³] cementitious materials content	117
Figure 35. Strength development of concrete produced at W/CM of 0.32 at 279 kg/m ³ [470 lb/yd ³] cementitious materials content	119
Figure 36. Strength development of concrete produced at W/CM of 0.41 at 250 kg/m ³ [420 lb/yd ³] cementitious materials content	119
Figure 37. Strength development of concrete based on different cements produced at W/CM of 0.42 and 279 kg/m ³ [470 lb/yd ³] cementitious materials content.....	120
Figure 38. The RCP of concrete with cementitious materials content of 279 kg/m ³ [470 lb/yd ³].....	124
Figure 39. The RCP of concrete with cementitious materials content of 250 kg/m ³ [420 lb/yd ³].....	125
Figure 40. The mass loss of concrete with cementitious material content of 279 kg/m ³ [470 lb/yd ³]at 300 freezing-thawing cycles	126
Figure 41. The mass loss of concrete with cementitious material content of 250 kg/m ³ [420 lb/yd ³] at 300 freezing-thawing cycles	127

LIST OF TABLES

Table 1. Fly ash classification per ASTM 618 – 12a [3].....	8
Table 2. The example of SHRP table for concrete mixture proportion based on maximum aggregate packing [21].....	22
Table 3. The K value for different compaction methods [26]	27
Table 4. Chemical composition of portland cement	41
Table 5. Physical properties of portland cement.....	41
Table 6. Chemical composition of fly ash	42
Table 7. Physical properties of fly ash.....	43
Table 8. Chemical composition and physical properties of blast furnace slag.....	43
Table 9. Properties of chemical additives	44
Table 10. Designation and sources of aggregates.....	45
Table 11. Physical characteristics of aggregates in oven dry (od) and saturated surface dry (SSD) Conditions	45
Table 12. Bulk density and void content of aggregates in loose and compacted state	45
Table 13. Grading of coarse aggregates.....	46
Table 14. Grading of intermediate aggregates.....	46
Table 15. Grading of fine aggregates (sand).....	46
Table 16. Chloride ion penetrability based on charge passed.....	54
Table 17. Test results for concrete mixtures with various southern aggregate blends	66
Table 18. Test results for concrete mixtures with various northern aggregate blends	67

Table 19. Southern aggregate properties used for Toufar model.....	79
Table 20. Northern aggregate properties used for Toufar model.....	79
Table 21. Mix design for preliminary mixtures without SCMs.....	94
Table 22. Fresh and hardened properties of preliminary mixtures without SCMs.....	95
Table 23. Mix design for preliminary mixtures with class F fly ash	96
Table 24. Fresh and hardened properties of preliminary mixtures with class F fly ash ...	97
Table 25. Mix design for preliminary mixtures with class C fly ash.....	98
Table 26. Fresh and hardened properties of preliminary mixtures with class C fly ash...	99
Table 27. Mix design for preliminary mixtures with slag	100
Table 28. Fresh and hardened properties of preliminary mixtures with slag.....	101
Table 29. Mixture proportioning of final optimized concrete mixtures at cementitious materials of 279 kg/m^3 [470 lb/yd^3].....	109
Table 30. The fresh properties of final optimized concrete mixtures at cementitious materials of 279 kg/m^3 [470 lb/yd^3].....	110
Table 31. The mechanical performance of final optimized concrete at cementitious materials of 279 kg/m^3 [470 lb/yd^3].....	111
Table 32. Mixture proportioning of final optimized concrete mixtures at cementitious materials of 250 kg/m^3 [420 lb/yd^3].....	112
Table 33. The fresh properties of final optimized concrete mixtures at cementitious materials of 250 kg/m^3 [420 lb/yd^3].....	113
Table 34. The mechanical performance of final optimized concrete at cementitious materials of 250 kg/m^3 [420 lb/yd^3].....	114
Table 35. The durability of concrete with cementitious materials content of 279 kg/m^3 [470 lb/yd^3]	122

Table 36. The durability of concrete with cementitious materials content of 250 kg/m³
[420 lb/yd³] 123

LIST OF ABBREVIATIONS

PCE/SP:	Poly Carboxylic Ether Superplasticizer
SNF/SP:	Sulfonated Naphthalene Formaldehyde Superplasticizer
MD/P (mid-range):	Mid-Range Plasticizer
P/SP:	Plasticizer/Superplasticizer
HRWRA/WRA:	High-Range Water Reducing / Water Reducing Admixtures
AE(A):	Air Entraining Admixtures
L:	Cement I (Type I)
H:	Cement II (Type I)
S:	Cement III (Type I)
SCM:	Supplementary Cementitious Material
AF:	Class F Fly Ash
AC:	Class C Fly Ash
SL/GGBFS:	Ground Granulated Blast Furnace Slag (Slag Cement)
CPD.:	Compacted Packing Degree
LPD:	Loose Packing Degree
PSD:	Particle Size Distribution
DF:	Durability Factor
W/C:	Water to Cement Ratio
W/CM:	Water to Cementitious Materials Ratio
PC:	Power Curve

Concrete Mixture Notations: Cement - Aggregate - (H)WRA – SCM - Reduced

ACKNOWLEDGMENTS

I would like to thank Professor Konstantin Sobolev for his endless support throughout this research. This work would not have been possible without his insight, discernment, and contributions. His guidance and support throughout my graduate studies has been endless. I would also like to thank Prof. Konstantin Sobolev, Prof. Habib Tabatabai, and Dr. Bruce Ramme for being part of my thesis defense jury.

I would also like to thank Dr. Ismael Flores-Vivian for the immense hours he has spent working on experiments especially at the early ages of the project, optimization of admixtures, and providing terrific thoughts within this research. Additionally, this work could not have been performed without the contribution of graduate assistants at UW-Milwaukee Rani Pradoto, Scott Muzenski, Justin Flickinger, Brandon Bosch, Brent Kriha, Emil Bautista, Seth Walsdorf, and Le Pham at UW - Madison for assistance with durability tests.

I would like to give a special thanks to all the students that helped me with all the mixtures, tests and heavy works in concrete lab. These students include: Nathaniel Havener, Katie LeDoux, Gaven Kobes, Jason Atchison, Craig Vindedahl, Clayton Cloutier, Chris Ball, Mark Moyle, Alper Kolcu, Kristian Nygaard, Andrew Sinko, Jesus Cortes, Jayeesh Bakshi, Tyler Beinlich.

Finally, I would like to thank my parents, for their love, support, and enthusiasm they have offered me throughout my studies and my life. I would not have had the opportunities that I've had and would've not been able to succeed without their support.

1. INTRODUCTION

In 2013 American Society of Civil Engineers (ASCE) estimated that an annual investment of \$170 billion on roads and \$20.5 billion for bridges is needed to substantially improve the conditions. The report concludes that one-third of America's major roads are in poor or mediocre condition [1]. The pavement industry was challenged to establish advanced practices for improvement of concrete mixtures and pavement design that address both environmental and financial vitality [2]. On the other side, the concrete and pavement industry struggles to produce a "sustainable concrete" addressing the portland cement contribution to carbon dioxide (CO₂) emissions and short life cycle of concrete which are required for immediate improvement and reaching the sustainable concrete objective.

Traditionally, as part of the structural design, the concrete pavement design is focused on determining the thickness of the slab based on the traffic loads [2]. A "recipe-based" or prescriptive-based concrete design does not necessarily respond to the performance requirements and the best use of the materials used in the mixture. As a result, the proportioning of concrete for highway pavement applications is hindered from further advancements and is more focused to ensure that the mix is cost-effective for the manufacturer rather than the performance requirements. The "performance-based" design as opposed to "recipe-based" approach relies mainly on materials performance limits and determines the optimal design based on both performance and material's properties. However, the application of this method requires a deep knowledge of the materials properties, behaviors and time-dependent interactions.

The research on concrete and evaluations of new methods and tools is vital for enhancing the infrastructure performance and durability, updating the specification requirements, and to provide guidelines to the industry for emphasizing sustainable design methods and the use of suitable materials. Optimizing concrete proportions for enhanced performance and reduced cement content is a complicated task as several ingredients including various aggregate types, air-entraining, water reducing or high range water reducing admixtures (WRA/HRWRA), and SCMs are involved. Therefore, this research concentrates on optimization of individual components, which can be optimized at a smaller scale prior to the use in concrete mixtures. Optimized concrete mixtures can offer tremendous savings by reducing cement content by 12% to 35% versus those prescribed by current standards (e.g., WisDOT standard specifications, Part 5: Structures, Section 501: Concrete), and utilizing industrial by-products.

The modern mineral additives or supplementary cementitious materials (SCMs) and chemical admixtures (such as HRWRA, AEA) are common components in concrete pavement technology, but are not effectively used due to the complexity and variability in materials, processes, diverse effects on concrete performance. Therefore, the SCMs, WR/HRWR, and AE admixtures can be optimized at smaller scale in pastes and mortars prior to the use in concrete. This research is based on the results of SCM and WRA/HRWRA optimization from a separately conducted study. Hence, the results of this research are accurate for the scope of the materials used and to the extent of the materials characterized. These materials, even of the same standard grade, often show different characteristics and different behaviors due to the variation in raw materials manufacturing and processing.

In the past decades, traditional concrete proportioning specifications were challenged with difficulties in the past decades to establish a uniform design specification for concrete mixtures containing SCMs, WRA/HRWRA, and AE admixtures, partially due to the use of different component materials with various behaviors, different characteristics, and potential chemical incompatibilities. In addition, due to the processes involved in the production of cement in rotary kiln, the ASTM C150 Type I cement product is manufactured with different properties and behavior. Such variation includes the physical, chemical, and thermal properties as well as compatibility issues when used with different mineral additives and chemical admixtures. To address far-reaching results, this research proposed a novel optimization method concentrating on aggregates optimization based on extensive experiments with optimized contents of aggregates and other materials to evaluate the performance of mixtures containing different SCMs (type F and C fly ash, slag) and different common cements widely used in concrete pavements in the state of Wisconsin.

Aggregates comprise up to 60 to 75 percent of concrete volume, and so concrete performance is strongly affected by the aggregate's properties, proportioning and packing [3-11]. Optimized aggregate blends can provide concrete with improved performance or can be used to design concrete mix at lower cementitious material content. Due to complexities in aggregate packing, and irregularities in shape and texture, there is no universal approach to account for the contribution of aggregate's particle size distributions and packing degree affecting the performance of concrete in fresh and hardened states. The properties and behavior of portland cement concrete depends on the properties of their main constituent – the aggregates [3-11]. Therefore, the optimization

of aggregates is an attractive option to improve the engineering properties, reduce the cementitious materials content, reduce the materials costs, and minimize the environmental impacts associated with concrete production. Early reports on concrete technology have emphasized the important effects of aggregates packing and grading related to performance [7, 11-13]. Improving the main engineering properties of concrete, such as strength, modulus of elasticity, creep, and shrinkage can be achieved by fine-tuning of aggregates packing as extensively discussed in the literature [4-6, 9, 10, 13-20]. The advent of ready mixed concrete and the use of large capacity pumps for transporting concrete demanded the use of improved aggregate blends for mixtures with high workability as well as imposing new limitations on maximum size of aggregates (D_{max}). Furthermore, the optimization of aggregate blends by packing or particle size distribution (PSD) techniques can bring significant savings due to the reduction of the volume of binder [13].

Indeed, the importance of aggregate characteristics is widely discussed in the literature. Abrams stated that "...the problem is to put together the aggregates available in order to have the best concrete mixture we can for a given cost or at a minimum cost" [3, 4]. In 1961, Gilkey [3, 5] proposed the modification of Abrams' w/c to strength relationship by considering the ratio of cement to aggregate, grading, shape, strength of aggregate particles, and D_{max} [3, 5]. Other researchers also discussed the relevance and importance of these factors [6-11]. The theory of aggregates particle packing has been discussed for more than a century [18-33] and includes the discrete particle packing theories, continuous theories, and discrete element models (DEM). Discrete models include the interaction effects between the particles to calculate the maximum packing

density for binary, ternary or multi-component mixtures [24-27]. Continuous models are believed to reach the maximum theoretical density mixtures. It is postulated that the optimal PSD corresponds to the “best” or the densest packing of the constituent particles; however, modeling of the large particulate assemblies had demonstrated that the densest arrangements of particles correspond to random Apollonian packings, are not practically achievable in concrete [33]. The dense packings calculated by RAP methods for regular particles and corresponding PSD, are not utilized in concrete technology. The static or dynamic DEMs generate virtual packing structures from a given PSD on using random distribution of spherical particles [31-33]. The experimental packing depends on a loose or compacted condition of packing, packing energy, packing method, and has to be specified prior to correlating the experiments and the models. A better understanding of packing mechanisms for aggregates of various combinations and sizes, as required for concrete applications, needs further attention and is the primary objective of this study.

The PSD is a commonly known criterion towards the optimization of aggregate blends affecting the fresh and hardened properties of concrete. The effect of PSD on workability, density and compressive strength of concrete mixtures is reported in the literature [26, 34, 35]. Packing criteria for optimizing concrete mixtures are occasionally used for various applications including high-strength concrete, self-consolidating concrete, low cement concrete for pavement applications, and heavyweight concrete [8, 14, 15, 21, 36, 37]. The purpose of this study is to investigate the effect of combined criteria such as grading, the experimental packing (in loose and compacted state), and applicability of coarseness chart on properties of low cement concrete mixtures.

The use of packing degree as a specific tool to optimize the binary and ternary aggregate blends for the minimal void content (or the maximal packing degree) was accomplished by some researchers [8]. The problem of the best-possible aggregate packing and its beneficial effects on concrete has been the subject of experimental and theoretical investigations [6-15, 37-41]. Other researchers have proposed a comprehensive theory and scientific insight providing a better understanding of the role of aggregates on compressive strength [15, 26, 33, 36, 37, 42-44]. To improve the aggregate mixture proportions, ACI Education Bulletin E1-07 recently recommended using an intermediate aggregates (IA) fraction to compensate for the “missing” grain sizes [12], and ACI 211 Technote drafted a document for the use of multiple criteria for aggregates optimization. In spite of several reports discussing the importance of theoretical models representing the packing of natural or artificial aggregate assemblies [37, 38, 45], the empirical approach remains very important tool to verify the models by testing different aggregate combinations and correlating the packing degree to the strength characteristics of particular composites [35-37, 46].

The identification of the best aggregate blends for concrete and the relationship between the packing and performance, still remains an ambiguous task for further research. To address the objective of this research, the best aggregate blend for concrete is selected using multiple criteria, and the effect of maximal aggregate packing is investigated by simulation and experiments. These criteria include the grading techniques with power curves (PC), coarseness factor chart, and the experimental and simulated packing. The experimental PSD and corresponding packing values are compared with

associated packing simulations based on the best fit to corresponding PC. The effect of aggregates packing on concrete strength is further examined.

The development of optimized aggregate blends with the use of ternary aggregate blends (as commonly used in asphalt industry) and specified packing degree can be suggested as a unique criterion based on the experiments which can, therefore, reduce the voids between the aggregates in the mix. As a result, reduced volume of cement paste is required to fill in the voids and so cement (and water) content can be reduced for the same unit volume. The optimization of aggregate blends by packing or particle size distribution (PSD) techniques can bring significant savings due to the reduction of the volume of binder. In addition to this the aggregate packing can be used as a tool to optimize concrete mixtures and improve the compressive strength.

The use of supplementary cementitious materials (SCMs) including industrial by-product such as ground granulated blast furnace slag (also known as slag cement) and fly ash, can potentially reduce the cement consumption by 50% and 30%, respectively, as typical replacement volumes prescribed by WisDOT standard specifications for concrete. Also, the use of SCMs can provide a cementitious matrix with a better packing density. In blend with portland cement, slag cement is chemically activated cement and, therefore, provides long-term cementitious properties. Pozzolanic by-products (especially class F fly ash) can also react with CH and cement alkalies (K_2O and Na_2O) minimizing potential aggregate-alkali-silica reaction due to pozzolanic reactions. Fly ash suitable for concrete applications is defined by ASTM 618 and is based on total volume of Si_2O_3 , Al_2O_3 , Fe_2O_3 .

Table 1. Fly ash classification per ASTM 618 – 12a [3]

Class	Description	Requirements
F	Pozzolanic properties	$\text{Si}_2\text{O} + \text{Al}_2\text{O}_3 + \text{Fe}_2\text{O}_3 > 70\%$
C	Pozzolanic cementitious properties	$\text{Si}_2\text{O} + \text{Al}_2\text{O}_3 + \text{Fe}_2\text{O}_3 < 70\%$

Superplasticized concrete with enhanced performance containing HRWRAs (superplasticizers) is applicable for heavily reinforced elements such as floors, foundations, bridges decks, and pavements. Superplasticizers release the excessive water from the paste by better dispersion of cement particles [47]. This type of concrete is characterized by enhanced workability, flowability, as well as reduced permeability, improved durability, and reduced shrinkage. However, WRAs (plasticizers) are more common in concrete pavements where low slump mixes are required and superplasticizers are common in high workability applications, such as structures with congested reinforcements. Due to exceptional water-reducing properties, modern superplasticizers enable the production of very economical concrete with reduced content of cementitious materials content without any detrimental effects on the performance. Therefore, superplasticizers can find a better place in concrete pavement technology enhancing the mechanical performance and fresh properties achieved at reduced water to cement (W/C) ratio. Although superplasticizers introduce remarkable advantages in concrete, there are some limitations with their use. The compatibility of plasticizer/superplasticizers with other admixtures such as retarders, accelerators and air-entraining agents, and SCMs must be investigated.

Air-entraining admixtures are intended to provide desired air void system in concrete. The air void structure can provide extra space required to accommodate the stresses from freezing water inside the air pockets and; therefore, enhance the freezing and thawing resistance. In regions exposed to freezing and thawing cycles, it is required to have certain air content to be able to perform adequately. However, the AE admixtures may have incompatibility with SCMs, specifically with fly ash containing high carbon content. Therefore, the design of Air-Entrained concrete mixtures often requires preliminary investigation to determine the AE admixture dosage that can provide the required air content.

The use of aggregate packing to optimize concrete mixtures can provide a good prediction for the compressive strength, explain the difference in concrete performance, and provide the correlation between the packing degree and compressive strength. The concrete compressive strength can be and, consequently, the enhanced performance can be used to reduce the cementitious materials content. The optimized concrete mixtures with SCMs use up to 30% of class C or class F, and up to 50% ground granulated blast furnace slag enhancing the concrete performance. The main goal of concrete optimization is to provide the enhanced performance, durability for additional life cycles, sustainability and environmental benefits.

2. LITERATURE REVIEW

2.1. CONCRETE OPTIMIZATION

Optimizing concrete mixture is a broad term used for fine tuning of various types of concrete for several performance aspects and desirable properties. More specifically, the optimization of concrete mixture proportioning deals with selection of the most efficient proportions of aggregates blend, SCMs, chemical admixtures, and minimization of cementitious materials content. Concrete mixture proportioning was holistically represented by many researchers [48-56]. The subject was further approached by performance based modeling [56], computer-aided modeling for a system of ingredient particles [42, 57, 58], sustainability concept [2, 59, 60], aggregates optimization, including the effect of aggregates on concrete strength [18, 31, 37, 46, 50, 55, 61-63], and statistical optimization of concrete mixtures [64]. The main purpose of reported researches however, was varying from obtaining a computer model for optimized proportioning [56-58], a sustainable mix proportioning by using by-products [65-67], improving the existing mix design methods by incorporating the aggregate characteristics related to packing density [68], studying the feasibility of cost effective mixtures by lowering cement content [21, 37, 55, 69], or developing software products based on packing theories that can aid the industry[70].

The optimization of aggregates in concrete as an approach covering theories, simulation, and experimental assessment of particle packing, the effect of aggregate packing, and optimal gradations as required for proportioning of a range of cement based materials including mortar, high-performance concrete (HPC), self-consolidating

concrete (SCC), light-weight concrete (LWC), structural concrete, and concrete for pavements [8, 9, 11, 20-22, 24-33, 40, 50, 51, 59, 69, 71-104]. Some researchers used the aggregate optimization methods to investigate the practicality of lowering cementitious materials content in concrete pavements as a result of optimized packing of aggregates [21, 69].

2.2. AGGREGATE OPTIMIZATION

The state of the art on aggregate optimization is based on experimental and theoretical methods and approaches to quantify the best combination of aggregates for particulate composites. These include but not limited to maximal packing degree, minimum void content, optimal particle size distribution (PSD) of aggregate's combinations, optimal individual percentage retained (IPR), and optimal coarseness and workability factors known as coarseness chart for various types of aggregates. Additionally, other effects such as a size, shape and geological properties of aggregates can be taken into account on the selection of optimal aggregates combinations or blends. A concrete mixture is largely constituted of aggregates and not only the concrete optimization depends on the aggregates, but also the prediction of concrete performance is strongly depends on aggregates. This section discusses the literature on aggregates packing, and the use of coarseness chart for optimization of packing.

2.2.1 Theories of Particle Packing

Aggregate packing is an approach for the selection of aggregates types and combinations and its purpose is to reach the lowest void content (or the maximal packing degree) [8]. The packing of particles, however, is not limited to concrete industry and was a major field of interest to other industries as material design, ceramics, asphalt, and

powder metallurgy [8]. The packing concept is based on the use of smaller particles to fill in the voids between the larger particles and as a result reducing the volume of voids. In 1968 Powers stated that the best aggregate mixtures for concrete industry is not necessarily the one with lowest void content: “The production of satisfactory concrete nevertheless requires aggregates with low content of voids even if not the lowest possible, and this requires finding proper combinations of sizes within the allowable size range” [78]. In concrete, the reduction of volume of voids is equal to the reduction in cement paste that must be used to fill in the voids between the aggregates [8]. At the same time, the necessity of concrete to flow imposes the limitations on the desired degree of packing of aggregates. This problem is even more pronounced for concrete with low cement content and, possibly, low to zero slump [37].

In this approach the packing density or packing degree α of a specific aggregate or aggregate combination is defined as the ratio between the bulk density of aggregate (ρ_{bulk}) and grain aggregate density (ρ_{grain}) or, in other words, volume of particles V_p in a unit volume V_b [8]:

$$\alpha = \frac{\rho_{\text{bulk}}}{\rho_{\text{grain}}} = \frac{V_p}{V_b} = \frac{m_p}{\rho_{\text{grain}} \cdot V_b} \quad (1)$$

As a result, the packing is characteristic of the aggregate type and minimum cement paste required to fill in the voids. The void content or porosity (ε) is then:

$$\varepsilon = 1 - \alpha \quad (2)$$

The design of optimal aggregate combination can be achieved by packing simulations.

This may be based on experiment, modeling, or both. The use of aggregates packing

simulation for predicting of concrete behavior, or to design the optimal mix is widely discussed in the literature and industrial projects since 1900s [69, 72-75], but the need for realistic packing model still requires further attention. Minimizing the number of experiments by implementation of a reliable packing simulation model is worthwhile to make the model practical and user-friendly to the industry.

The particle packing is approached in two fundamental directions: as discrete models and continuous models. The discrete models are based on the assumption that each class of aggregates packs to its highest density in the assigned volume and are classified into (a) binary (b) ternary and (c) multimodal mixture models [71].

2.2.1.1. Discrete Models

Discrete models are usually based on few assumptions including, but not limited to: (a) the aggregates are perfect disks or spheres; (b) aggregates are monosized; (c) fine and coarse aggregates differ in characteristic diameters. These assumptions can have conflicts with experimental packing of realistic aggregates and combinations.

2.2.1.1.1. Binary Packing Models

One of the earliest works on ideal packing of spheres was accomplished by Furnus in 1929 and 1931 [10, 18]. In Furnas theory, spherical binary blends of particles are assumed to provide the ideal packings. The second assumption was that the use of fine particles is required to fill in between the coarse particles [71].

Depending on the volume fraction of fine particles (y_1 or r_1) and volume fraction of coarse particles (y_2 or r_2), two possible cases are defined as (1) r_2 is larger than r_1 and is

called “fine grain dominant” or (2) r_2 is larger than r_1 and is called “coarse grain dominant” [76]. These two cases are conditional and possible only if diameter d_1 of fine particles is significantly smaller than diameter d_2 of the coarse particles ($d_1 \gg d_2$) [76].

In first case, the small particles are added to a container packed by large particles with partial volume of φ_1 , volume fraction of r_1 , and packing density of α_1 . By addition of small particles the total volume and packing density increases from α_1 to $\alpha_1 + \varphi_2$ as follows, where the φ_1 is restricted by α_1 (maximum packing density of large particles) [20]:

$$\alpha_t = \varphi_1 + \varphi_2 = \alpha_1 + \varphi_1 \quad (3)$$

Assuming $\alpha_1 = \varphi_1$

$$\Rightarrow \alpha_t = \frac{\alpha_1}{1 - r_2} = \frac{\alpha_1}{r_1} \quad (4)$$

In the second case, large particles are added to occupy the rest of the container [20]. As a result, the packing density contribution of large particles is their partial volume added (φ_1). The rest of unit volume is filled with small particles of partial volume of $(1-\varphi_1)$ and maximum packing density of α_2 [20]:

$$\alpha_t = \varphi_1 + \varphi_2 = \varphi_1 + \alpha_2(1 - \varphi_1) \quad (5)$$

$$\Rightarrow \alpha_t = \frac{1}{r_1 + \left(\frac{r_2}{\alpha_2}\right)} \quad (6)$$

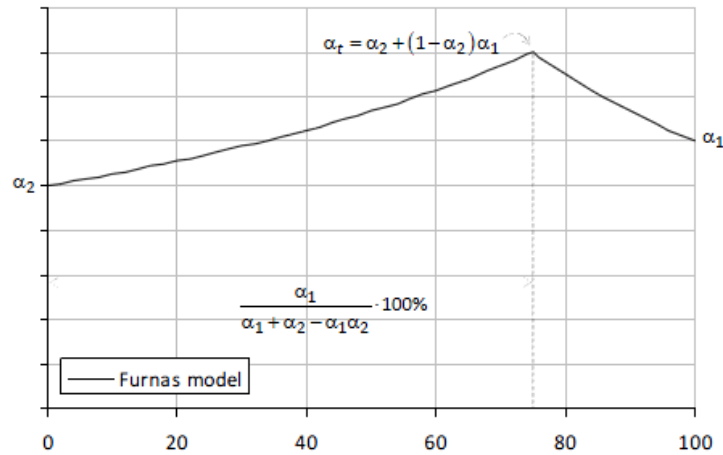


Figure 1. Packing of two monosized particle classes [20].

The wall effect occurs when the amount of fine particles is much higher than the amount of coarse particles and the presence of coarse particles increases the void in the vicinity of coarse particles because the small particles cannot be packed as high as their maximum bulk density. The loosening effect occurs due to interaction of fine particles on large particles when the fine particles are no longer able to fit in the voids between the interstices of coarse particles and therefore, disturb the packing density of large particles. These two effects are shown in *Figure 1* and both effects reduce the packing degree and thus are accounted in the model with factors representing the reduction in packing degree [51].

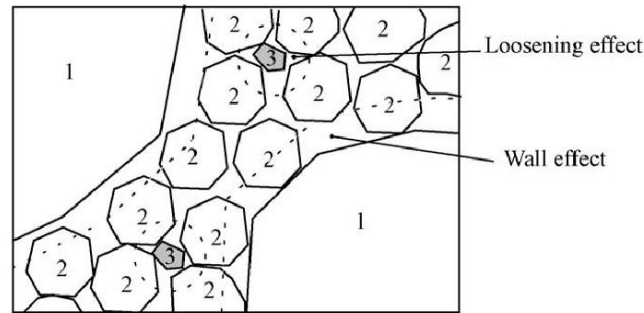


Figure 2. The interaction effects between the aggregates [51].

Similar to other packing models, Furnas model prescribing total packing density (α_t), is valid for two monosized classes of particles when there is no interactions between the particles [59] and the aggregates are of different sizes ($d_1 \gg d_2$). If the diameters of the spheres are close to each other, an additional interaction occurs that is not considered in the model. Furnas published another method of calculating the maximum packing density of multiple classes of particles and their interaction at the maximum packing density [59].

Furnas work was followed by Westmann and Hugill in 1930 [77]. They used a discrete particle packing theory and developed an algorithm for multiple classes of particles; however, they did not include the interaction in their work [59].

Aim and Goff in 1967 suggested a model that takes into account the wall effect with a correction factor for calculating the packing density for binary mixture of particles [24, 71]. This model takes into account the interaction of large particles with smaller particles based on Furnas model [20]. The assumption of this model is similar to other discrete models and considers two cases as fine and coarse dominant mixtures for which there are two equations suggested for packing degree as follows:

$$\phi = \frac{\phi_2}{1 - y_1} \quad \text{for} \quad y_1 < y^* \quad (7.1)$$

$$\phi = \frac{1}{\left[\frac{y_1}{\phi_1} + (1 - y_1) \times \left(1 + 0.9 * \frac{d_1}{d_2}\right)\right]} \quad \text{for} \quad y_1 > y^* \quad (7.2)$$

where ϕ_1 and ϕ_2 are the eigenpacking degree of fine and coarse aggregates respectively, y_1 and y_2 are the grain volume of the fine and coarse aggregates, and d_1 and d_2 are the characteristic diameter of fine and coarse aggregates. The packing degree of individual fine and coarse aggregates is called Eigen packing degree.

The y^* defines the border of two cases between the fine and coarse aggregate dominance. In the first case the amount of coarse particles is much higher and in the second case the amount of fine particles is much higher. The y^* is the dividing point of packing degree and is defined as:

$$y^* = p/(1 + p) \quad (8)$$

$$p = \frac{\phi_1}{\phi_2} - \left(1 + 0.9 * \frac{d_1}{d_2}\right) * \phi_1 \quad (9)$$

This model includes the correction factor for wall effect in both describing the limits and the packing degrees. The model describes the effect that the fine aggregates fill the voids between the coarse aggregates.

In 1968 Powers reported on a void ratio of concrete aggregates [22]. The particle interactions (wall and loosening effect) were taken into account and an empirical relationship to estimate the minimum void ratio of binary mixtures of particles was proposed [8].

Reschke in 2000 [82] developed the model of Schwanda 1966 [81] that incorporated both interactions of large and small particles. In contrary, in their earlier model, Aim and Goff only incorporated the wall effect in their earlier model [20, 81, 82].

2.2.1.1.2. Ternary Packing Models

2.2.1.1.3. In 1976 Toufar et al., for the first time introduced an additional group of particles to the packing density model of binary mixes [25]. The model was developed to calculate the packing density of binary mixes, and the model was capable to estimate the packing of ternary mixes [20]. This model assumes that smaller particles (at a diameter ratio < 0.22) are too small to fit in the interstices of larger particles and hence the packing density consists of packed areas of larger particles and packed areas of smaller particles. The larger particles are assumed to be distributed discretely throughout the matrix of smaller particles [71]. For ternary groups of particles each of two components form a binary mixture and the resulting blend is used as a binary group with third set of particles. In this way, the proposed approach can be applied to multi-component mixtures as well [71]. The total packing degree is described as α_t :

$$\Rightarrow \alpha_t = \frac{1}{\frac{r_1}{\alpha_1} + \frac{r_2}{\alpha_2} - r_2 \left(\frac{1}{\alpha_2} - 1 \right) k_d k_s} \quad (10)$$

where α_1 and α_2 are the eigenpacking degree of fine and coarse aggregates, respectively, r_1 and r_2 are the grain volume of the fine and coarse aggregates, and d_1 and d_2 are the characteristic diameters of fine and coarse aggregates. The k_d is a factor that considers the diameter ratio of two particles in the packing density and the k_s is a statistical factor

that considers the probability of the number of interstices between coarse particles and a fine particle surrounded by four coarse particles [20]:

$$k_d = \frac{d_2 - d_1}{d_2 + d_1} \quad (11)$$

$$k_s = 1 - \frac{1 + 4x}{(1 + x)^4} \quad (12)$$

$$x = \frac{(\text{bulk volume of fine particles})}{(\text{void volume between the coarse aggregates})} = \frac{r_1}{r_2} \frac{\alpha_2}{\alpha_1(1 - \alpha_2)} \quad (13)$$

Without interaction, Toufar model uses $k_d = 1$, which is similar to Furnas model ($d_1 \gg d_2$) and the corresponding packing density for two cases ($r_1 \gg r_2$ and $r_2 \gg r_1$). This model can be extended for multi-component mixes, however, it was found that such approach tends to underestimate the packing density and is not suitable for many size classes [20]. Europack is a computer program that uses the Toufar model and calculates the proportions of aggregates that produce the maximum or the desired packing degree. However, Europack cannot be used as concrete proportioning method alone and would require the use of another proportioning method such as prescribed by ACI 211 [70]. Europack uses a stepwise method to overcome the underestimation for multi-component mixes by calculating the packing density of binary mixes with larger diameters first and blending the combined mix with the fine size material in a secondary binary model.

Goltermann et al in 1997 favored the use of modified Toufar and Aim model associated with Rosin-Raimmler size distribution parameters that are used to represent the characteristic diameter of aggregates [8]. The model proposed three experimental values to overcome the conflicts between the models and realistic aggregates observed

for discrete models. The characteristic diameter parameter was proposed to represent the non-spherical aggregates in the model. The characteristic diameter is defined as a position parameter of the Rosin-Raimmler-Sperling-Bennet size distribution curve (D') for which the cumulative probability that the diameter of the particle is less than D is 0.368.

This parameter can be used to adjust the theoretical model to assemblies of realistic aggregates. A minor correction factor to k_s is based on the assumption that each fine particle is placed in the space between four coarse particles:

$$k_s = \frac{0.3881x}{0.4753} \quad \text{for} \quad x < 0.4753 \quad (14)$$

$$k_s = 1 - \frac{1 + 4x}{(1 + x)^4} \quad \text{for} \quad x > 0.4753 \quad (15)$$

The third parameter added to the Toufar model is the grain density of each group of particles [2]. It was pointed out that the assumption of fine aggregates filling the void between the coarse aggregate is not realistic when the two aggregates have overlapping grain sizes and therefore, the Aim's model overestimates the packing in the areas where $y_1 < y^*$ (finer than corresponding to the maximum), although the characteristic diameters are different [8].

As discussed by modified Toufar and Aim discrete models, the Rosin-Rambler distribution can be used to defined the Rosin-Rambler Coefficient (D') also named as characteristic diameter of aggregates [8]. From Rosin-Rammler (R-R) equation, D' can be calculated:

$$R(D) = 1 - F(D) = \exp \left(\frac{D}{D'} \right)^n \quad (16)$$

where, $R(D)$ is the R-R distribution, $F(D) = P(d < D)$ is the cumulative probability that the diameter d is less than D . These parameters D and n describe the R-R distribution and can be calculated from the following transform:

$$\ln\left(\frac{1}{R}\right) = (D/D')^n \quad (17)$$

$$\ln\left(\ln\frac{1}{R}\right) = n \ln D - n \ln D' \quad (18)$$

On a ln-ln paper, the $\ln 1/R$ vs. D plot can provide the slope n intercepting at $-n \ln D'$ that follows the calculations of D' as:

$$\ln D' = \frac{\text{intercept}}{n} \quad (19)$$

$$D' = \exp\left(-\frac{\text{intercept}}{n}\right) \quad (20)$$

The Strategic Highway Research Program (SHRP) has developed a computer packing model of dry packed particles, based on the Toufar et al. [25, 94] and Aim and Goff work [79]. This discrete dry packed model was used to calculate the packing density of polydispersed system of particles including cement, fine and coarse aggregates [69,70]. The packing degree of each class and characteristic diameters from Rosin-Rammler distribution was used in a similar way as described by Toufar and Aim models. The Cement and Concrete Association (CCA), Portland Cement Association (PCA), and Pennsylvania Department of Transportation (PennDOT) recommended concrete formulations based on theoretical equations [21]. The packing calculation results are usually presented by in ternary diagrams with isodensity lines and in a numeric table format as illustrated by *Figure 3* and *Table 1*.

$$\text{PHI} = 1 - (\% \text{ voids} / 100) \quad (21)$$

For dry weight packing density PHI (ϕ) as described above.

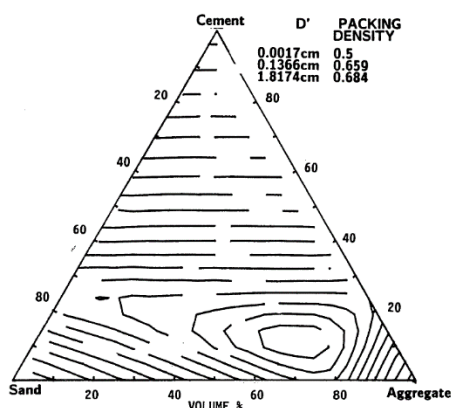


Figure 3. The ternary diagram and isodensity lines calculated for cement, sand, and coarse aggregate blends [21].

Table 2. The example of SHRP table for concrete mixture proportion based on maximum aggregate packing [21].

SAND		COARSE AGGREGATE		VOLUME %	MAXIMUM
d'	PHI, 0	d'	PHI, 0	COARSE AGGREGATE	DENSITY
1.5	0.50	13.0	0.55	74.0	0.70
1.5	0.55	13.0	0.55	72.0	0.71
1.5	0.60	13.0	0.55	70.0	0.73
1.5	0.65	13.0	0.55	68.0	0.74
1.5	0.70	13.0	0.55	66.0	0.76

It was found that the location of recommended concrete mixture on the ternary diagram is within the area of optimal packing [21]. The developed mixtures were supported theoretically to possess the maximum dry packing density [21].

It was reported that “the correlation between the rheology and packing of the mix has found that the workability of concrete is mainly controlled by the binary packing of coarse and aggregate at a fixed cement content and w/c ratio” [25]. The optimal

workability then can be found and compared for mixtures with the maximum packing of fine and coarse aggregates [25].

The purpose of these studies were to provide the means to determine the optimal proportion of fine and coarse aggregates and to calculate the theoretical packing based on the experimental aggregate specific gravity and size (i.e. packing and characteristic diameter) and correlate that with the optimal strength and workability and compare that with recommended mixtures of PCA and State DOTs [21]. As a result, the packing tables in SHRP-C-334 [21] to determine the volume of coarse aggregates based on the maximum packing, were intended for the use in conjunction with ACI 211 (or other mix design methods) to produce a more workable mix and concrete with lower permeability and improved durability. The report [21] concludes that the fluctuations in proportioning of concrete have a very little effect on the dry packing density.



Figure 4. Ternary diagram with isodensity lines and equal sand to coarse aggregate ratio [21].

Figure 4 represents the fine-coarse-cement packing system with a vertical isoline for fixed fine to coarse aggregate ratio [21]. The vertical line also equals to a maximum

binary packing of coarse and fine aggregates. Therefore, at each point on the line the optimal workability can be found at a fixed cement content and w/c ratio. The other advantage of this graph is that concrete mixture can be produced with the lowest w/c ratio and the optimal use of component materials.

This graph demonstrates that the “concrete strength then can be optimized along the line by decreasing and increasing the cement just enough to reach desired workability” [21]. On the right of the line the coarse aggregates exceed the sand fraction and, therefore, in this zone the separation may occur for concrete with low cement and bleeding at high cement contents [21].

The report defines the problem of the best optimal blends and states that “on this background it is apparent that the design of the optimal highway concrete may be reduced to the problem of first finding the optimal volume ratio of the sand to the coarse aggregate and then to find the lowest possible cement content, that with the necessary water content for the desired workability will give the desired strength” [21].

2.2.1.1.4. Multi-Modal Packing Models

Linear packing density model (LPDM) was developed by Stovell and De Larrard in 1986 [83]. The LPDM is based on the improved Furnas model and the use of multi-component combined with the geometrical interaction between the particles [20]. The α_t stated in the Furnas model is always the smallest of two α_t calculated. The reason for that is in case of $r_1 \gg r_2$, the smaller particles cannot be completely packed because there is no small particles to completely fill up the voids between the large particles and in case

of $r_2 \gg r_1$, the larger particles cannot be completely packed because of insufficient space for all fine particles to be placed [20].

Stovell et al. demonstrated that the packing degree is always the minimum of α_t and the size class with the lowest α_t is the dominant class [20]. This concept was extended to multi-component mixtures by representing at least one packed class as dominant and describing the packing density as follow:

$$\Rightarrow \alpha_t = \underset{i=1}{\text{minimum}}^n \left\{ \frac{\alpha_i}{1 - (1 - \alpha_i) \sum_{j=1}^{i-1} r_j - \sum_{j=i+1}^n r_j} \right\} \quad (22)$$

where $i = 1$ indicates the largest particle class.

This equation does not consider the interaction between the particles and it assumes $d_i \gg d_{i+1}$. If the assumption is not valid, then the geometrical wall and loosening interaction effects are considered as follows:

$$\Rightarrow \alpha_t = \underset{i=1}{\text{minimum}}^n \left\{ \frac{\alpha_i}{1 - (1 - \alpha_i) \sum_{j=1}^{i-1} g(j, i)r_j - \sum_{j=i+1}^n f(i, j)r_j} \right\} \quad (23)$$

The function $f(i, j)$ represents the local expansion of larger particles with introduction of the small particles into the mix (loosening effect) and the function $g(j, i)$ represents the reduction of packing degree of the small particles at the vicinity of large particles (wall effect). In this equation, i -class is the dominant fully packed class size and j is partially packed size classes. The interaction between j -size classes is neglected and, therefore, it is anticipated that when these class sizes reach their maximum packing at higher r_j then the calculation becomes less accurate [20]. The other feature of LPDM is that it can be

used to optimize the grading when if enough multiple class sizes are used and the packing density of each class is known. It is an interesting finding that the first equation (without interaction) is similar to the continuous model described by Funk and Dinger in the form of optimization curve.

In 1994 de Larrard and Sedran suggested another model called solid suspension model (SSM) which can be used for packing density calculations of small particles and cementitious materials reaching high packing densities [9, 71].

In 1999 de Larrard introduced a new model for compaction of the mixture via virtual compaction as compressible packing model (CPM) [26]. This model includes the process of packing and compaction effort in describing the packing degree and can be considered as an extension of LPDM [20]. With introduction of a virtual packing density (β) and index K to calculate the actual packing density (α_t). The parameter β is defined as the maximum potential packing density of the mix (if the particles were placed to minimize the voids); versus as if a random packing was placed the resulting packing degree would be lower β . For n size classes and the i category as the dominant class:

$$\beta_{ti} = \frac{\beta_i}{1 - \sum_{j=1}^{i-1} \left[1 - \beta_i + b_{ij}\beta_i \left(1 - \frac{1}{\beta_j} \right) \right] r_j - [1 - \alpha_{ij}\beta_i/\beta_j]r_j} \quad (24)$$

where the β_j can be determined from an experimentally determined packing degree (α_j) and the following equation. The virtual packing (β) is higher than the real packing (α_t) and the effect of applied compaction energy is considered in experimentally determining the packing degree of each class size where k can be determined from *Table 3* [20]:

$$\alpha_j = \beta_j / \left(1 + \frac{1}{k}\right) \quad (25)$$

where, α_j , α_{ij} , b_{ij} can be calculated as follow:

$$\alpha_{ij} = \sqrt{1 - \left(1 - \frac{d_j}{d_i}\right)^{1.02}} \quad (26)$$

$$b_{ij} = 1 - \left(1 - \frac{d_j}{d_i}\right)^{1.50} \quad (27)$$

Table 3. The K value for different compaction methods [26]

Packing method		K value
Dry	Pouring	4.1
	Sticking with rod	4.5
	Vibration	4.75
	Vibration + compression 10kPa	9
Wet	Smooth thick paste (Sedran and Larrard, 2000)	6.7
	Proctor test	12
Virtual	-	∞

The real packing density α_t tends to virtual packing β_t as K tends to infinity and can be implicitly calculated from the following equation [20]:

$$k = \sum_{i=1}^n k_i = \sum_{i=1}^n \frac{r_i/\beta_i}{1/\alpha_t - 1/\beta_{ti}} \quad (28)$$

This model is not limited to aggregate particles and can be used as a proportioning method and allows the use of as many fractions of aggregates and cement as needed [50]. Another feature of this model was to evaluate the “filling diagram” of different mixtures which indicate the filling ratio of the i-th fraction in the void left by the coarser fractions

[50]. It provides the information on deficiencies of certain size classes and the soundness of the overall distribution [50] and can be used for the approximation of particulate composites. The commercial software BETONLABPRO and RENE LCPC use this model to predict the optimal mixture composition and maximum packing density, respectively [20]. Given the experimentally determined packing degree and a joint K index for each class, the model can calculate the packing degree of any mixture and combination. The CPM is the first model that takes into account the experimental compaction method. de Larrard suggests using vibration plus pressure (10 kPa) for measuring the dry packing density as an input for the compressible packing model (CMP) [50].

Theory of particle mixture (TPM) developed by Dewar is a model that calculates the void ratio of two single-sized component mix based on mean size, void ratio and relative density [27]. The theory is relied on the concepts of Power's work including the particle interference and the disturbance of structure of both fine and coarse materials and the generation of additional voids when the fine materials fill the voids between the coarse materials. The theory can be applied to powders as well as the aggregates and can be extended to mixtures with more than two components by combining two components at a time. The void ratio (U) is calculated as the ratio of void to solid volume:

$$U = \frac{1}{\alpha} - 1 \quad (29)$$

For each class U_i represents the void ratio of the class i and d_1 being the diameter of the smallest size class, the overall packing density of mixtures of n size classes can be determined by using of the characteristic (average) diameters [20]. Each time the new

characteristic diameter and the void ratio should be calculated between the two sets of particles [20]. The Mixsim software is developed based on this model.

This method can also be applied for mortar or concrete mixtures with a minimum void content and the mean diameter for binder particles can be determined from the Blaine fineness when the particle size distribution (PSD) of powders is not available. Dewar suggests using loose packing density for TPM model. This method was later adopted by British Standard BSI 812: Part 2.

While Toufar et al. [25], Stovall et al. [83] and Yu and Standish [84] work emphasized the advantages of multi-particle packing based on Furnas model, Dewar [27] stepwise approach is based on the assumption that smaller particles are packed in the voids of larger particles [59].

Schwanda model [81] calculates the maximum void ratio U based on the minimum void ratio ε and maximum packing density α as follows [20]:

$$U = \frac{\varepsilon}{\alpha} \quad (30)$$

In addition to two cases considered by Furnas for small and large particle dominant cases to calculate the void ratio, case 3 is defined where the transition between two zones occurs and the void ratio increases due to the interaction of small particles incapable to fit between the large particles. The interaction is determined using the size-ratio of classes [20]. The packing is calculated from maximum void ratio as follow:

$$\alpha = \frac{1}{1 + U_{\max}} \quad (31)$$

The model can be used for fine sands as well as aggregate blends and takes into account the shape and texture of the particles through the void and packing, but does not take into account the surface forces and packing structure.

2.2.1.1.5. Comparison of Discrete Models

Aim and Goff found the best fit of the theoretical and experimental packing densities for small particle diameter ratios [24]. Goltermann et al. also compared the packing values suggested by Aim model, Toufar model and Modified Toufar model to the experimental packing degree of the binary mixtures [8]. The Aim model predicts a sharp maximum, whereas the Toufar model predicts a flat maximum. For experimental dry packing, Dewar suggests loose packing density, de Larrard suggests vibrated and pressure packing, and Andersen suggests dry rodded packing density. The latter was adopted by ASTM C 29 [50].

Currently, the transfer from binary to multi particle mixtures is facilitated with developed software programs based on the theoretical models. The commercial particle packing software based on theoretical packing models can calculate the packing density based on various compositions based on the aggregate's PSD and packing density. Several mixture compositions can be evaluated to determine the maximum packing density achievable based on the used model. Each model assumes the different particle interactions and energy implemented in the mathematical equations of the model.

2.2.1.2. Continuous Models

Continuous models are also known as optimization curves, focus on the effect of aggregates on concrete performance and assume that all particle sizes are present in the

distribution and there is no gap between the different size classes [71]. Optimization curves can be studied from a particle size distribution (PSD) point of view and optimization can be achieved by the analysis of the curves corresponding to the describing the minimum void content or highest packing.

Ferret in 1892 [30] demonstrated that the packing of aggregates is affecting the concrete properties by reducing porosity of the granular mixes and maximizing the strength. In this regard, the continuous grading of particulate composite can be used to improve the properties of concrete [30, 71].

In 1907 Fuller and Thomson proposed the gradation curves for maximum density known as Fuller's "ideal" curves [11]. These curves can be plotted using the following equation which relates each size to the maximum size of particles:

$$\text{CPFT} = 100 (d/D)^n, \quad n = 0.5 \quad (32)$$

The CPFT is the Cumulative (volume) Percent Finer Than, and n is the power n=0.5 was suggested initially as shown in *Figure 5* and later was changed to 0.45. Talbot and Richard described the Fuller curve as in equation above [85]. Power 0.45 curve found its application in grading of aggregates in asphalt industry.

In 1930 Andreassen et al. tried to improve the Fuller curves and proposed Andreassen equations for ideal packing and a range for exponent n between 0.33-0.5. Andreassen ideal packing curve for n=0.37 is shown in *Figure 5* [100]. In that model the exponent had to be determined experimentally and, as a result, is affected by the aggregates properties [20]. Andreassen assumes that the smallest particle in the mix must be infinitesimally small.

In 1980 Dinger and Funk realized [87, 88] [103, 104] that Andreassen equations need to have a finite lower size limit as a finite smallest particle. Therefore, an important advancement in continuous gradings was developed, in contrast to Fuller curves, by considering not only the largest particle size into equation, but the smallest size as well. The modified Andreassen equations are proposed as follow:

$$\text{CPFT} = \left\{ \frac{(d - d_0)}{(D - d_0)} \right\}^n \cdot 100 \quad (33)$$

where, d is the particle size,

d_0 is the minimum particle size of distribution,

D is the maximum particle size, and

n (also demonstrated as q) is the distribution exponent.

The exponent n is proposed to be 0.37 for optimum packing as shown in *Figure 5* and is suggested to be taken as 0.25-0.3 for high-performance concrete.

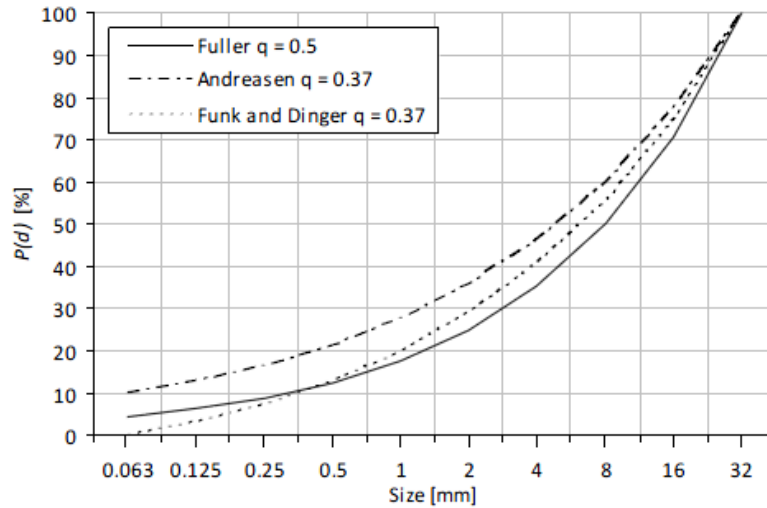


Figure 5. Ideal distribution curves developed by Fuller, Andreassen, and Funk and Dinger [20]].

Also, by selection of exponent n the effect of aggregate shape can be taken into account. For example, for angular coarse particles the lower n can describe the ideal curve because more fines are needed to fill in the coarse particles with irregularities in the shape [20, 86]. As the target and application of the optimization curves is to reach the mixtures of the highest density, the effect of shape on packing density is considered by many researchers [86]. Zheng et al. tried to determine q (or n) as an average of all q -values of all classes used by varying the particle shape [90]. Peronius et al. tried to calculate the porosity of the mixtures of particles with different shapes based on the roundness and the deviation from Fuller curves [92]. This relates the highest packing (or porosity) to the shape and the deviation from a set criterion (Fuller curve) for each shape. Funk and Dinger model was used by other researchers for optimization of mixtures by adjusting the q -value based on the required workability and other experimental results [20, 28, 29, 86, 92, 93].

2.2.1.2.1. Comparison of Continuous Models

The optimization curves can be used to optimize different blends of particles. Three curves represented in *Figure 5* can lead to mixtures with the highest packing density when different particle sets are optimized to fit these curves; however the shape of the particles is not taken into account [20]. The selection of the suitable range for the exponent n , must consider the workability level requirements of concrete mixtures. For higher workability, smaller n leads to the use of higher volumes of fine particles and vice versa for zero slump mixtures.

De Larrard compared and demonstrated the differences between the various types of grading i.e., continuous, gap, uniform, Fuller, Faury, Dreux, maximum density, minimum segregation and segregation potential [26].

The segregation potential is lowest for PSD corresponding to maximum density. The highest segregation potential though occurs for gap graded PSDs, and PSD can provide a very high packing density which is close to maximum possible density and random apollonian packing (RAP) algorithm [26]. However, the change in packing density is not significant for slight variation in the coarse to fine ratio near the maximum packing for slight variation in the coarse to fine ratio.

2.2.1.3. Discrete Element Models (DEM)

The DEM are able to generate the virtual particle structure from a given size distribution. The particles are randomly positioned in a definite space and the packing density can be calculated [59]. The early models were static simulations with fixed positions of assigned particles. The later models evolved to dynamic simulations and,

therefore, enabled the relocation, and the potential for expanding and sliding of the particles under the forces exerted. A dynamic model can be used to consider the gravity and collision forces applied on the particles. Both static models or dynamics models can lead to loose or compacted packing and a dynamic model is not necessarily required to achieve the highly compacted packing assemblies.

Random dispersion of particles can be achieved in many different ways. Large particles can be positioned first or smaller particles can be pre-packed before filling in the space between the larger particles to increase the computational speed required for generating the structure. The particle can overlap, contact, or stay separate. The initial model such as a model used by Zheng and Stroeven [95] has no contacts and, therefore, results in unrealistic packing structure in which the particles form a loose “suspension” structure as represented by Figure 6.

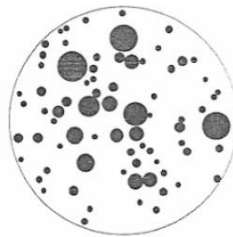


Figure 6. The DEM generating unrealistic random distribution of particles [95].

Other dynamic DEM were able to model loose packing of particles by exerting the gravity on the polydisperse particles as described by Fu and Dekelbab (2003), in *Figure 7* [31, 95]. These models generate a loose packing structure and then reduce the volume of container to reach a compacted state as proposed by Stroeven et al. [40]. Other approaches enable the particles to overlap initially and then enlarge the container with

rearranging the particles until no overlap occurs as proposed by Kolonko et al. in 2008 [32].

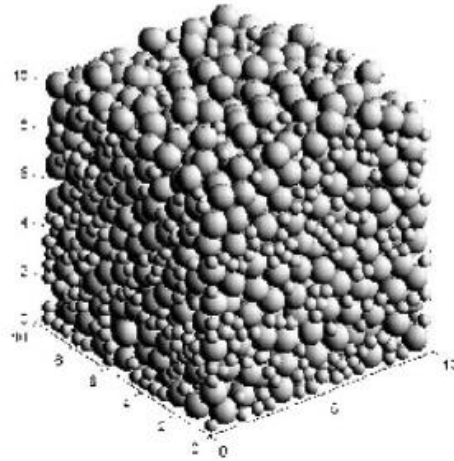


Figure 7. The DEM (dynamic) generating stable loose packing structure of particles [95].

Sobolev et al. solved problems related to both dynamic and static DEM in the sequential packing algorithm (SPA) by assigning several factors that can generate different packing assemblies including loose packing, compacted packing, and packing of particles with defined distribution [44]. In addition, spacing between the particles was introduced and was adjusted in a constant range starting with an initial separation coefficient as the particles are positioned. The diameter of the particles can be reduced at a constant range starting with the D_{\max} to allow the smaller particles pack between the larger particles. Number of trials parameter was introduced to allow the desired packing efforts to fit a particle at a certain diameter range with certain spacing before it reduces the current size and the spacing [44]. *Figure 8* demonstrates the 2D and 3D visualization of the algorithm.

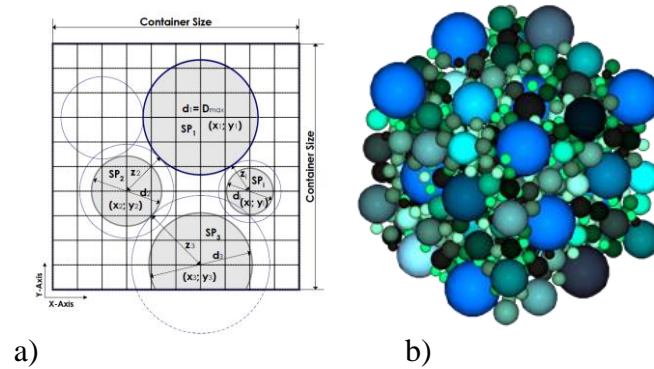


Figure 8. The 2D (sequential packing model) and 3D visualization of the algorithm [37].

The DEM offers an additional information and great potential of modeling for other properties of concrete that may not be possible with discrete or continuous models. The particle structure reveals the particle size distribution, packing degree, size, shape (if not assumed spherical) and the location of particles, and contact points. The model can also be used as a basis for modeling the stress transmission by aggregates and matrix, flow properties, load resistance and permanent deformation capacity [96-98]. These models can help to predict the volumes of cementitious materials, water and admixtures by calculating the spacing or the paste thickness between the particles for a certain viscosity of paste to achieve a certain workability or strength needed. This can minimize the need for extensive experiments to specify the optimized mixtures.

The most important feature of these models is capabilities to find the best particle size distribution (i.e. aggregate blends) corresponding to highest packing. Several mixture compositions must be simulated at a cost of computational efforts as the number of small particles increases. It should be noted that the ultimate selection of the best aggregates

mix should be based on the workability requirements, segregation potential, strength and stiffness requirements achieved at the highest packing density possible.

2.2.2 Coarseness Chart

The coarseness factor chart defines the Workability Factor (WF) and Coarseness Factor (CF) limits for various aggregate blends and relates the grading and concrete performance by specifying Zone II as desired well graded zone as demonstrated in *Figure 9*. The empirical WF and CF parameters depend on composition, grading and cement content of the mix:

$$WF = P_{2.36} + 0.045 (C - 335) \quad (34)$$

$$CF = R_{2.36} / R_{9.5} \quad (35)$$

where $P_{2.36}$ percent passing 2.36 mm (#8) sieve;

C cement content of the mix, kg/m³;

$R_{2.36}$ cumulative percent retained on 2.36 mm (#8) sieve;

$R_{9.5}$ cumulative percent retained on 9.5 mm (3/8") sieve.

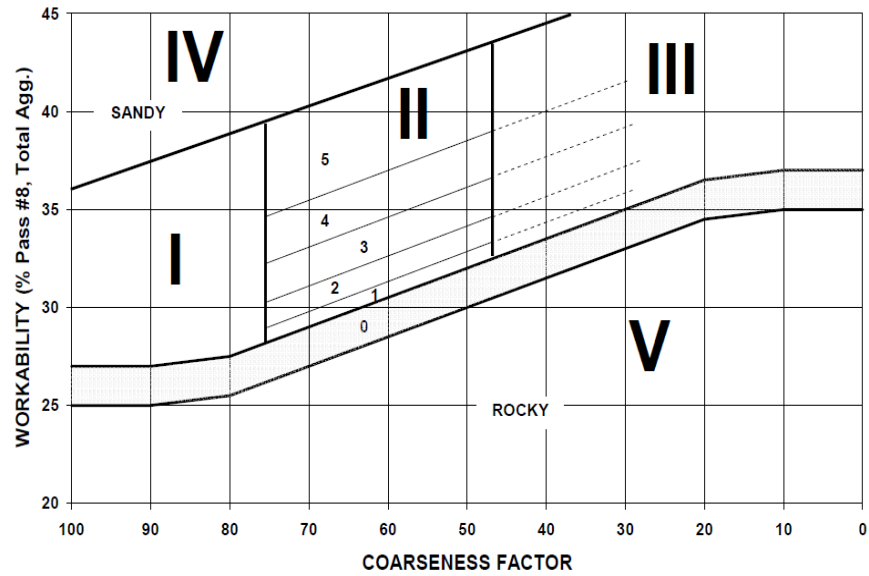


Figure 9. Coarseness chart of aggregate mixtures [18]

The coarseness chart can assist in elaborating the level of workability and coarseness of the blends with binary, ternary or multi-class aggregates. It can also assist to investigate the effect of combined criteria such as grading, the location on coarseness chart, corresponding experimental packing (loose vs. compacted state), and on properties of low cement concrete mixtures.

3. MATERIALS AND METHODS

This chapter discusses the properties of materials used, the experimental matrix, and the testing methods for measuring fresh properties, hardened properties, and durability of concrete.

3.1. MATERIALS

3.1.1. Portland Cements

ASTM Type I portland cements from three different sources were used for the research. The chemical composition and physical properties of cements are presented in *Table 4* and *Table 5*, respectively, along with the requirements of ASTM C150 Standard Specification for Portland Cement. The chemical composition of cements were tested using X-Ray Fluorescence (XRF) technique and reported by the cement manufacturer.

Table 4. Chemical composition of portland cement

CHEMICAL				
Parameter	ASTM C150	Test Result		
	Limits	Lafarge	Holcim	St Marys
SiO ₂ , %	-	19.8	19.4	18.6
Al ₂ O ₃ , %	-	4.9	5.3	5.5
Fe ₂ O ₃ , %	-	2.8	3.0	2.6
CaO, %	-	63.2	63.2	61.1
MgO, %	6.0 max	2.3	2.9	4.3
SO ₃ , %	3.0 max	2.9	3.3	3.9
Na ₂ O, %	-	0.2	0.3	0.3
K ₂ O, %	-	0.5	0.7	0.6
Others, %	-	0.6	0.9	1.5
Ignition loss, %	3.0 max	2.8	1.1	1.5
Potential Composition				
Al ₂ O ₃ / Fe ₂ O ₃		1.8	1.8	2.1
C ₄ AF, %	-	8.5	9.1	8.0
C ₃ A, %	-	8.2	8.9	10.1
C ₂ S, %	-	10.3	9.9	11.3
C ₃ S, %	-	61.6	60.7	55.8
Na ₂ O _{equi} , %	0.6 max	0.5	0.8	0.7

Table 5. Physical properties of portland cement

PHYSICAL				
Parameter	ASTM C150	Test Result		
	Limit	Lafarge	Holcim	St Marys
Density, g/cm ³	-	3.13	3.08	3.07
Time of setting, minutes				
Initial	45 min	103	88	93
Final	375 max	264	222	228
Compressive strength, MPa				
1 day	-	12.1	18.1	21.2
3 days	12.0 MPa	21.7	28.7	26.2
7 days	19.0 MPa	28.3	34.3	29.4
28 days	28.0 MPa	36.5	40.1	34.6

3.1.2. Fly Ash

ASTM Class C and F Fly Ash (from We Energies) were used in this research. The chemical composition and physical properties of two types of fly ash are summarized in *Table 6* and *Table 7*, respectively, along with the requirements of ASTM C618, “Standard Specification for Coal Fly Ash and Raw or Calcined Natural Pozzolan for Use in Concrete”.

Table 6. Chemical composition of fly ash

Chemical Parameter	Class F (AF)	Class C (AC)	ASTM C618 limits	
			Class F	Class C
SiO ₂ , %	46.9	32.7	-	-
Al ₂ O ₃ , %	22.9	17.6	-	-
Fe ₂ O ₃ , %	19.2	5.9	-	-
Total, SiO ₂ +Al ₂ O ₃ +Fe ₂ O ₃ , %	89.0	56.2	70 min 5.0	50 min 5.0
SO ₃ , %	0.3	2.0	max	max
CaO, %	3.8	27.3	-	-
MgO, %	0.8	6.6	-	-
K ₂ O, %	1.7	0.4	-	-
Na ₂ O, %	0.6	2.2	-	-
Moisture Content, %	0.1	0.8	3.0 max	3.0 max
Loss on Ignition, %	2.3	0.3	6.0 max	6.0 max

Table 7. Physical properties of fly ash

PHYSICAL				
Parameter	Class F (AF)	Class C (AC)	ASTM C618 limits	
			Class F	Class C
Specific Gravity	2.50	2.83	-	-
7 Days Strength Activity Index, %	77.5	82.9	75 min 105	75 min 105
Water Requirement, %	102	91	max	max

3.1.3. Blast Furnace Slag

The ASTM Grade 100 ground granulated blast furnace slag (GGBFS or slag cement, SL) was used as Supplementary Cementitious Material (SCM) in this research. The chemical composition and physical properties of SL are presented in *Table 8*, along with the requirements of ASTM C989, “Standard Specification for Ground Granulated Blast Furnace Slag for Use in Concrete and Mortars”.

Table 8. Chemical composition and physical properties of blast furnace slag

CHEMICAL			PHYSICAL		
Parameter	ASTM C989 Limit	Test Result	Parameter	ASTM C989 Limit	Test Result
SiO ₂ , %	-	33.4	Specific Gravity	-	3.01
Al ₂ O ₃ , %	-	10.1	7 Days Strength Activity Index, %	75 min	88.1
Fe ₂ O ₃ , %	-	0.7			
SO ₃ , %	4.0 max	2.5			
CaO, %	-	42.8			
MgO, %	-	10.0			
K ₂ O, %	-	0.4			
Na ₂ O, %	-	0.3			
Loss on Ignition, %	-	1.0			

3.1.4. Chemical Admixtures

Air-entraining, mid-range and high-range water-reducing admixtures were used in this study. Locally used chemical admixtures were supplied by BASF. *Table 9* shows the type, specific gravity, solid content and recommended dosage of admixtures used in the project.

Table 9. Properties of chemical additives

Designation	Admixture	Brand Name	Composition	Specific gravity, g/cm ³	Solid Content, %	Manufacturer recommended dosage ^a
ADA	Air-Entraining	Daravair 1000	Resin and Rosin Acids	1.007	4.3	30-200 mL (0.5-3 fl oz)
AMA	Air-Entraining	Micro Air	Tall Oil, Fatty acids, Polyethylene Glycol	1.007	12.3	8-98mL (0.13-1.5 fl oz)
RP8 (Mid-range)	Water-Reducing Admixture	Pozzolith 80	4-chloro-3-methyl phenol	1.200	40.3	195-650 mL (3-10 fl oz)
HG7 (PCE)	High-range water-reducing	Glenium 7700	Polycarboxylate Ether	1.062	34.0	325-520 mL (5-8 fl oz)
HR1 (SNF)	High-range water-reducing	Rheobuild 1000	Naphthalene Sulphonate	1.193	40.3	650-1,600 mL (10-25 fl oz)

^a The dosage of chemical admixtures is expressed by 100 lbs of cementitious material

3.1.5. Aggregates

Coarse, intermediate and fine (natural sand) aggregates of two different types were used in this project.

Table 10 provides a summary of the aggregates types and sources supplied for the project. Physical characteristics of aggregates are summarized in *Table 11*. Bulk density and void content for loose and compacted aggregates are listed in *Table 12*.

Table 13, Table 14, and Table 15 provide the sieve analysis of aggregates.

Table 10. Designation and sources of aggregates

Designation	Type	Location
C1	1" Limestone	Sussex Pit - Sussex, WI
C2	1" Glacial	Northern WI
I1	5/8" Limestone	Lannon Quarry - Lannon, WI
I2	5/8" Glacial	Northern WI
F1	Torpedo Sand	Sussex Pit - Sussex, WI
F2	Glacial Sand	Northern WI

Table 11. Physical characteristics of aggregates in oven dry (od) and saturated surface dry (SSD) Conditions

Aggregate	Specific Gravity (OD)	Specific Gravity (SSD)	Apparent Specific Gravity (SSD)	Density (OD), kg/m ³	Density (SSD), kg/m ³	Apparent Density (SSD), kg/m ³	Abs., %	Material <75µm, %
C1	2.730	2.765	2.829	2723.1	2758.1	2822.3	1.29	0.78
C2	2.706	2.741	2.803	2699.5	2733.9	2795.9	1.27	0.81
I1	2.684	2.734	2.824	2677.5	2726.8	2816.9	1.84	0.79
I2	2.659	2.715	2.816	2652.8	2708.1	2808.5	2.09	0.94
F1	2.566	2.637	2.762	2559.3	2630.1	2754.9	2.77	1.19
F2	2.563	2.620	2.720	2556.6	2612.7	2709.0	2.20	0.78

Table 12. Bulk density and void content of aggregates in loose and compacted state

Aggregates	Loose			Compacted		
	Bulk Density (OD), kg/m ³	Bulk Density (SSD), kg/m ³	Void Content, %	Bulk Density (OD), kg/m ³	Bulk Density (SSD), kg/m ³	Void Content, %
C1	1561.8	1582.0	42.7	1638.2	1659.3	39.9
C2	1548.9	1568.6	42.7	1674.7	1696.0	38.0
I1	1465.7	1492.6	45.3	1605.2	1634.7	40.1
I2	1508.3	1539.8	43.2	1610.6	1644.2	39.3
F1	1781.5	1830.8	30.4	1868.3	1919.9	27.0
F2	1680.9	1717.8	34.3	1797.3	1836.8	29.7

Table 13. Grading of coarse aggregates

Aggregate	Amount finer than each sieve (mass %)				
	25 mm (1 in)	19 mm (3/4 in)	9.5 mm (3/8 in)	4.75 mm (No. 4)	2.36 mm (No. 8)
No. 67: 3/4 - No.4 (ASTM C33)	100	90-100	40-70	0-15	0-5
C1	100	97.4	23.4	1.1	0.2
C2	100	97.9	34.1	3.6	0.7

Table 14. Grading of intermediate aggregates

Aggregate	Amount finer than each sieve (mass %)						
	19 mm (3/4 in)	12.5 mm (1/2 in)	9.5 mm (3/8 in)	4.75 mm (N. 4)	2.4 mm (N. 8)	1.2 mm (N. 16)	0.3 mm (N.50)
No. 7: 1/2 - No.4 (ASTM C33)	100	90-100	40-70	0-15	0-5	-	-
I1	100.0	87.6	58.5	12.8	2.5	-	-
No. 89: 3/8 - No.16 (ASTM C33)	-	100	90-100	20-55	5-30	0-10	0-5
I2	-	100.0	99.8	29.3	7.8	5.5	2.1

Table 15. Grading of fine aggregates (sand)

Aggregate	Fineness Modulus	Amount finer than each sieve (mass %)						
		9.5 mm (3/8 in)	4.7 mm (N. 4)	2.4 mm (N. 8)	1.2 mm (N. 16)	0.6 mm (N. 30)	0.3 mm (N. 50)	0.15 mm (N. 100)
Sand (ASTM C33)	2.3-3.1	100	95- 100	80- 100	50-85	25-60	3-50	0-10
F1	2.43	100	99	83	70	58	35	13
F2	2.64	100	99	89	74	47	23	5

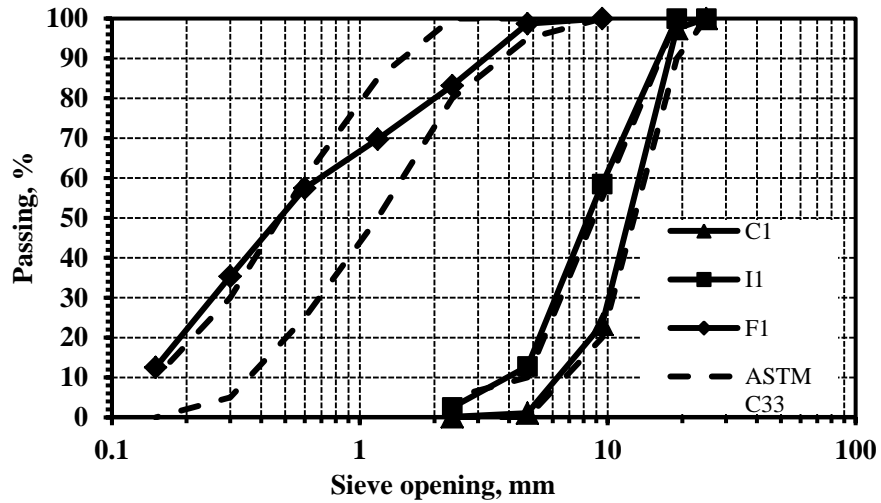


Figure 10. Sieve analysis of southern aggregates (C1,F1,I1)

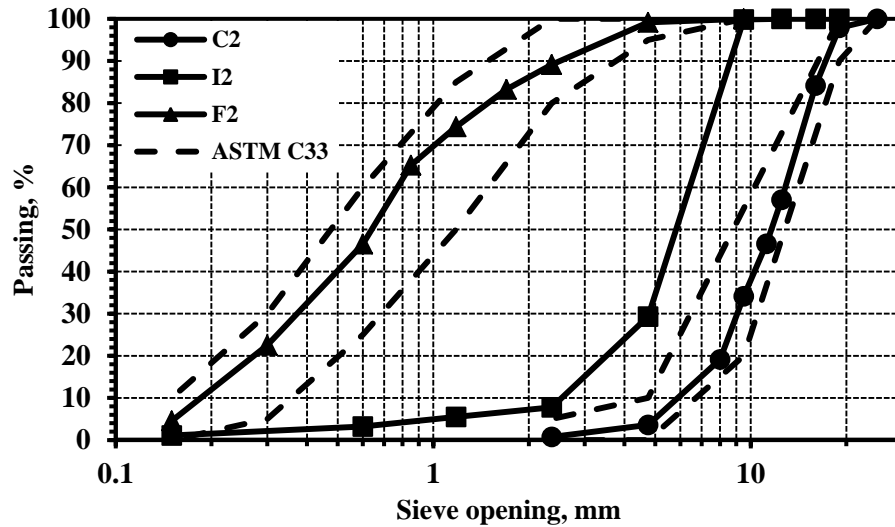


Figure 11. Sieve analysis of northern aggregates (C2,F2,I2)

3.2. EXPERIMENTAL PROGRAM AND TEST METHODS

Concrete mixtures were batched, mixed, cured, and the concrete specimens were cast, and tested for fresh and hardened concrete properties, according to the ASTM and AASTHO standards. The data were obtained using the required number of specimens for various tests. For each testing days and each test results reported in this research, 3 specimen compressive strength, 2 specimen for modulus of rupture, 2 specimen for rapid-

chloride permeability testing, and 3 specimen for freezing-thawing specimen were used. The errors and standard deviations for all testing results of final batches were calculated and the outliers were eliminated from the results according to the limitations of associated standards for compressive strength, modulus of rupture, and durability tests.

3.2.1. Experimental Testing Methods for Packing Density

The VB apparatus was initially developed for zero slump concrete and is currently used to measure the consistency and density of roller-compacted concrete. In this research, the VB vibro-compacting apparatus is adopted (from the ASTM C1170, method A) to test the packing of aggregate combinations. Different aggregate blends (with a total weight of 5.0 kg) were selected and tested for density and packing degree in loose and compacted conditions. Aggregates were thoroughly mixed before the entire sample was placed into the cylindrical mold of the VB consistometer to form a conical pile. The conical pile was carefully flattened to a uniform thickness by spreading the aggregates with a scoop. An aluminum disk attached to the base was placed into the cylinder on the top of the aggregate sample. The distance between the bottom of the mold and the bottom of the disk for loose and compacted aggregates was then determined using four different points. For compacted samples, the trials with different combinations of aggregates were performed to determine the time required for compaction. A time period of 45 seconds was used as an appropriate time for compaction. At least five tests were performed for each aggregate combination, and bulk packing density (BPD) was determined using the following equation:

$$\gamma = BPD = 4000 \left(\frac{W}{(H-\Delta h)\pi D^2} \right), \quad \text{kg/m}^3 \quad (36)$$

where: γ : Bulk packing density of combined aggregates in loose or compacted conditions, kg/m^3

W: Mass of combined aggregates, kg

H: Height the container, mm

D: Diameter of the cylindrical container, mm

Δh : Height reduction of the compacted materials in cylindrical container, mm

Loose and compacted densities of aggregates and aggregate's blends were determined by the following equation:

$$\varphi = \gamma \cdot \sum_{i=1}^n \frac{A_i}{\rho_i} \quad (37)$$

where: γ : Packing density of aggregates blend, kg/m^3

ρ_i : Grain density of aggregates fraction, kg/m^3

A_i : Percentage of aggregates fraction, %

n: Number of aggregate fractions



Figure 12. VB apparatus used for experimental packing test

3.2.2. Preparation, Mixing, and Curing

The concrete batching and mixing, as well as casting and curing of the specimens were accomplished according to ASTM C192 “Standard Practice for Making and Curing Concrete Test Specimens in the Laboratory”. The mixing procedure included mixing of aggregates with 20% of the water for 30 seconds. Then cement was added to the mix and then SCMs were added. The rest of water was added upon the addition of cementitious materials followed by the addition of sand. The mixing was continued for additional 3 minutes using a drum mixer suitable for the volume of the batch. The mix was left in the drum mixer at rest for a period of 3 minutes and was mixed for another 2 minutes.

3.2.3. Slump

Concrete slump was tested according to ASTM C143 as a measure of workability level of plastic concrete. This test is widely used for testing concrete pavement mixtures in the field to measure the suitability for slip-forming, however there may be other characteristics of such as finishability that are not accounted by using this test. The test was repeated after 30 min upon addition of water and cement to measure the slump loss. The apparatus and equipment used per ASTM C143.

3.2.4. Density of Fresh Concrete

Density of concrete was tested in a fresh state per ASTM C34. All the mixtures regardless of the slump, were consolidated using rodding according to the standard and tapping the side of the container with a rubber mallet repeated in 3 layers. The top of the container is stroke-off and the weight was measured on the scale as per as ASTM C34 and fresh density was calculated accordingly.

3.2.5. Air Content of Fresh Concrete

Air content was tested in the fresh state. Since AE admixture creates air bubbles within the mix it is important to determine the air content. Optimized mixtures were designed to reach 6 ± 1.5 % air content; however, some changes occurred due to the variation in type of HRWRA and SCMs. Air content was tested using an air meter (*Figure 13*) per ASTM C231. In this test, concrete material is placed within the container and the lid is placed on and sealed. The container is then pressurized to allow all the voids within the container to be accessible to the air. A valve is then released, allowing air to flow into the container and resulting in a pressure decrease which is proportional to the amount of air the was originally in the fresh specimen. This air content can then be read on the apparatus and recorded.



Figure 13. Air meter used for air test

3.2.6. Temperature

Fresh concrete temperature was tested according to ASTM C164 using a temperature measuring device capable of measuring a ± 1 °F throughout a range of 30° to 120° to

monitor the potential effect of temperature. The temperature can be used to track any potential variation due to moisture loss and heat of hydration, and different batches.

3.2.7. Compressive Strength

Compressive strength tests were performed on cylinders with a diameter of 100 mm and height of 200 mm according to ASTM C39. These specimens were tested with an ADR-Auto ELE compression machine and loaded at a rate of 2.4 kN/sec. The maximum load and maximum compressive stress were recorded. The test was performed at different ages including 1, 3, 7, 28, 90, and 360 days.

3.2.8. Flexural Strength (Modulus of Rupture)

Flexural tests were performed on 101.6 x 101.6 x 355.6 mm beams according to ASTM C293. These specimens were tested using an ADR-Auto ELE machine suitable for center-point loading method and loaded at a rate of 1.4 kN/sec. The width and height of the sample at two cross sections were measured prior to testing and the maximum load was then recorded upon testing. The modulus of rupture at 3, 7, 28, and 90 days was calculated as follow:

$$R = \frac{3PL}{2bd^2} \quad (38)$$

where: R : Modulus of rupture,

P : Maximum load, N

L : Length of the specimen, mm

b : Width of the specimen, mm

d : Height of the specimen, mm

3.2.9. Chloride Permeability

Preparation and testing for Rapid Chloride Permeability follow procedures in the Standard Test Method for Electrical Indication of Concrete's Ability to Resist Chloride Ion Penetration ASTM C1202 (equivalent AASHTO T259). From each batch of concrete, there were two 4" x 8" cylinders, one for 30-day testing and the other for 90-day testing. The cylinders were moist-cured in a wet room under temperature of 70 F until two days prior to their testing dates.

Two days prior to the testing date, two 2-inch thick slides were cut from the cylinder for test specimens. Before this cutting, a slide of approximately ½-inch thickness was removed from the end of the cylinder so that testing surfaces of both specimens have similar conditions. The slides were let dry for about one hour before epoxy was applied to their side surfaces. All holes on the side were covered in this process. Attempts were made to avoid letting epoxy stick to the testing surfaces of the specimens. After the epoxy was cured for about 12 hours, the specimens were ready for vacuum saturation process. Two-part marine grade epoxy PC-11 was used.

The two slides were kept in a container which was put in a desiccator under vacuum in dry condition for 3 hours. Then water, which was tap water vigorously boiled for 20 minutes and cooled to room temperature, was let into the container through a pipe attached on the side of the desiccator. Vacuum pump was kept running for an additional hour. After that, vacuum was released and the specimens were kept under water, usually overnight, for 18±2 hours.

The specimen was removed from water and mounted between the two test cells. Four bolts were used to secure the specimen to the cells. Silicone caulk was applied to seal the

gap between the specimen and the cells. After the caulk was let dry for about one hour, one cell, which would be connected to the negative terminal of the power supply, was filled with 3% NaCl solution and the other, which would be connected to the positive terminal, was filled with 0.3N NaOH solution. The power was turned on and maintained at 60 ± 0.1 V. Current and voltage readings were automatically recorded every 30 or 60 seconds by a computer program. Tests were run for 6 hours. The charge passed through the specimen was calculated by integration of the current with time and then adjusted to account for the diameter of the specimen as equation (2) in the ASTM C1202 standard as follow:

$$Q=900 (I_0+2I_{30}+2I_{60}+\dots+2I_{300}+2I_{330}+I_{360}) \quad (39)$$

Where,

Q=charge passed (coulombs)

I_t =current passed (amperes) at time t after voltage is applied

The lower the charge passed the lower the chloride ion permeability will be. The specimen can then be analyzed using the following table.

Table 16. Chloride ion penetrability based on charge passed

Charge Passed (coulombs)	Chloride Ion Penetrability
>4,000	High
2,000–4,000	Moderate
1,000–2,000	Low
100–1,000	Very Low
<100	Negligible

3.2.10. Freeze Thaw Durability

From each batch of concrete, there are three 3" x 4" x 16" beams. Preparation and testing for freeze-thaw durability follow procedures in the Standard Test Method for Resistance of Concrete to Rapid Freezing and Thawing ASTM C 666 (equivalent AASHTO T161) Procedure A and Standard Test Method for Fundamental Transverse, Longitudinal, and Torsional Resonant Frequencies of Concrete Specimens ASTM C 215 with the following exceptions:

- ✓ 3% NaCl solution (by weight) was used instead of water;
- ✓ The specimens were moist-cured for 28 days and then kept in lab conditions with relative humidity of 50% and temperature of 70 F.

On its 54th day, each specimen was saturated in 3% NaCl solution for 48 hours. The purpose of this saturation process is to make initial measurements comparable to later measurements of the specimen. This follows the instructions for conditioning beams cut from hardened concrete stated in provision 8.1 in the ASTM C666.

Immediately after the conditioning period above, on their 56th day, fundamental traverse frequency of the specimen was measured according to the ASTM C215 standard. Mass, average length and cross-section dimensions were measured within the tolerance required in Test Method C215.

Freezing-and-thawing tests were started by placing the specimens in 3% NaCl solution at the beginning of the thawing phase of the cycle. The specimens were removed from the apparatus, in a thawed condition, at intervals of between 30 and 36 cycles and tested for fundamental traverse frequency and mass. The specimens were then returned to the apparatus in 3% NaCl solution. Each specimen was continued testing until it has been

subjected to 300 cycles or until its relative dynamic modulus of elasticity reaches 60 % of the initial modulus, whichever occurs first. Relative dynamic modulus of elasticity of each tested specimen was calculated as follows:

$$P_c = (n_c/n_0)^2 \times (M_c/M_0) \times 100 (\%) \quad (40)$$

where:

P_c = relative dynamic modulus of elasticity, after c cycles of freezing and thawing, percent,

n_0 and M_0 are fundamental transverse frequency and mass respectively, after 0 cycle of freezing and thawing and

n_c and M_c are fundamental transverse frequency and mass respectively, after c cycles of freezing and thawing.

The above equation was modified from equation (1) in the ASTM C 666 standard to account for mass change as mentioned in Note 9 of the same document.

Durability factor of each specimen was calculated as follows:

$$DF = PN/M \quad (41)$$

where:

P is relative dynamic modulus of elasticity at N cycles, %,

N is number of cycles at which P reaches the specified minimum value for discontinuing the test or the specified number of cycles at which the exposure is to be terminated, whichever is less, and

M is specified number of cycles at which the exposure is to be terminated which is 300.

Length change was not measured.

4. RESULTS AND DISCUSSION

This chapter discusses the optimization of aggregates as the major component of concrete, the preliminary optimization of HRWRA/WRA, and air-entraining admixtures, water to cement ratio adjustment in concrete, and final optimized concrete mixtures investigated for fresh properties, hardened properties, such as strength development, and flexural behavior.

4.1. AGGREGATES OPTIMIZATION

This section reports on theoretical, simulation, and experimental aspects of aggregate optimization and the common techniques, characteristics of aggregate blends, applicability of gradation techniques, and coarseness chart. The aggregates were also evaluated in concrete mixtures in order to make a comparison between the aggregates optimization and the performance of corresponding blends in concrete.

4.1.1. Experimental Packing of Aggregates

The experimental bulk density and void content for loose and compacted aggregates are summarized in *Table 17* and *Table 18*. Higher densities of aggregate blends correspond to the lower void content of the material. As demonstrated by *Figure 15* and *Figure 16*, loose and compacted density of 40 different southern Wisconsin aggregate blends and 40 different northern Wisconsin aggregate blends were used to determine the experimental packing degree. Selective combinations of aggregates and the density before and after compaction are summarized in *Table 17* and *Table 18*. As illustrated by *Figure 15* and *Figure 16*, in Southern aggregates (top of ternary diagram), the packing

degree tends to increase at 50% to 70% of fine aggregates and in Northern aggregates the best packings were achieved at 40% to 60% of fine aggregates at different levels of IA.

From both *Figure 15* and *Figure 16* it can be observed that the use 10% intermediate aggregates tend to increase the packing degree of all mixtures based on both Northern and Southern aggregates, and as a result provides the highest packing in both loose and compacted states. For both types of aggregates the impractical zone of the diagram corresponds to mixtures with less than 40% of coarse aggregates. The experimental packing degree as high as 79% for compacted and 68% for loose states, were achieved as illustrated in *Figure 15* for Southern aggregates and as high as 78% for compacted and 68% for loose states as illustrated in *Figure 16* for Northern aggregate. For Northern aggregate the packing test results indicate that the intermediate aggregates have a high compactibility with other aggregate fractions, therefore, can contribute to dense packing and better aggregate blends for both Southern crushed and Northern round aggregates.

4.1.2. Proposed Packing Simulation Model

The sequential particle packing simulation algorithm developed by Sobolev and Amirjanov [33, 43] used for this research assumes that the particles are spherical (or circular in a 2D educational model) [40]. Spherical particles with radii in the range of $r_{min} < r \leq r_{max}$ are sequentially placed into the cube with the centers glued to the node of a very fine lattice grid [33]. The radius r_{max} is defined depending on the container size and is fixed at the beginning of simulation, but r_{min} is decreased gradually by a controllable procedure, thus allowing larger spheres to be placed prior to the placement of smaller ones [33]. To realize the packing routine, a set of parameters including the reduction rate of the minimal size of the particle (K_{red}), the initial separation between the

particles (K_{del}), the step of separation (S), and the number of packing trials are defined as inputs. Before locating the sphere with radius r_i , the various conditions are examined: a) the center of a new sphere cannot be located inside of any already packed spheres; b) new sphere cannot cross any already packed sphere; and c) the minimum distance to the surface of any already packed sphere should be greater than r_{min} [33]. The cube can be pre-packed with initial objects including intersecting spheres enabling the combinations of different packing rules to assemble the “real world” particulate composite.

In this study, the simulation of aggregate packing established by Sobolev et al. [33] was used for the optimization of concrete mixtures. The performance of the proposed algorithm is illustrated by a 2D packing achieved with a limited number of objects (500 disks) and a relatively low reduction coefficient ($K_{red}=1.001$) as represented in *Figure 14.a*. Higher initial separation coefficient value (K_{del}) results in larger initial separation between the particles [33]. The separation was introduced to provide the spacing between the larger objects, but allows for smaller separation between the midsize and small particles as achieved by the use of separation with a reduction coefficient ($S=1.001$) proportional to the grain size. For the reported example in *Figure 14*, the initial separation (K_{del}) of 1.5 was used. This 2D packing resulted in a packing degree of 86.2% (*Figure 14.a*).

Further, the 3D simulations of particulate composites with a large number of particles, up to 20 million can provide a very realistic packing arrangement in respect to size distribution and degree of packing used in “real world” concrete. In this research, a simulation experiment with 5 million particles is compared with ASTM 33 limits and with 0.55 power curve as coarse and combined aggregates benchmark, respectively.

Preliminary exploration of the simulation with 5 million spheres was used for the virtual experiment. The error from each of these curves was minimized by selection of suitable packing parameters. The final 3D packing simulation experiment was conducted for the combination of a reduction coefficient of $K_{red}=1.01$ and a relatively low number of packing trials, 10 corresponding to a low packing energy (i.e. Loose Initial Packings, LIP), but at a relatively large separation with $K_{red} = 5$ and 10 with a step of separation of $S=1.025$ to achieve two different compositions corresponding to 0.7 and 0.55 power curves as demonstrated in *Figure 14.b*.

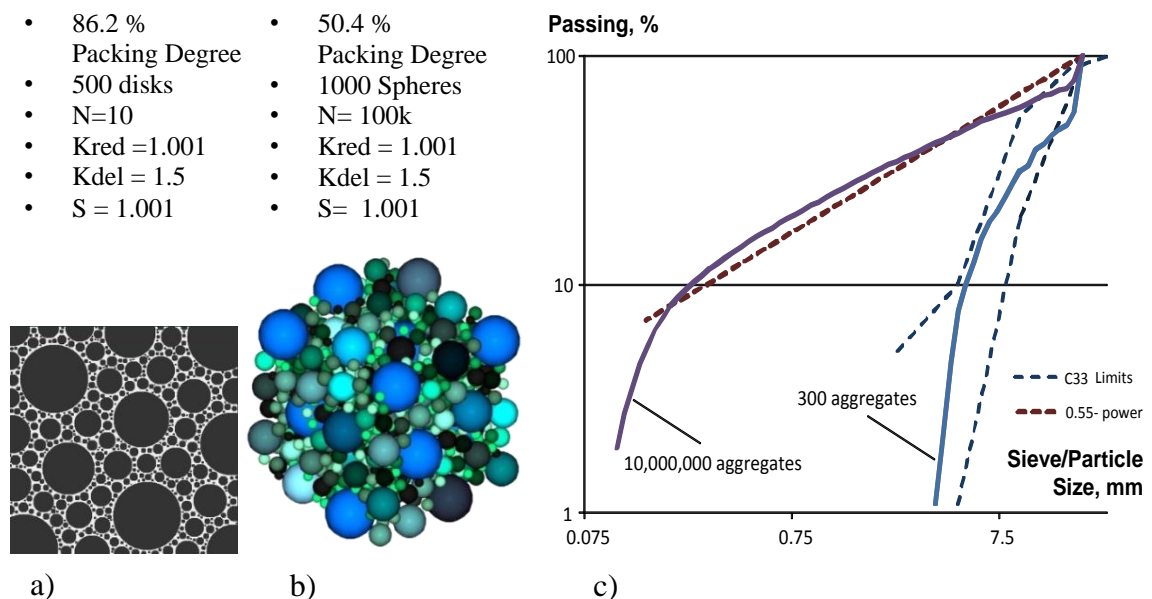


Figure 14. The output of packing algorithm: a) representation of Apollonian Random Packing with LIP separation b) 3D visualization and c) the associated PSD the output of packing algorithm

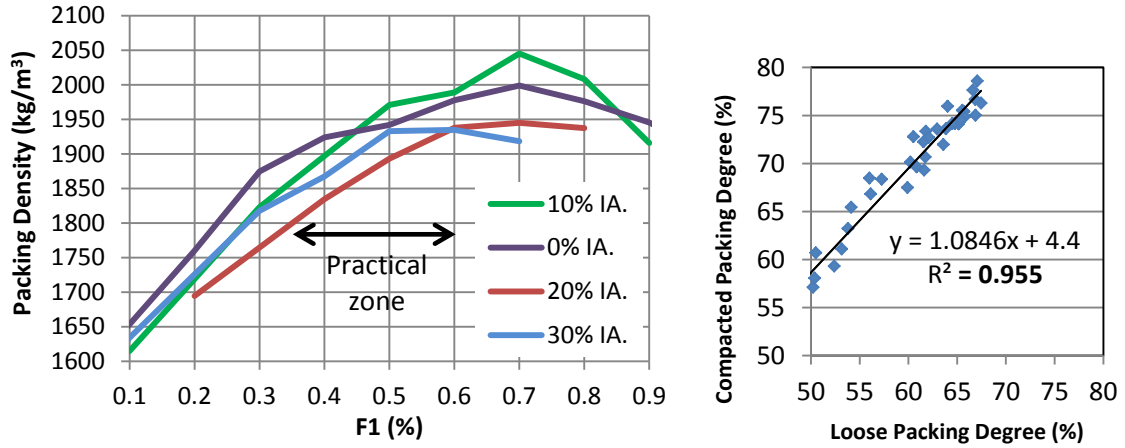
4.1.3. Packing Simulation

Two combinations were selected for 3D packing simulation with an initial separation of 5 and 10 (Figure 17.a) corresponding to realistic packing arrangements of compacted

aggregates. The compositions were developed to achieve the best PSD fit to 0.7 (Fit 1) and 0.45 (Fit 2) power curves. The resulting packing degree of 74.5% and 78.8% and the corresponding square error from 0.7 and 0.45 power curves respectively are given in Table 17. This was achieved by proper selection of input variable parameters of the simulation: a reduction coefficient, K_{red} of 1.01, initial separation, K_{del} of 5 and 10, and step of separation, S of 1.025 resulting in desirable particle size distributions as illustrated by Figure 17.a. In the 3D model, realistic packing can be achieved with a step of separation higher than the reduction coefficient. The experimental blends of Southern aggregate with the best fit to 0.7 and 0.45 power curves and associated aggregate combinations are presented in Figure 17.b. Table 17 compares the packing degrees and parameters obtained by the simulation and experiment. Table 18 represents similar experimental results for Northern aggregates.

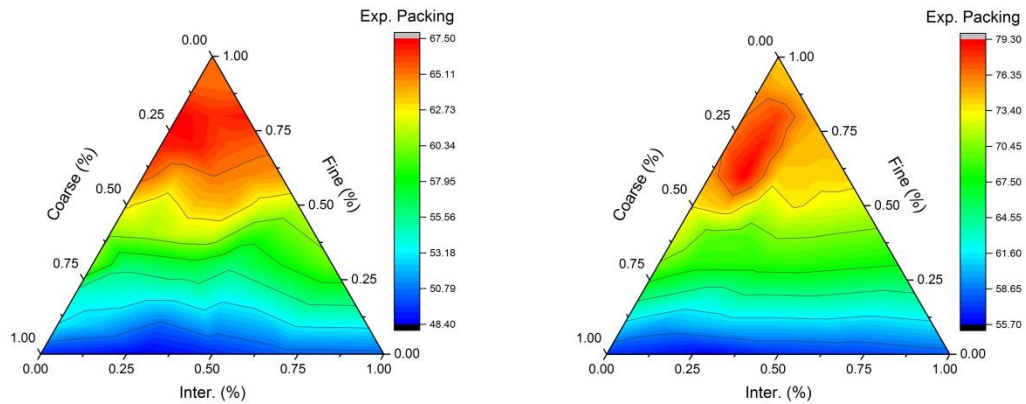
Among 16 mixtures investigated for Southern aggregates and 10 mixtures investigated for Northern aggregates, the experimental mixtures with the best fit to 0.7 and 0.45 power curves were selected. In southern (S) mixtures the binary mixture S1 has the best fit to the 0.7 power curve and mixture S13 with 50% of fine aggregates has the closest fit to the 0.45 power curve. Other mixtures such as S8 are also close to 0.45 power curve, but have a slightly higher deviation compared to mixture S13 with 50% fine aggregates. For Northern (N) mixtures the binary mixture N1 has the best fit to the 0.7 power curve and mixture N7 with 45% fine aggregates has the closest fit to the 0.45 power curve. The most of the real world aggregate combinations would fall in between 0.7 and 0.45 power distributions as boundary mixtures. Other mixtures such as N3 and N9 are also close to

0.45 power curve, but have a slightly higher deviation compared to N7 with 45% fine aggregates.



a)

b)



c)

d)

Figure 15. The experimental packing degree of Southern aggregate a) compacted vs. loose; b) the effect of fine aggregates; c) ternary diagrams d) compacted packing

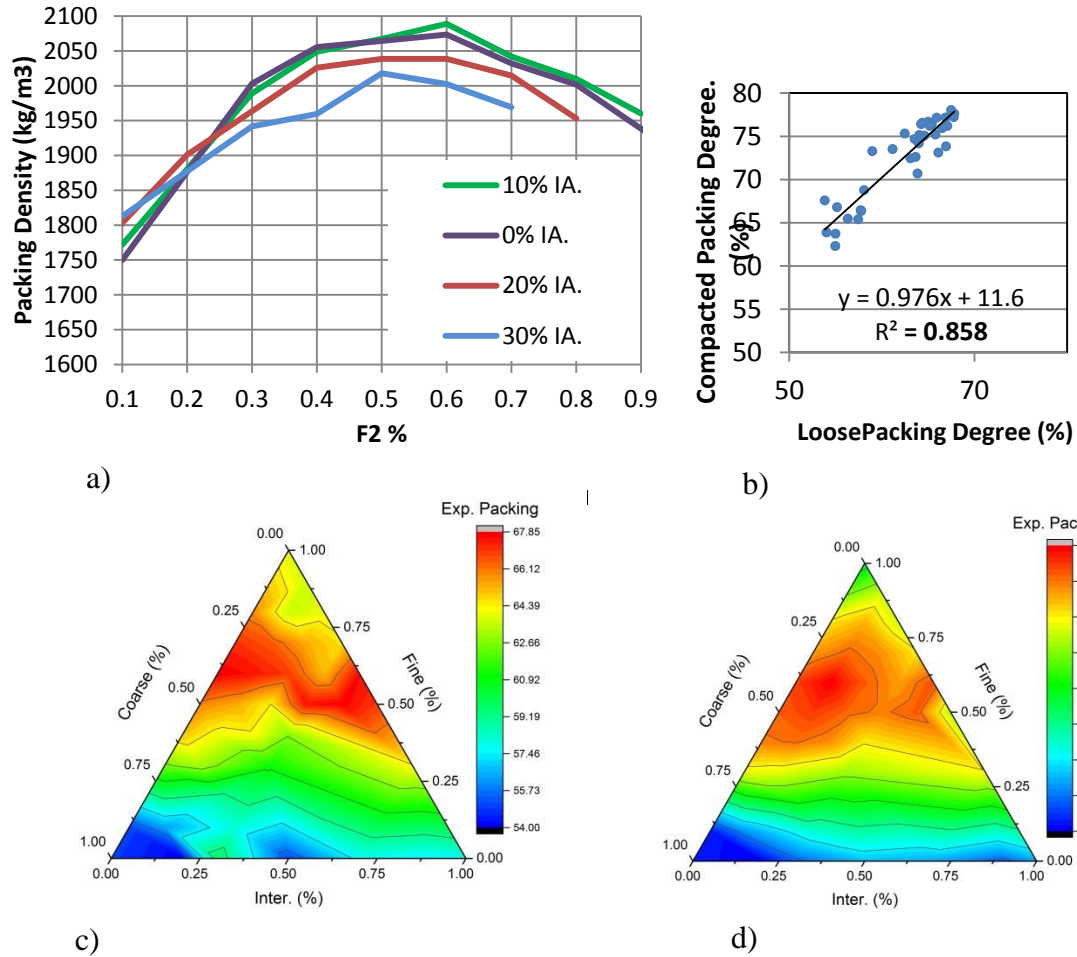


Figure 16. The experimental packing degree of Northern aggregates a) compacted vs. loose; b) the effect of fine aggregates; c) ternary diagrams d) compacted packing

The use of simulation algorithm provides the PSD suitable for the desired power curve and can be correlated to the particular type of concrete. The simulation with realistic parameters such as number of particles, packing trials and reduction coefficients then can be used for the representation of various aggregate blends. Table 17 provides the difference between the errors and standard deviation for simulated and experimental compositions. As it appears from *Figure.17.b*, “Fit 1” (corresponding to mixtures S13, N7, and 0.45 power distribution) has a higher error and standard deviation than “Fit 2” corresponding to mixtures S1, N1, and 0.7 power distribution. Simulated compositions

have S shape PSD converging to 0.7 power curve at diameters smaller than $0.02D_{max}$ mainly due to the limited number of small particles, where the experimental mixtures have a reverse S shape due to the PSD of individual components.

Lower initial spacing results in fitting of particles with larger diameter (Fit 2). The packing degrees obtained by the simulation are higher than those corresponding experimental blends. This can be explained by the irregularities in the real aggregates vs. the use of ideal round spheres and also a better particle positioning achieved by simulation.

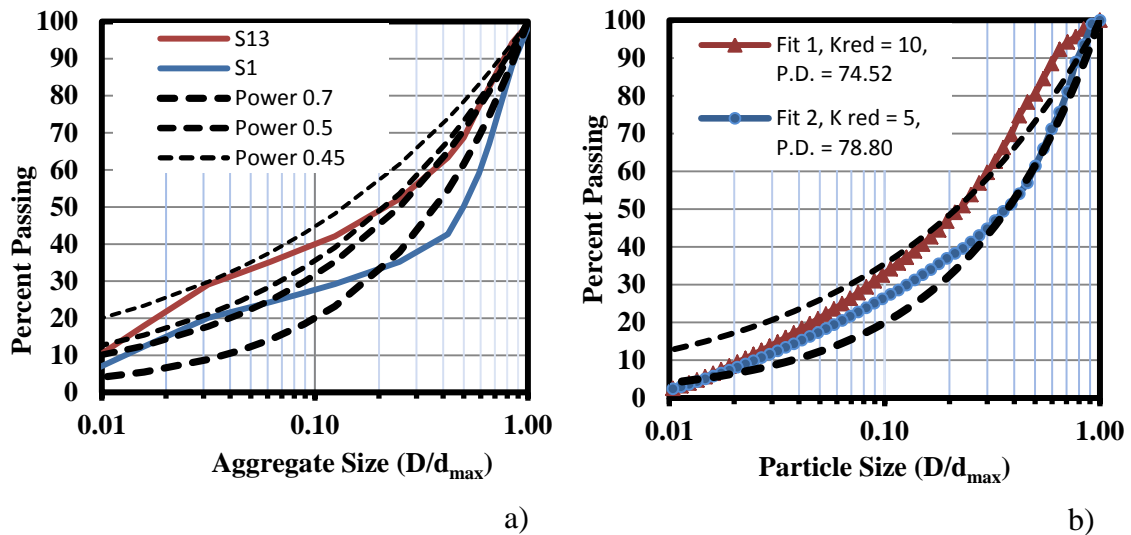


Figure 17. The PSD corresponding to a) the best fit to experimental blends and b) 3D packing simulation and

Table 17. Test results for concrete mixtures with various southern aggregate blends

Mix ID	Packing Degree, %		Aggregate Combinations, %			Experimental Results					Power Distribution					
	Loose	Comp.	CA	IA	FA	Slump, mm	Bulk density, kg/m ³	Air (Pressure) %	Compressive Strength, MPa		Power n	Statistical Parameters				
									7 days	28 days		Square Error	MSE	Root MSE	NRM SE %	Std. Dev.
S1 Fit 2	60.4	71.5	65	0	35	76	2480	1	15.6	22.8	0.70	943	67.4	8.2	73.0	53.7
	-	78.8	-	-	-	-	-	-	-	-	0.70	204	-	-	-	14.8
S2	60.5	72.8	60	0	40	70	2477	0.8	20.2	25.5	0.59	893	63.8	8.0	65.2	55.4
S3	61.7	73.2	55	0	45	191	2463	1	20.4	25.8	0.51	796	56.9	7.5	65.5	53.7
S4	62.9	73.6	50	0	50	191	2435	1.3	21.2	25.7	0.46	676	48.3	6.9	68.6	42.8
S5	65.7	75.4	40	0	60	165	2406	2.2	23.0	27.8	0.36	471	33.6	5.8	64.7	31.3
S6	58.5	68.2	55	10	35	205	2480	0.9	16.5	23.6	0.64	649	46.4	6.8	61.9	39.7
S7	61.3	71.5	45	10	45	191	2449	1.2	20.3	27.6	0.49	497	35.5	6.0	60.0	32.8
S8	61.8	73.4	40	10	50	191	2435	1.2	22.4	28.0	0.43	405	28.9	5.4	59.6	27.2
S9	62.4	74.0	37.5	10	52.5	191	2446	1.3	23.0	31.3	0.40	372	26.6	5.2	59.0	26.5
S10	62.9	74.7	35	10	55	171	2446	1.8	22.5	30.8	0.39	326	23.3	4.8	60.3	21.4
S11	59.7	67.8	45	20	35	181	2469	0.9	17.7	20.9	0.6	427	30.1	5.5	64.8	27.8
S12	61.6	69.3	40	20	40	175	2460	0.9	17.9	24.9	0.53	360	25.7	5.1	64.3	24.0
S13 Fit 1	63.6	72.0	30	20	50	156	2463	1.2	23.5	30.2	0.42	227	16.2	4.0	66.8	15.2
	-	78.8	-	-	-	-	-	-	-	-	0.45	943	-	-	-	53.7
S14	59.5	69.5	35	30	35	166	2483	0.9	17.7	22.4	0.57	268	19.1	4.4	64.3	18.6
S15	61.7	70.7	30	30	40	146	2457	1.1	22.9	30.1	0.51	218	15.6	3.9	65.4	14.5
S16	63.8	73.6	20	30	50	165	2443	1.3	21.6	30.4	0.40	151	10.8	3.3	45.2	14.0

Table 18. Test results for concrete mixtures with various northern aggregate blends

Mix ID	Packing Degree, %		Aggregate Combinations, %			Experimental Results					Power Distribution					
	Loose	Comp.	CA	IA	FA	Slump, mm	Bulk density, kg/m ³	Air (Pressure) %	Compressive Strength, MPa		Power n	Statistical Parameters				
									7 days	28 days		Square Error	MSE	Root MSE	NRM SE %	Std. Dev.
N1	63.7	76.0	65	0	35	32	2544	0.75	19.4	29.5	0.62	521	37.2	6.1	32.4	33.9
N2	64.9	76.0	60	0	40	93	2525	0.8	21.7	28.0	0.55	513	36.6	6.1	39.0	31.9
N3	65.9	77.1	50	0	50	70	2473	2.2	21.5	33.1	0.44	495	35.4	5.9	65.7	28.8
N4	67.8	77.6	40	0	60	20	2410	2.8	17.4	27.7	0.36	587	41.9	6.5	38.5	51.9
N5	65.5	76.9	55	10	35	36	2502	1	20.2	31.6	0.58	305	21.8	4.7	29.0	25.7
N6	64.0	75.1	50	10	40	43	2524	1.3	24.8	32.4	0.52	301	21.5	4.6	37.1	23.3
N7	64.7	75.8	45	10	45	70	2486	0.8	23.8	30.2	0.46	308	22.0	4.7	56.5	24.2
N8	64.2	76.4	40	20	40	33	2477	1.6	21.9	30.9	0.49	229	16.4	4.0	42.5	18.8
N9	64.3	76.5	30	20	50	30	2476	3	21.1	26.7	0.40	520	37.1	6.1	48.4	35.7
N10	66.1	73.1	30	30	40	44	2490	1.8	20.9	29.0	0.40	520	37.1	6.1	69.2	22.4

4.1.4. Concrete Mixtures

Sixteen mixtures with different combined aggregate gradations and different packing degrees were tested to determine the effect of aggregate proportions on fresh properties and mechanical performance of concrete as summarized in *Table 17* for Southern aggregates and similar test were conducted on ten mixtures for Northern aggregates. The workability of fresh concrete is affected by other parameters such as air content, aggregate surface area and also the volume of fines. Cement paste volume was held constant by holding the W/C ratio and cement content constant. All mixtures were produced without air entraining admixture in order to minimize the contribution of air. Therefore, all the mixtures listed in each of the *Table 17* and *Table 18* had the same aggregate volume, W/C ratio, and cement content, but different combined aggregate gradings. The mixtures were produced at a relatively high water to cement ratio of 0.6 for Southern aggregate and 0.53 for Northern aggregates in order to provide sufficient workability important for the detection of difference in performance.

4.1.5. Gradation Techniques - Particle Size Distribution (PSD) Curve

The selection of the best power curve for the optimized aggregate blends was performed using the least standard deviation. The exponent n that generates the square error from the aggregate's combined PSD curve is reported in *Table 17* for Southern aggregates and *Table 18* for Northern aggregates. The square error from suggested power curve (PC) is an important parameter to evaluate the best fit PC. As expected, the blends with finer PSD find the better fit to the smaller exponents in a range that vary between 0.36 to 0.7 for both types of aggregates. In addition to square error, other statistical

parameters including standard deviations are calculated and reported in *Table 17*. The normalized root of mean square error (NRMSE) is calculated as follow:

$$NRMSE (\%) = \frac{RMSE}{e_{max} - e_{min}} * 100 \quad (42)$$

where, e_{max} and e_{min} are the maximum and minimum errors (deviations) from the associated power curve respectively. The NRMSE takes into account the maximum and minimum deviations from the PC as well as the root mean square error. The correlation between the NRMSE and both loose and compacted packing degree indicates the relationship between the deviation from the power curves and the experimental packing degree. For a given composition, the best fit can be associated with either lower RMSE from the curve or a lower difference between the maximal and minimal errors. The best fit blend therefore demonstrates the lowest errors and highest NRMSE.

Figure 18 and *Figure 19* illustrate the PSD for coarsest and finest mixtures of different levels of IA and provide the range for practical mixtures. The use of IA assists in shifting the coarsest and finest mixtures to the middle zone confined by the 0.45 and 0.7 power curves for both southern aggregates. The same trend is observed for Northern aggregates, however Northern aggregates have a smaller size distribution than Northern aggregates.

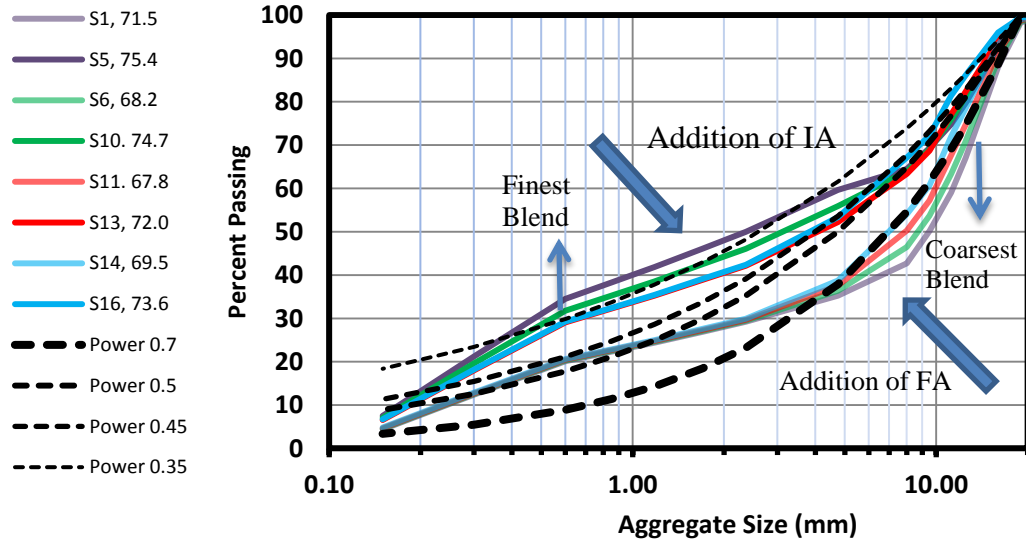


Figure 18. The PSD of experimental southern aggregate blends

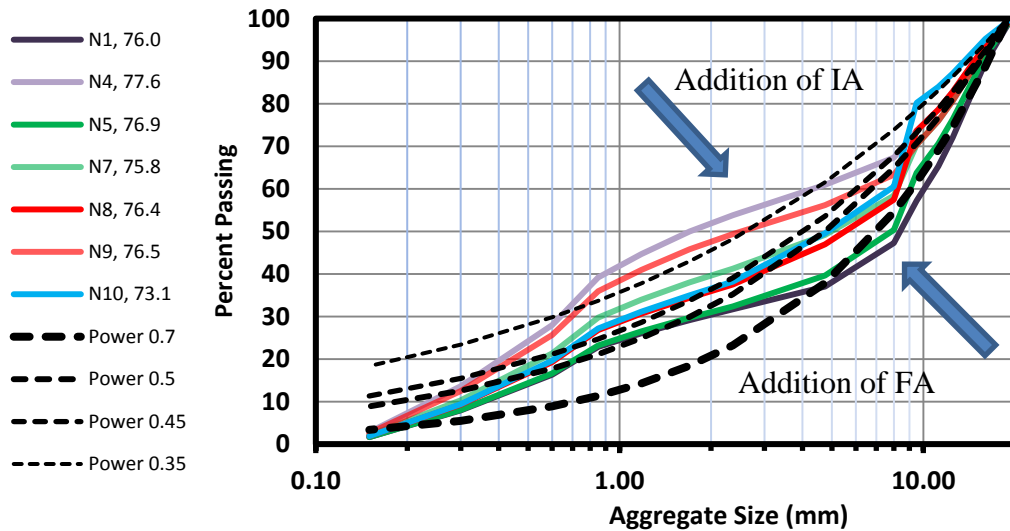


Figure 19. The PSD of experimental northern aggregate blends

4.1.6. Coarseness Chart

The coarseness factor (CF) and workability factor (WF) are defined in section 2.2.2. The chart correlates the individual and the cumulative passing of certain aggregate sets and cement content. The WF thus is controlled mainly by the fine aggregate content, and the CF is controlled by the ratio of fine aggregates to combined fine and intermediate aggregate size groups. The effect of intermediate and fine aggregates on these factors is

illustrated by *Figure 20* and *Figure 21*. Sharp increase in WF and gradual decrease in CF due to the replacement of coarse aggregates with sand at different levels of IA can be observed in *Figure 20* for a range of mixtures including sequence of S1-S5, S6-S10, S11-S13, and S14-S16. The reason for such trend is due to the increase in percent passing the 2.36 mm (#8) sieve, which is mostly controlled by the volume of fine aggregates.

The addition of intermediate aggregates leads to the improvement of CF in some blends, but is negligible for WF. The improvement of CF is more pronounced with higher fine aggregate content. As the cumulative percent retained on the 9.5 mm (3/8") sieve is decreasing at a higher rate with the addition of sand (for example, S4-S8-S13-S16 sequence), the cumulative percent retained on the 2.36 mm sieve (#8) does not change throughout the IA replacement for all contents of fine aggregates. The cumulative percent passing on the 9.5 mm (3/8") sieve increases faster and cumulative percent retained on the 9.5 mm sieve decreases faster when there is more fine aggregates in the mix. This effect is observed in mixes with similar sand content such as represented by sequences of S1 to S14, S2 to S15, and S4 to S16 observed on the row of the chart.

With up to 50% sand, all the mixtures were able to reach Zone II-5, which is desirable for low cement content mixtures such as those used for typical concrete pavement operations. However, from the workability standpoint, Zones II-2 and II-3 can be more desirable for slip-form concrete; those mixtures (e.g. S2) prone to low cement content and reduced paste volume can provide the robust performance required in the field. The replacement of coarse aggregates with intermediate fraction provides a horizontal shift of the mixtures to lower CF and higher WF enabling to pass the cautious workability 0 band

towards a more sandy subzone of Zone II. In such way, the chart can be used to estimate the performance of low cement concrete with different aggregate blends.

The use of 40% to 50% fine aggregates improves the particle to particle contacts in the mixtures and reduces the coarseness factor compared to mixes with 35% FA for southern aggregate mixtures (S1, S6, S11, and S14). These mixes that appear between the Subzone 1 and 5 of Zone II are considered ideal for slip form paving, but may further require higher quantities of fine aggregates. The mixtures in this zone such as S8 and N7 can be beneficial to low cement concrete pavements. The best blend however depending on the workability need of the mix.

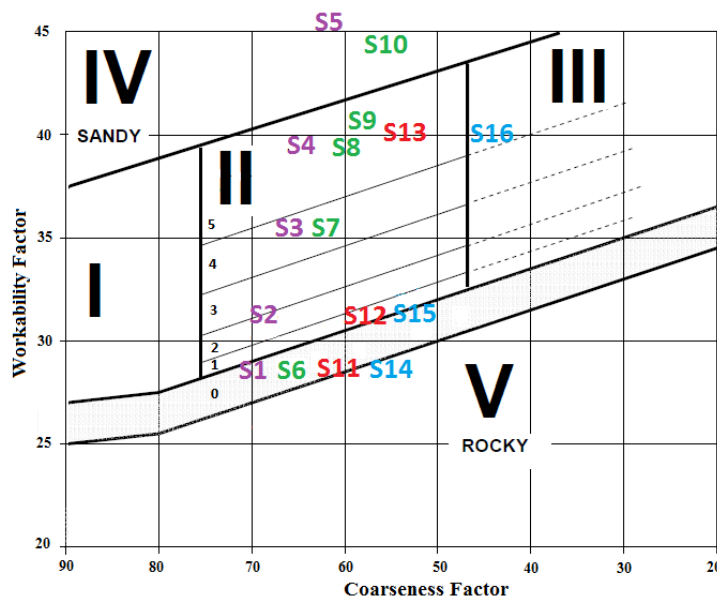


Figure 20. Coarseness chart of Southern aggregate mixtures [18, 105]

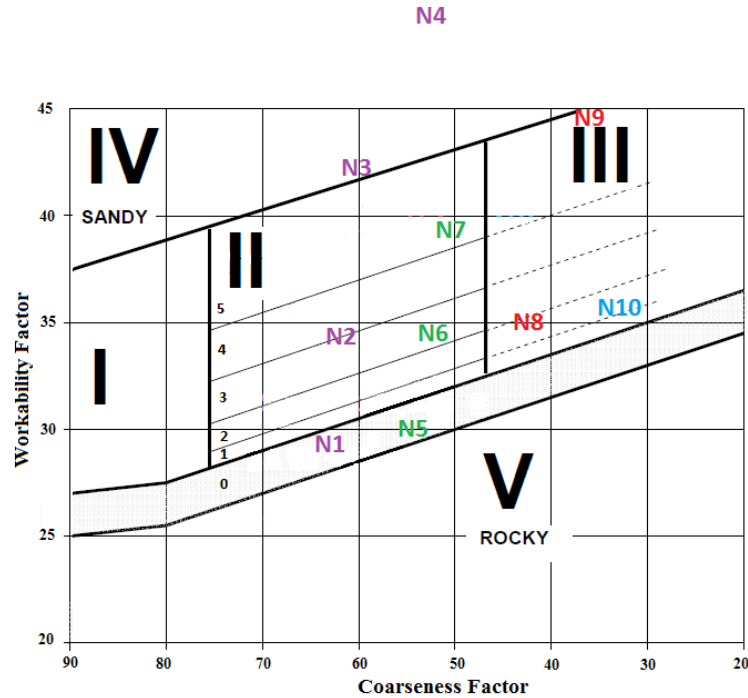


Figure 21. Coarseness chart of Northern aggregate mixtures [18, 105]

4.1.7. Evaluation of Concrete Mixtures

Table 17 and Table 18 demonstrate the results of experimental packing, the statistical deviation from corresponding power curve for the mixtures, concrete strength, and other performance characteristics for Southern and Northern aggregates. Table 17 and Table 18 are arranged by the IA content. The entrapped air content is less than 2% for almost all the mixtures, providing little interference with observed relationships. As demonstrated in Table 17 and Table 18, the mixtures with minimal square error at each level of IA result in the highest strength for both types of crushed southern aggregates and round northern aggregates. As it was demonstrated by the experimental packing mixtures, lower deviation from the power curve represents better packing degrees. This verifies that the high density mixtures are achievable with different power curves.

The correlation between the 7-day and 28-day compressive strength and aggregate packing degree is demonstrated by Figure 22 for southern aggregates. The highest correlation was found to be between the loose packing degree and 7-day compressive strength for southern aggregates. In addition, the correlation of 0.95 between the loose and compacted packing is demonstrated in this research for southern aggregates (Figure 15.b). The correlation between 7-day and 28-day compressive strength and aggregate packing degree doesn't provide any significant relationship. One reason for no correlation between northern aggregates may be that the experimented blends have already reached the highest packing degree achievable by concrete aggregates with the use of crushed intermediate aggregates combined with round coarse aggregates. Also the effect of various combinations in such a narrow range of blends between 30% to 60% of fine aggregates and 0% to 20% of intermediate aggregates may be difficult to observe.

The experimental results for southern aggregate demonstrate that a mixture with 50% of fine aggregates had a higher compressive strength than concrete with lower sand content (except for ternary mixes with 10% IA). At a relatively low cement content (279 kg/m³), higher volumes of fine aggregates are required for better packing as demonstrated by *Table 17*, and the requirement for an additional volume of fine materials to fill the voids in coarse aggregates is better addressed.

For Northern aggregate, the experimental results demonstrate that a mixture with 50% of fine aggregates had a higher compressive strength than concrete with lower and higher sand content (except for ternary mixes with 10% IA). At a relatively low cement content (279 kg/m³), 40% of fine aggregates are required for better packing of Northern aggregates as demonstrated by *Table 18*.

Figure 22 shows that southern aggregate mixtures with the highest strength are located in Zone II-5. For the level of cement content used in this research (279 kg/m^3), this seems to be a suitable area for southern aggregates; however, zones II-2 and II-3 are known to be excellent for concrete pavements with low cement content (in the range of 310 to 350 kg/m^3). The improvement in strength from S1 to S5 mixtures, and similarly, for other concrete mixtures with different contents of IA, is directly proportional to the improvement of coarseness and the workability factors as demonstrated by *Figure 23* and *Table 17*.

Figure 23 shows that northern aggregate mixtures with the highest strength are mostly located in Zone II. For the level of cement content similar to the one used for Southern aggregates (279 kg/m^3), this seems to be a slightly lower sand requirement for Northern aggregate.

Some binary Southern aggregate mixtures had a better packing versus mixtures with 20% and 30% of IA; however, ternary mixtures achieve higher compressive strength as presented in *Table 17*. The highest compressive strength was achieved in mixtures with 10% of IA matching the experimental packing results.

Some binary Northern aggregate mixtures had a better packing versus mixtures with 10%, 20%, and 30% of IA. However, some of the binary mixtures achieved higher compressive strength with 50% FA, the highest compressive strength with ternary mixtures achieved at 40% FA as presented in *Table 18* and matches the experimental packing results.

The density of fresh mixtures was decreased mainly due to the addition of sand for both types of aggregates. This means that the packing degree is affected by the positioning of the particles rather than the density of each fraction.

Mixtures with the sand content ranging between 45% to 50% for Southern and 40% to 50% for northern aggregates had higher workability than those outside these limits as observed for the binary and ternary mixtures with 0% and 10% IA content for southern aggregates. Mixtures with 45% and 50% FA in coarseness chart (S3-S4, S7-S8, S13-14, S15-16) demonstrates they are all located in the middle of the Zone II and the mixtures with 40% to 45% FA in coarseness chart (N2, N6-N7, N8) are all located in the middle of the Zone II and edge rocky side of Zone III. The use of higher sand volumes signifies higher WF for Southern aggregate and the use of lower sand volume signifies lower WF for Northern aggregates, but further research is required to explore the effect of WF on workability, including slump. Where all the southern aggregate mixtures with 50% FA stand at the same WF in the chart, the slump of mixture with 20% and 30% of IA was lower. The same trend was observed at 45% of FA (*Figure 22* and *Table 17*). For northern aggregates all the mixtures with 40% FA stand at the same WF of the coarseness chart (N2, N6, N8, N10), the workability is lower for ternary aggregates.

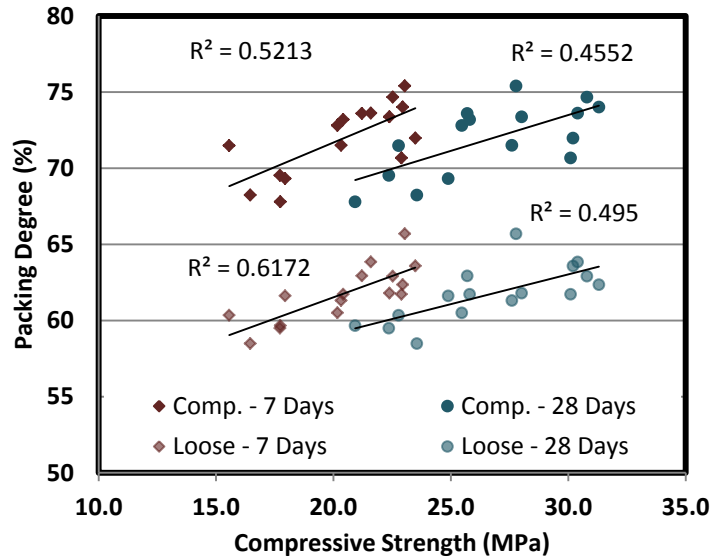


Figure 22. The correlation between the compressive strength and packing degree of Southern aggregates

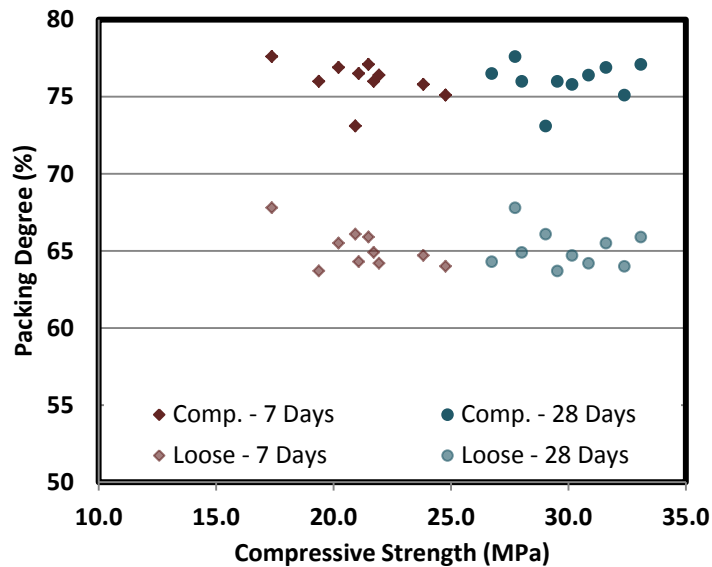


Figure 23. The correlation between the compressive strength and packing degree of Northern aggregates

4.1.8. Modeling vs. Experimental Packing

The aggregate packing degrees obtained from Vebe packing experiment were compared to some of the theoretical discrete models to ensure the obtained packing degrees were reasonable compared to commonly known models. The practicality of this

comparison is to verify the experimental packing results and associated best blend in terms of maximum packing with the models and also use the models as a tool to investigate the blends. Also, such comparison can evaluate the separate effects of each of the fine, coarse and intermediate aggregate on packing degree in the models versus the experiments. Aim Model [83] was used as a classical model able to describe the packing degree of binary blends and modified Toufar model [25] was used to describe the packing degree for binary and ternary blends. Both models are based on Furnas model and were described in section 2.2.1.1.1 and 2.2.1.1.2. Aim model takes into account the wall effect to calculate the packing degree and the Toufar model take into account the diameter ratio of the particles, probability of the number of interstices between the coarse particles and also uses the characteristic diameter, Eigenpacking degree, and grain density of each individual class of particles to calculate the packing degree. These properties are aggregate specific and are measured for each class and types of aggregates. The properties of aggregates used for Toufar model are summarized in Table 19. and

Table 20.

Grain density was obtained from specific gravity of the aggregates. The compacted packing degree used in the model was taken from Vebe packing experiment for each type of the aggregates. The characteristic diameter was determined as the position of the size distribution curve at the cumulative probability at which the diameter is less than 0.368 for each class of aggregates as stated in section 2.2.1.1.2.

Table 19. Southern aggregate properties used for Toufar model

Southern Aggregate	Grain density, kg/m ³	Eigenpacking degree		Characteristic, diameter, mm
		compact	loose	
C1	2730	0.57	0.49	14.1
I1	2684	0.58	0.50	10.0
F1	2566	0.74	0.65	0.87

Table 20. Northern aggregate properties used for Toufar model

Northern Aggregate	Grain density, kg/m ³	Eigenpacking degree		Characteristic, diameter, mm
		compact	loose	
C2	2706	0.6231	0.5498	13.3
I2	2659	0.6636	0.5777	8.4
F2	2563	0.7068	0.6385	0.83

Figure 24., Figure 25., and Figure 26. demonstrate the binary representation packing degree of the southern aggregates and Figure 27. to Figure 29. demonstrate the binary representation of northern aggregates based on Aim and Toufar models. Figure 30 demonstrates the ternary packing degree based on Toufar model for both southern and northern aggregates.

As demonstrated for C1-F1, I1-F1, C2-F2, and I2-F2 binary blends and illustrated in Figure 24. Figure 25., and Figure 26. the maximum packing based on the Aim model occurs at slightly higher fine material content than the maximum packing based on the Toufar model.

The maximum experimental packing, however occurs, at coarser fractions of fine class size content compared to both models for C1-F1, I1-F1, C2-F2, and I2-F2 binary blends.

In comparison to experimental packing the Aim model overestimates the packing degree versus the experimental data by about 10% at the vicinity of maximum packing for C1-F1, I1-F1, C2-F2, and I2-F2 binary blends. The Toufar model, on the other hand, closely follows the experimental trend observed for both southern and northern aggregates. The maximum packing prediction as illustrated by *Figure 24* and *Figure 25* from the Toufar model is less than 5% different from the experimental results for southern aggregate blends C1-F1 and I1-F1. The Toufar model prediction of maximum packing as shown in *Figure 28* and *Figure 29* is even less than 3% different from the experimental packing results for northern aggregate blends C2-F2 and I2-F2.

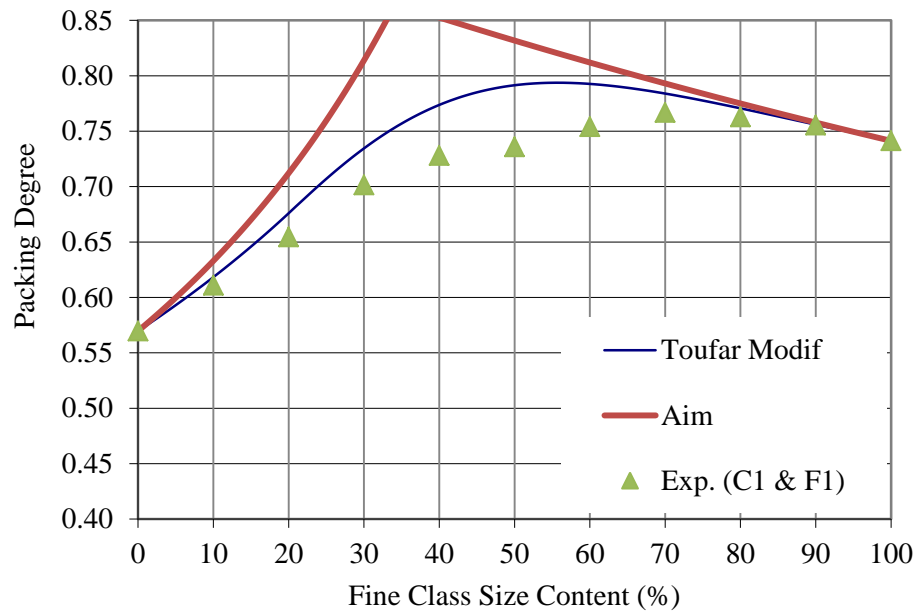


Figure 24. Toufar and Aim model versus packing degree of binary blends (C1 and F1)

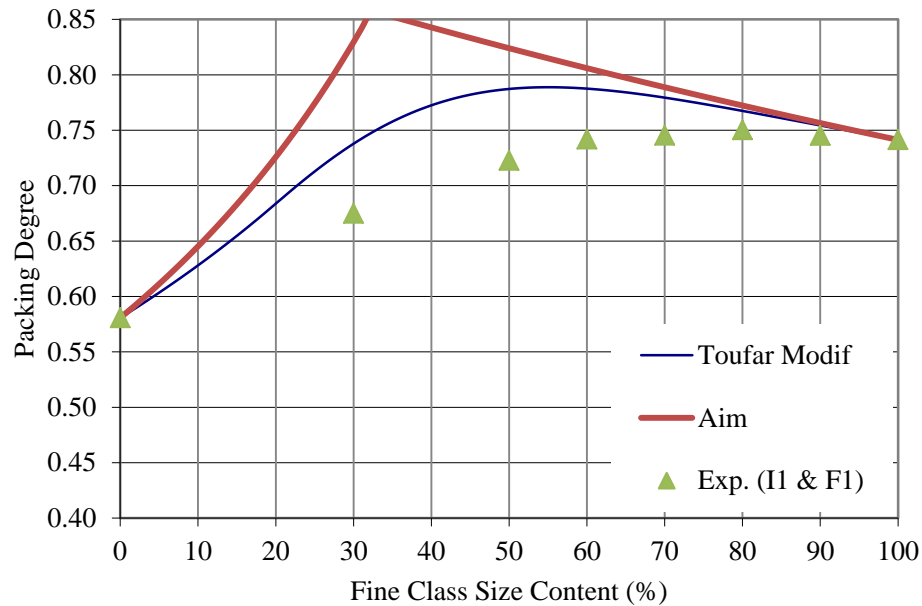


Figure 25. Toufar and Aim model versus packing degree of binary blends (I1 and F1)

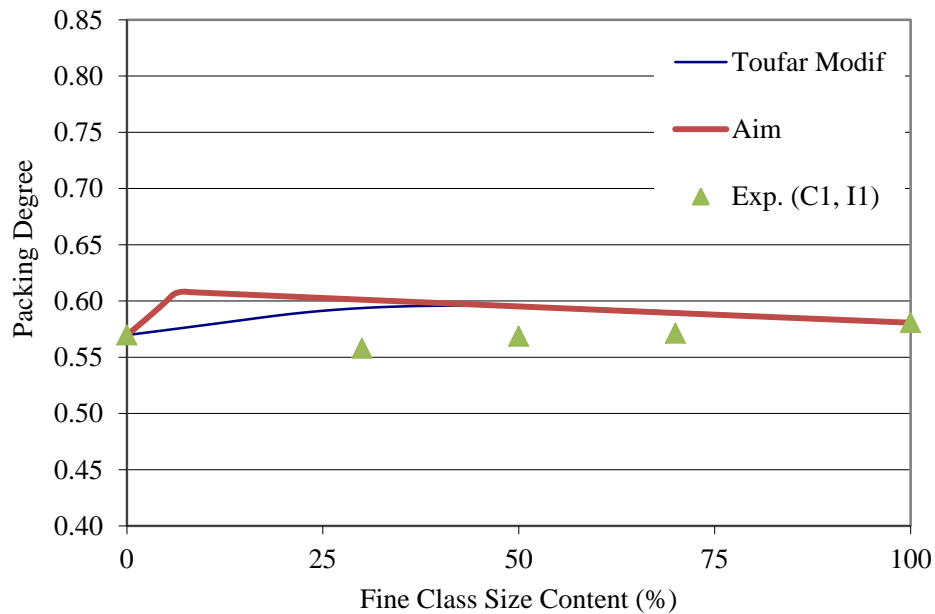


Figure 26. Toufar and Aim model versus packing degree of binary blends (C1 and I1)

The packing degree for the binary blend of fine and coarse southern aggregates tends to increase with increase in fine content up to 70% where the Toufar model shows the

maximum packing degree is achieved at 55% fine content as illustrated in *Figure 24*. Similar trend can be observed for the binary blend of intermediate and fine southern aggregates as illustrated in *Figure 25*.

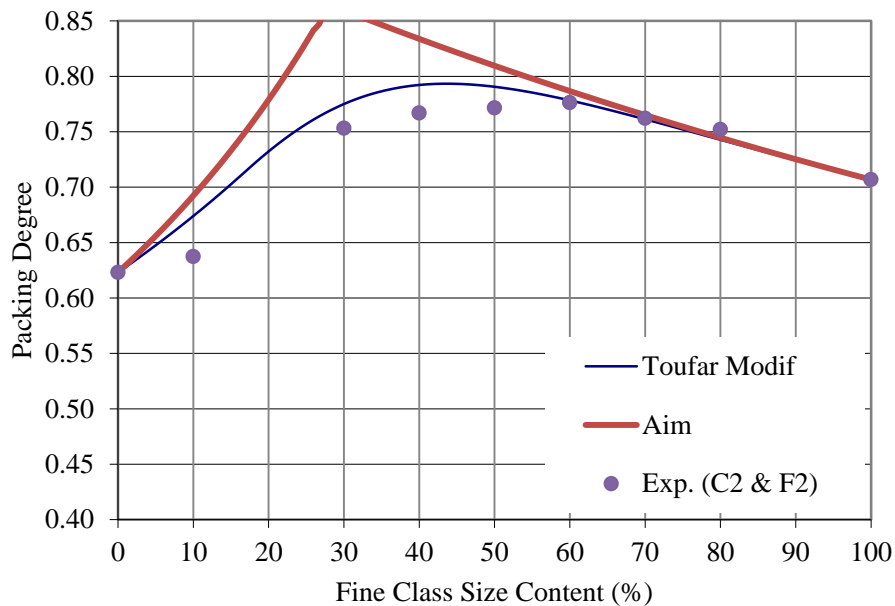


Figure 27. Toufar and Aim model versus packing degree of binary blends (C2 and F2)

Figure 27 illustrates that the packing degree for binary blends of fine and coarse northern aggregates tends to increase with the increase in fine material content up to 60% where the Toufar models predicts the maximum packing degree at 45%. Similar trend was observed for binary blends of intermediate and fine northern aggregate as illustrated in *Figure 28*.

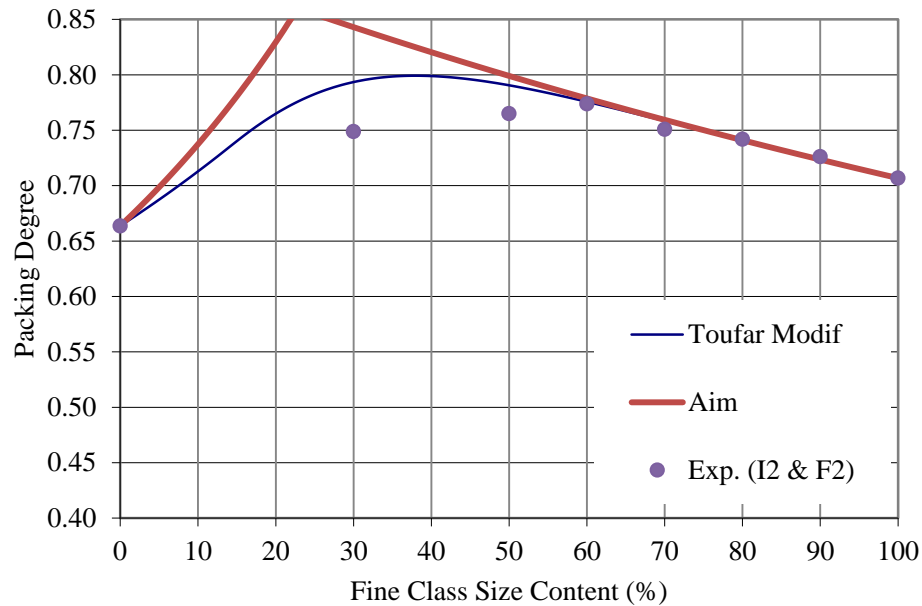


Figure 28. Toufar and Aim model versus packing degree of binary blends (I2 and F2)

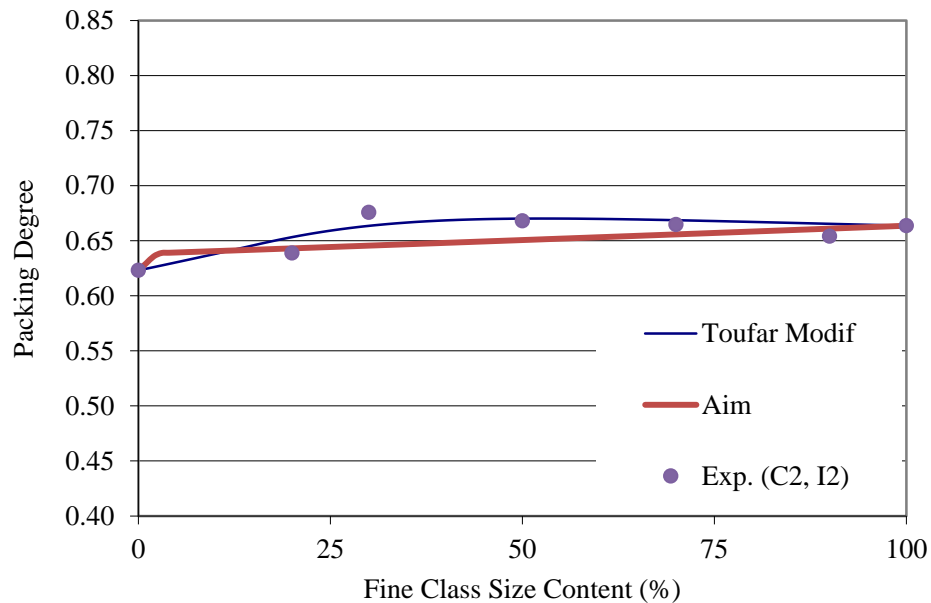


Figure 29. Toufar and Aim model versus packing degree of binary blends (C2 and I2)

Figure 30 shows the packing degree for ternary blends of fine, coarse and intermediate aggregates for southern and northern aggregates using Toufar model.

Comparing *Figure 30* with *Figure 15* and *Figure 16* demonstrates the difference between the location of maximum packing and the packing degree for both types of aggregates. The maximum experimental packing degree of about 75% to 76% occurs at 55% to 60% fine aggregates and 0% to 10% intermediate aggregates for southern blends which was close to the maximum packing degree of 79% at 55% fine aggregates and 20% intermediate as predicted by Toufar model.

For northern aggregate blends the maximum packing degree of about 78% for blends with a broad range of fine aggregates from 60% to 40% fine aggregates and 0% to 20% intermediate aggregates which is close to Toufar maximum packing degree of 81% at 40% fine aggregates and 20% intermediate aggregate. As a result, using Toufar model could lead to the same optimized blend in terms of packing degree for both types of aggregates.

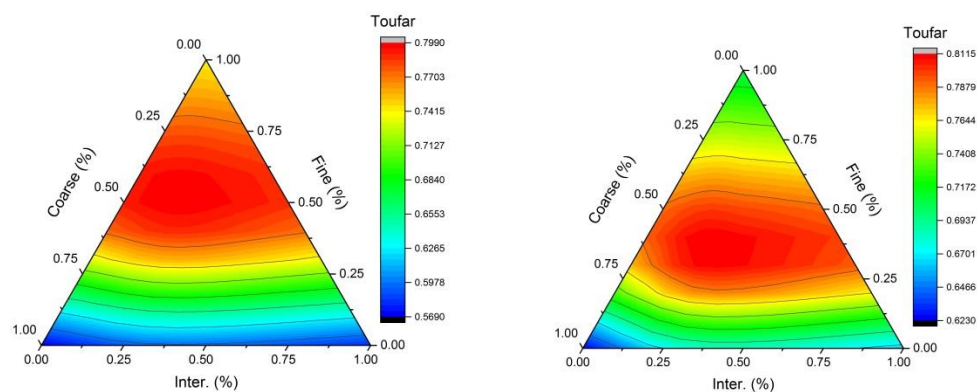


Figure 30. a) Southern 3D Toufar b) Northern 3D Toufar

For southern blends, the results of Toufar model for southern aggregates provided the best blend to be about 50% fine and 30% intermediate aggregates which the experimental

packing test suggested using 55% fine aggregates with 0% to 20% intermediate aggregates (*Table 17*). The mechanical performance, on the other hand, aims the best blend to be 52.5% fine with 10% intermediate aggregates. The workability was similar for mixtures with 50% to 55% fine aggregates and 10% intermediate aggregate; however, the mixtures with intermediate aggregates had more cohesiveness compared to binary mixtures which had some segregation potential. As a result, and for other practical reasons, the best blends used for the preliminary concrete mixtures were selected using 50% of fine aggregates, 10% of intermediate aggregates, and 40% of coarse aggregates.

For northern aggregates, the results of Toufar model suggested the best blend to be about 40% fine and 20% intermediate aggregates where the experimental packing proves the use of 40% to 60% of fine and 0% to 10% of intermediate aggregates blends (*Table 17*). On the other hand, the mechanical performance was the best for the blend with 40% fine and 10% intermediate aggregates. The workability was similar for mixtures with 35% to 40% fine aggregates and 10% intermediate; however, the mixtures with intermediate aggregates had more cohesiveness compared to binary mixtures. As a result, and for practical reasons, the best blends selected for preliminary concrete testing with southern aggregates were the proportions with 50% of fine aggregates, 10% of intermediate aggregates, and 40% of coarse aggregates.

4.2. MIXTURE OPTIMIZATION

Concrete mixtures were optimized based on the results of aggregate optimization using the multi-scale procedure. The concrete mixtures, therefore, use the best aggregate combinations was selected by using PSD, packing degree, coarseness, and performance in concrete criteria was optimized in terms of strength and workability. The durability of the mixtures was also evaluated. The benefit of aggregate optimization is to gain an “additional” strength and potentially reduce the required cement content. The following concrete mixture phases therefore, were optimized using constant aggregate combinations of 50% fine, 10% intermediate, and 40% coarse aggregate for the mixtures with southern aggregate as discussed previous section. This section does not report on the concrete mixtures based on northern aggregates. This section discusses the preliminary optimization of admixtures, and the results of final optimized mixtures.

4.2.1. Preliminary Admixture Optimization

The purpose of preliminary batches were to identify the dosage of AE admixture in concrete mixtures to achieve suitable air content, and assist in achieving required slump. All preliminary mixtures were tested for 7 and 28 days compressive strength to ensure that the required strength is achieved. Another study was conducted to investigate the thermal effects of plasticizing admixtures on hydration of portland cement systems. The results of that study were used for testing the optimal range of WRA/HRWRs used in preliminary batches. For this research the effect of plasticizer, superplasticizers, AE admixtures in achieving the required levels of workability was investigated. To optimize the dosage, the lowest desirable W/CM ratio that meets the specification requirements of

50-100 mm (2-4 in) slump, 6 to 7 \pm 1.5% air content, and early compressive strength of 20.6 MPa (3000 psi) were targeted. The cement content was varied at 2 levels of 279 kg/m³ [470 lb/yd³] and 249.2 kg/m³ [420 lb/yd³]. However, this section of the study does not report on preliminary mixtures with 249 kg/m³.

The design concept of concrete mixtures includes the first step of achieving best aggregate blends. The cement content was determined for a 12% reduction from current WisDOT specifications. The W/CM ratio was then defined based on preliminary study (as a starting point). The ratio was adjusted in 0.05 increments for most of the mixtures. The volume of the cement paste was calculated from the volume of the cementitious materials and water. The volume of the cement paste, admixtures, and the tentative air content of 6% was then subtracted from the total volume of the mix. The remaining aggregate volume is then split between the coarse, intermediate, and fine aggregates based on optimal proportions.

Four sets of experiments were conducted for concrete mixtures with constant aggregate ratio including plain concrete mixtures without any SCM, with class F fly ash, class C fly ash, and slag as reflected in *Table 21*, *Table 23*, *Table 25*, and *Table 27* respectively.

The fresh and hardened properties of preliminary mixtures including reference mixtures without SCM, with class F fly ash, class C fly ash, and slag are presented in *Table 22*, *Table 24*, *Table 26*, and *Table 28*, accordingly. All the mixtures were compared with reference mixture CM 64 (L-S-M) without mid-range WRA and without any air-entraining admixture in *Table 21* to *Table 28*. For each set of mixtures three different

WRA/HWRAs were used (*Table 21 to Table 28*). These three admixtures used (as described in *Table 9*) were mid-range, SNF, and PCE type admixtures. The mixtures were used to achieve the required air and slump parameters without increase of W/CM ratio with the goal of obtaining optimal mechanical performance. Commonly, higher compressive strength can be achieved at lower W/CM ratio but this may result in impractical workability levels in some cases.

For reference mixtures without SCM and with mid-range water reducing admixture (plasticizers), the mixture CM69 obtained the required performance in terms of air content (8.2%) and slump (45 mm) *Table 22 and Table 23*. The compressive strength is lower than the reference mixture CM64 without AE because an additional 4.2% less air content. Comparing the workability of mixture CM69 with mid-range WR admixture proves that this admixture can assist in reduction of W/C ratio and maintain the slump at almost the same levels when used in plain mixtures. For mixtures with PCE HRWR admixtures, the mixture CM79 achieved the optimal performance with 4.4% air content and 44 mm slump. The compressive strength was similar compared to the reference concrete (CM64) especially at early ages. Comparing slump of the mixture CM79 with reference demonstrates that even at 10% reduction of W/CM ratio the slump is almost equal to the reference, indicating the superior qualities of PCE admixtures in terms of workability and W/C ratio reduction. For mixtures with SNF admixtures, the mixture CM101 achieved the optimal performance with 5.8% air content and 65 mm slump. Comparing slump of the mixture CM101 with reference demonstrates that even at 5% lower W/C ratio the slump is equal to the reference, indicating the desirable qualities of SNF admixtures in terms of workability and W/CM ratio reduction. At 28 days, the

compressive strength of CM101 was similar to reference but lower the reference at early ages. Compared to reference mixture CM64, the mixture with PCE (CM79) has the closest strength at early ages and the mixture with SNF (CM101) has the closest strength at 28 days. The W/C ratio achieved with PCE admixtures was about 5% lower than the W/C ratio achieved by mid-range and SNF admixtures for plain no SCM mixtures *Table 22*.

Table 22 and *Table 23* represent the mix design and the test results for mixtures with class F fly ash used at 30% portland cement replacement levels. For mixtures with mid-range admixture, the mixture CM72 obtained the required performance in terms of air content of 4.5%. The 10 mm slump is lower than required and therefore must be adjusted by increasing the W/CM in the design of the final mixture. The compressive strength was reduced versus the reference mixture CM64 (without AE), mainly because of the effect of class F fly ash on hydration at replacement level of 30% of cement. For mixtures with PCE admixtures, the mixture CM108 achieved the optimal performance with 5.8% air content and 130 mm slump at W/C ratio reduced by 0.05 versus other two mixtures (CM72 and CM71) and even by 0.10 when compared to the reference (CM64). Comparing the slump of the mixture CM108 with reference it can be observed that even at a reduced (0.10) W/CM ratio, the slump is double than that of the reference, indicating the desirable benefits of PCE admixtures in terms of workability and W/C ratio reduction. The increase in slump from 40 mm (CM79 for plain mixtures with no SCM) to 130 mm (CM108 for mixture containing class F fly ash) can be explained by 1.4% extra air content and addition of class F fly ash. The compressive strength was lower compared to the reference at all tested ages mainly due to the delayed pozzolanic reaction of class F

fly ash. The long-term tests were conducted for final mixtures as discussed in next sections. For mixtures with SNF admixtures, the mixture CM71 achieved the optimal performance with 6.5% air content and 90 mm slump. The compressive strength of CM71 was lower than that of the reference. Compared to reference mixture CM64, the mixture with PCE (CM108) had very close strength with the reference at early and later ages. This proves that the use of class F fly ash requires the application of PCE (HRWRAs) and adjustment of air content to reduce the W/CM.

Table 22 and *Table 23* represent the mix design and results for mixtures with class C fly ash at 30% portland cement replacement level. These mixtures demonstrated superior performance. For compositions with **mid-range** admixture, the mixture CM84 obtained the required performance in terms of air content of 7.5% and 50 mm slump. The compressive strength is very similar to the reference mixture CM64 at 7 days and exceeded that of the reference at 28 days (even at 3.5% higher air content). The beneficial properties of class C fly ash enables to assist in workability. For mixtures with PCE admixtures, the mixture CM103 achieved the optimal performance at 7% air content and 95 mm slump with W/CM ratio reduced by 0.05 versus optimal mixtures (CM84 and CM85) and even by 0.10 versus the reference (CM64). The increase in slump from 40 mm to 95 mm compared to plain mixture with PCE (CM79) can be explained by an additional 2.6% extra air content and by the effects of class C fly ash. Also, higher slump compared to the reference at reduced W/CM ratio, indicates the synergic effect of PCE admixtures, and class C fly ash and the perfect compatibility of between two additives. In spite of higher air content, the compressive strength of this concrete was very high compared to the reference at both ages due to extreme reduction of W/CM ratio. For class

C fly ash mixtures with SNF admixtures, CM85 achieved the optimal performance with 7.5% air content and 70 mm slump. The compressive strength was similar to the reference and the workability was higher and achieved at reduced W/CM ratio. Compared to the reference mixture CM64, the PCE based concrete (CM84) has achieved 20% higher compressive strength at all ages. This proves that the use of PCE admixtures with class C fly ash can achieve superior performance in terms of workability improvement and strength gain.

Table 22 and *Table 23* represent the mix design and the results for mixtures with slag replaced with 50% portland cement. These mixtures had superior performance. For mixtures with mid-range admixture, the mixture CM86 obtained the required fresh properties in terms of air content of 6% and 59 mm slump even at higher air content. The compressive strength of CM86 was slightly higher when compared to the reference mixture CM64 even at higher air content. Similar chemical composition and compatibility of the slag and portland cements had a great contribution to mechanical performance. The PCE based mixtures (CM89) achieved the optimal performance with 3.5% air content and 50 mm slump at the W/CM ratio reduced by 0.05 versus other optimal mixtures (CM86 and CM77) and 0.10 as compared to the reference. Due to similarity between portland cement and slag in terms of superplasticizer absorption the slump values remain close to the reference mixtures. The slag is reactivated when used in alkali environment which is provided by portland cement. As a result, this mixture at 28 days had even higher strength compared to the plain mixtures with PCE (CM79). Also, similar slump compared to the reference at reduced W/CM ratio indicates the beneficial effect of PCE in slag mixtures improves workability. The compressive strength of slag

concrete was slightly reduced compared to the reference at both ages due to relatively high replacement level of 50%. For concrete mixtures with SNF, the mixture CM77 achieved the optimal performance with 6% air content and 68 mm slump. For this type of admixtures the compressive strength was similar to the reference at 7 days and was higher at the age of 28 days. The workability was very similar to reference, but achieved lower W/C ratio (reduced by 0.10). Compared to the reference mixture CM64, the slag mixture had similar performance as the reference mixture, but at higher air contents required for the freeze-thaw resistance.

It was found from the preliminary study that density, air content, and compressive strength has a strong relationship and the mixtures with various air contents (including the reference) can be represented by the fresh density-air content graph as illustrated in

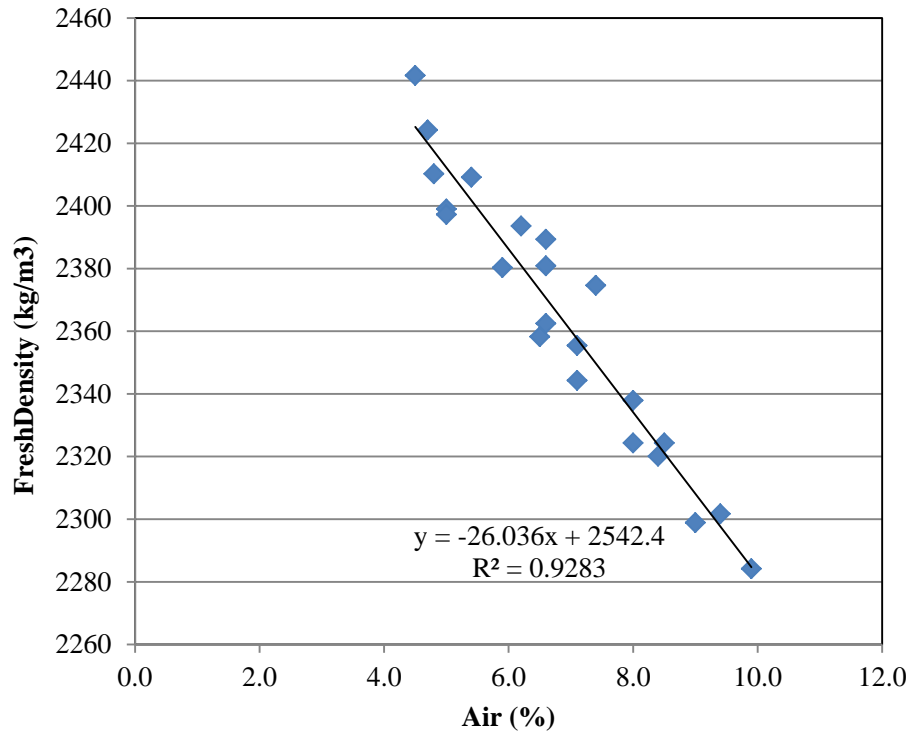


Figure 31. To meet the WisDOT specifications some of the optimized mixtures based on preliminary study required further minor adjustments of the dosage of AE admixture before use for final large volume batches, so such relationship was very useful for air content of fresh concrete mixtures and fine tuning the AE admixture.

Table 21. Mix design for preliminary mixtures without SCMs

Labels	Chem. Admix. (%)				Cement Content	SCM	Agg. (SSD) (Kg/ m ³)			Total Agg.	SP	AE	Total W	W/CM	YIELD
	PCE	SNF	Mid-Range	AE	kg/m ³	kg/m ³	CA	IA	FA	kg/m ³	kg/m ³	kg/m ³	kg/m ³		
L-S-M CM64			0.15	0.00	278.9	0.0	801	198	955	1954	1.038	0.000	132.8	0.48	0.97
L-S-M CM81			0.20	0.01	278.9	0.0	749	185	893	1828	1.384	0.227	121.5	0.44	1.02
L-S-M CM65			0.15	0.008	278.9	0.0	816	202	973	1991	1.038	0.181	118.3	0.42	1.01
L-S-M CM57			0.20	0.015	278.9	0.0	816	202	972	1990	1.384	0.340	118.7	0.43	1.07
L-S-M CM69			0.15	0.01	278.9	0.0	816	202	973	1991	1.038	0.227	118.4	0.42	1.02
L-S-P CM66	0.15			0.01	278.9	0.0	816	202	973	1991	1.230	0.227	118.6	0.43	1.00
L-S-P CM100	0.15			0.02	278.9	0.0	765	189	912	1866	1.230	0.453	107.1	0.38	0.96
L-S-P CM96	0.20			0.02	278.9	0.0	765	189	911	1865	1.641	0.453	107.4	0.38	0.93
L-S-P CM79	0.15			0.015	278.9	0.0	765	189	912	1866	1.230	0.340	107.0	0.38	0.92
L-S-N CM68		0.40		0.02	278.9	0.0	814	201	970	1985	2.768	0.453	119.7	0.43	1.00
L-S-N CM80		0.50		0.02	278.9	0.0	746	184	890	1821	3.460	0.453	123.1	0.44	0.98
L-S-N CM83		0.40		0.015	278.9	0.0	763	189	909	1861	2.768	0.340	107.9	0.39	0.93
L-S-N CM91		0.50		0.015	278.9	0.0	762	188	908	1859	3.460	0.340	108.4	0.39	0.94
L-S-N CM97		0.60		0.015	278.9	0.0	761	188	907	1856	4.152	0.340	108.8	0.39	0.93
L-S-N CM101		0.40		0.015	278.9	0.0	747	185	891	1823	2.768	0.340	122.5	0.44	0.92

Table 22. Fresh and hardened properties of preliminary mixtures without SCMs

Labels	Slump, mm	Air	Fresh Density	Temp.	Vol. of Agg.	Aggregate Proportions			Compressive Strength, MPa		Labels	Slump, in	Compressive Strength, psi	
	*	%	kg/m ³	°F	kg/m ³	C1, %	I1, %	F1, %	7 days	28 days			C.S. 7	C.S. 28
L-S-M CM64	63	4.0	2440	65	0.724	40	10	50	29.5	38.4	CM64	2.5	4273	5570
L-S-M CM81	95	15.0	2180	66	0.678	40	10	50	17.6	20.4	CM81	3.7	2555	2966
L-S-M CM65	26	7.0	2350	66	0.738	40	10	50	27.5	34.4	CM65	1.0	3988	4993
L-S-M CM57	68	12.0	2231	69	0.737	40	10	50	20.3	25.1	CM57	2.7	2940	3640
L-S-M CM69	45	8.2	2338	66	0.738	40	10	50	25.1	31.4	CM69	1.8	3635	4551
L-S-P CM66	150	5.4	2375	68	0.738	40	10	50	27.0	32.0	CM66	5.9	3919	4638
L-S-P CM100	95	6.5	2341	68	0.692	40	10	50	32.8	37.5	CM100	3.7	4755	5434
L-S-P CM96	30	5.0	2415	69	0.691	40	10	50	20.9	25.4	CM96	1.2	3033	3685
L-S-P CM79	40	4.4	2432	70	0.692	40	10	50	29.1	34.7	CM79	1.6	4224	5032
L-S-N CM68	29	6.2	2392	65	0.736	40	10	50	28.8	35.3	CM68	1.1	4173	5127
L-S-N CM80	100	10.0	2271	67	0.675	40	10	50	21.2	26.4	CM80	3.9	3073	3825
L-S-N CM83	10	4.8	2404	70	0.690	40	10	50	32.5	40.0	CM83	0.4	4719	5806
L-S-N CM91	11	5.5	2375	72	0.689	40	10	50	31.9	41.3	CM91	0.4	4633	5996
L-S-N CM97	25	4.7	2415	68	0.688	40	10	50	31.3	37.0	CM97	1.0	4537	5363
L-S-N CM101	65	5.8	2406	67	0.676	40	10	10	21.7	36.1	CM101	2.6	3144	5237

* immediately after mixing

Table 23. Mix design for preliminary mixtures with class F fly ash

Labels	Chem. Admix. Dos.(%)				Cement Content ($\frac{kg}{m^3}$)	AF ($\frac{kg}{m^3}$)	Agg. (SSD) (Kg/m3)			Total Agg. ($\frac{kg}{m^3}$)	SP ($\frac{kg}{m^3}$)	AE ($\frac{kg}{m^3}$)	Total W ($\frac{kg}{m^3}$)	W/CM	YIELD
	PCE	SNF	Mid-Range	AE			CA	IA	FA						
L-S-M CM64			0.15	0	278.9	0.0	801	198	955	1954	1.038	0.000	132.8	0.48	0.97
L-S-M-F CM88			0.15	0.02	195.2	83.7	742	183	884	1809	1.038	0.453	121.9	0.44	0.96
L-S-M-F CM72			0.15	0.01	195.2	83.7	808	200	963	1971	1.038	0.227	118.7	0.43	0.99
L-S-P-F CM70	0.15			0.015	195.2	83.7	808	200	963	1971	1.230	0.340	119.0	0.43	1.03
L-S-P-F CM87	0.15			0.015	195.2	83.7	757	187	902	1847	1.230	0.340	107.3	0.38	0.93
L-S-P-F CM92	0.15			0.015	195.2	83.7	772	191	921	1884	1.230	0.340	92.7	0.33	1.04
L-S-P-F CM98	0.20			0.015	195.2	83.7	772	191	920	1883	1.641	0.340	93.0	0.33	0.94
L-S-P-F CM102	0.10			0.02	195.2	83.7	757	187	903	1847	0.820	0.453	107.1	0.38	0.94
L-S-P-F CM107	0.10			0.015	195.2	83.7	758	187	903	1848	0.820	0.340	107.0	0.38	0.93
L-S-P-F CM108	0.15			0.015	195.2	83.7	757	187	902	1847	1.230	0.340	107.3	0.38	0.96
L-S-N-F CM71		0.4		0.025	195.2	83.7	806	199	960	1965	2.768	0.567	120.2	0.43	1.00

Table 24. Fresh and hardened properties of preliminary mixtures with class F fly ash

Labels	Slump, mm	Air	Fresh Density	Temp.	Vol. of Agg.	Aggregate Proportions			Compressive Strength, MPa		Labels	Slump, in	Compressive Strength, psi		
	*	%	kg/m ³	°F	kg/m ³	C1, %	I1, %	F1, %	7 days	28 days			C.S. 7	C.S. 28	
L-S-M	CM64	63	4.0	2440	65	0.724	40	10	50	29.5	38.4	CM64	2.5	4273	5570
L-S-M-F	CM88	88	9.5	2293	73	0.670	40	10	50	12.9	18.3	CM88	3.5	1869	2661
L-S-M-F	CM72	10	4.5	2395	66	0.731	40	10	50	18.3	25.9	CM72	0.4	2651	3754
L-S-P-F	CM70	175	8.0	2299	68	0.730	40	10	50	14.6	20.4	CM70	6.9	2113	2958
L-S-P-F	CM87	164	5.0	2389	67	0.684	40	10	50	21.7	20.7	CM87	6.5	3153	2998
L-S-P-F	CM92	0	7.2	2169	69	0.698	40	10	50	14.9	17.9	CM92	0.0	2159	2591
L-S-P-F	CM98	12	1.5	2401	69	0.698	40	10	50	11.6	14.8	CM98	0.5	1677	2142
L-S-P-F	CM102	15	5.6	2378	69	0.685	40	10	50	19.1	26.4	CM102	0.6	2766	3832
L-S-P-F	CM107	10	4.5	2398	71	0.685	40	10	50	20.7	28.7	CM107	0.4	3002	4159
L-S-P-F	CM108	130	5.8	2313	69	0.684	40	10	50	20.0	27.1	CM108	5.1	2894	3927
L-S-N-F	CM71	90	6.5	2367	65	0.728	40	10	50	16.6	24.0	CM71	3.5	2406	3474

* immediately after mixing

Table 25. Mix design for preliminary mixtures with class C fly ash

Labels	Chem. Admix. Dos.(%)				Cement Content ($\frac{kg}{m^3}$)	AC ($\frac{kg}{m^3}$)	Agg. (SSD) (Kg/m3)			Total Agg. ($\frac{kg}{m^3}$)	SP ($\frac{kg}{m^3}$)	AE ($\frac{kg}{m^3}$)	Total W ($\frac{kg}{m^3}$)	W/CM	YIELD
	PCE	SNF	Mid-Range	AE			CA	IA	FA						
L-S-M CM64			0.15	0.00	278.9	0.0	801	198	955	1954	1.038	0.000	132.8	0.48	0.97
L-S-M-C CM93			0.15	0.005	195.2	83.7	762	188	908	1858	1.038	0.113	106.7	0.38	1.06
L-S-M-C CM84			0.15	0.005	195.2	83.7	762	188	908	1858	1.038	0.113	106.7	0.38	0.96
L-S-M-C CM99			0.20	0.005	195.2	83.7	761	188	907	1857	1.384	0.113	107.0	0.38	0.96
L-S-M-C CM75			0.15	0.01	195.2	83.7	812	201	969	1982	1.038	0.227	118.5	0.43	1.04
L-S-P-C CM73	0.15			0.015	195.2	83.7	812	201	968	1981	1.230	0.340	118.8	0.43	1.06
L-S-P-C CM82	0.15			0.015	195.2	83.7	761	188	908	1857	1.230	0.340	107.1	0.38	0.97
L-S-P-C CM10 ₃	0.15			0.015	195.2	83.7	777	192	926	1895	1.230	0.340	92.5	0.33	0.95
L-S-N-C CM74		0.4		0.025	195.2	83.7	810	200	965	1975	2.768	0.567	120.0	0.43	1.03
L-S-N-C CM85		0.4		0.015	195.2	83.7	759	188	905	1852	2.768	0.340	108.1	0.39	0.95

Table 26. Fresh and hardened properties of preliminary mixtures with class C fly ash

Labels	Slump, mm	Air	Fresh Density	Temp.	Vol. of Agg.	Aggregate Proportions			Compressive Strength, MPa		Labels	Slump, in	Compressive Strength, psi	
	*	%	kg/m ³	°F	kg/m ³	C1, %	I1, %	F1, %	7 days	28 days			C.S. 7	C.S. 28
L-S-M CM64	63	4.0	2440	65	0.724	40	10	50	29.5	38.4	CM64	2.5	4273	5570
L-S-M-C CM93	0	5.4	2107	67	0.689	40	10	50	11.1	13.3	CM93	0.0	1610	1933
L-S-M-C CM84	50	7.5	2338	68	0.689	40	10	50	28.8	38.8	CM84	2.0	4182	5632
L-S-M-C CM99	50	7.0	2338	70	0.688	40	10	50	27.8	37.3	CM99	2.0	4027	5406
L-S-M-C CM75	110	12.0	2293	70	0.735	40	10	50	18.2	26.4	CM75	4.3	2642	3823
L-S-P-C CM73	180	12.0	2248	67	0.734	40	10	50	19.8	26.7	CM73	7.1	2868	3868
L-S-P-C CM82	215	9.0	2313	68	0.688	40	10	50	27.2	36.4	CM82	8.5	3941	5282
L-S-P-C CM103	95	7.0	2387	69	0.702	40	10	50	35.5	46.7	CM103	3.7	5154	6772
L-S-N-C CM74	120	12.0	2293	68	0.732	40	10	50	17.8	24.4	CM74	4.7	2580	3535
L-S-N-C CM85	70	7.5	2350	69	0.686	40	10	50	28.3	38.2	CM85	2.8	4099	5535

* immediately after mixing

Table 27. Mix design for preliminary mixtures with slag

Labels		Chem. Admix. Dos.(%)				Cement Content ($\frac{kg}{m^3}$)	Slag ($\frac{kg}{m^3}$)	Agg. (SSD) (Kg/m ³)			Total Agg. ($\frac{kg}{m^3}$)	SP ($\frac{kg}{m^3}$)	AE ($\frac{kg}{m^3}$)	Total W ($\frac{kg}{m^3}$)	W/C	YIELD
		PCE	SNF	Mid-Range	AE			CA	IA	FA						
L-S-M	CM64			0.15	0.00	278.9	0.0	801	198	955	1954	1.038	0.000	132.8	0.48	0.97
L-S-M-S	CM86			0.15	0.01	139.5	139.5	747	185	890	1822	1.038	0.227	121.4	0.44	0.94
L-S-P-S	CM76	0.15			0.015	139.5	139.5	813	201	969	1983	1.230	0.340	118.8	0.43	0.98
L-S-P-S	CM104	0.15			0.035	139.5	139.5	762	188	908	1858	1.230	0.794	107.5	0.39	0.93
L-S-P-S	CM89	0.15			0.025	139.5	139.5	762	188	908	1858	1.230	0.567	107.3	0.38	0.92
L-S-N-S	CM94		0.5		0.025	139.5	139.5	759	187	904	1851	3.460	0.567	108.7	0.39	0.96
L-S-N-S	CM77		0.4		0.025	139.5	139.5	811	200	966	1977	2.768	0.567	120.0	0.43	0.97

Table 28. Fresh and hardened properties of preliminary mixtures with slag

Labels	Slump, mm	Air	Fresh Density	Temp.	Vol. of Agg.	Aggregate Proportions			Compressive Strength, MPa		Labels	Slump, in	Compressive Strength, psi		
	*	%	kg/m ³	°F	kg/m ³	C1, %	I1, %	F1, %	7 days	28 days			C.S. 7	C.S. 28	
L-S-M	CM64	63	4.0	2440	65	0.724	40	10	50	29.5	38.4	CM64	2.5	4273	5570
L-S-M-S	CM86	59	6.0	2364	71	0.675	40	10	50	30.0	23.7	CM86	2.3	4346	3441
L-S-P-S	CM76	140	3.2	2429	70	0.735	40	10	50	21.8	29.9	CM76	5.5	3163	4336
L-S-P-S	CM104	200	5.0	2418	69	0.689	40	10	50	23.1	31.6	CM104	7.9	3349	4588
L-S-P-S	CM89	50	3.5	2432	72	0.689	40	10	50	28.3	36.8	CM89	2.0	4106	5336
L-S-N-S	CM94	71	8.5	2327	66	0.686	40	10	50	25.6	33.4	CM94	2.8	3711	4838
L-S-N-S	CM77	68	6.0	2437	66	0.733	40	10	50	26.4	40.1	CM77	2.7	3827	5811

* immediately after mixing

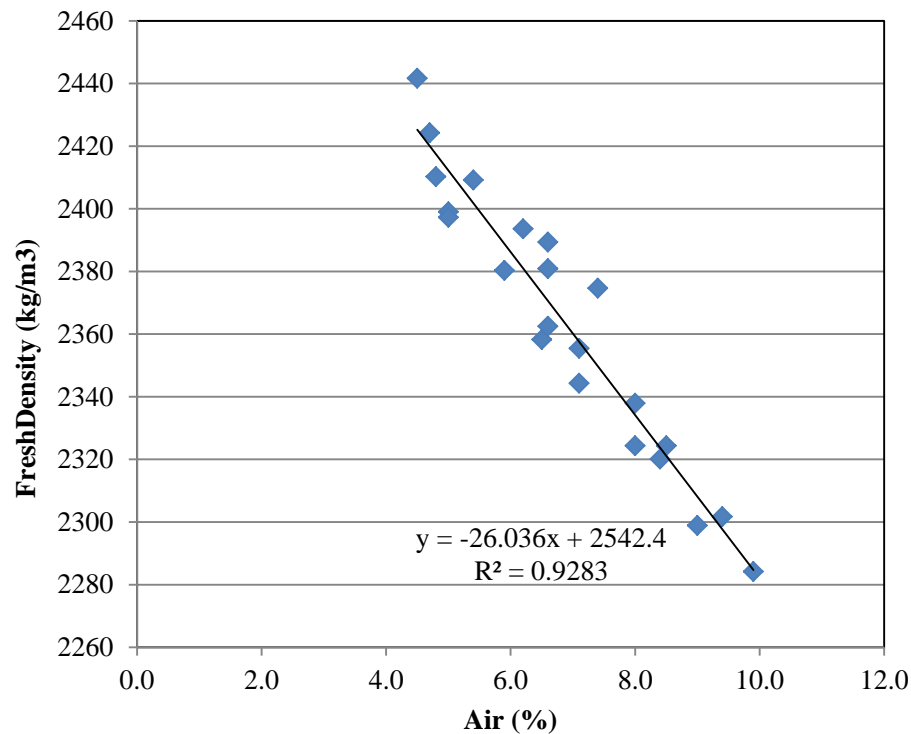


Figure 31. The relationship between air content and fresh density of tested final mixtures

4.2.2. Optimized Mixture Evaluation

Final optimized mixtures were produced using the results of aggregates optimization, admixture optimization, using the constant contents of SCMs and two levels of cementitious materials of 279 kg/m³ [470 lb/yd³] and 249.2 kg/m³ [420 lb/yd³]. The mixtures are classified in *Table 29* to *Table 34* based on the cement content level, the type of SCMs used, and the admixture type. To evaluate the mixtures for fresh properties the slump, air content, bulk density, and temperature was performed. To evaluated the mixtures for hardened properties the compressive strength at 1, 3, 7, 28, 90, and 360 days and flexural strength (modulus of rupture) at 3, 7, 28, and 90 days were performed. Durability of the mixtures were evaluated using the

freeze-thaw at 56 days and rapid chloride permeability tests at 30 days and 90 days (these tests were performed at UW-Madison). The preliminary mixtures were designed and tested based on optimized aggregate blends defined by this research. The mix design for final optimized mixtures was based on the adjustment of preliminary mixtures (AE admixture dosage and the W/CM ratio). The mix designs are presented in *Table 29* and *Table 32* for 279 kg/m^3 [470 lb/yd^3] and 249.2 kg/m^3 [420 lb/yd^3] of cementitious materials content, respectively.

4.2.3. Optimized Mixture: Fresh Properties

The fresh properties of final optimized mixtures were evaluated using slump test. The slump depends of various parameters including W/CM ratio, the quantity of cement (volume of cement paste), the type of admixtures (WRA/HRWRA), and quantity of air. The quantity and proportioning of aggregates were held constant for each level of cement content; therefore this parameter did not affect the slump results for a constant cement content level.

The workability of fresh concrete was evaluated right after mixing and at 30 minute after mixing water and cement as presented in *Table 29* and *Table 30*. Comparing mixtures based on Lafarge cement produced at the same W/CM ratio with reference mixture BB04 reveals that at the same W/CM ratio of 0.42 the mixtures containing slag (BB02, BB08) and class F fly ash (BB05, BB03) had a better workability (about 50 mm higher) than plain mixtures without SCMs. Such behavior was observed for both SNF admixture (BB04) and reference mid-range admixture (BB09). In case of W/CM ratio of 0.38 mixtures with slag (BB11) and PCE admixture had better workability than plain mixture (BB13) and the mixture with class C fly ash and mid-range admixture (BB06). All three mixtures had 0.05 reduced W/CM ratio than that of the reference

(BB04). In case of W/CM ratio of 0.33 only two mixtures with PCE containing class C and Class F fly ash (BB10, BB12) were able to reach such level of water reduction versus the reference (BB04). It must be noted that the effect of air content on slump is very significant and so all the compared mixtures assumed to have the same level of air content.

Comparing the mixtures based on Holcim cement at the same W/CM ratio (BB19, BB18, BB17) demonstrates the superior effect of PCE admixtures on slump and slump retention at 30 minutes after mixing. All three mixtures were produced at 0.05 reduced W/CM ratio than that of the reference (BB04) with Lafarge.

Comparing the mixtures based on St Marys produced at the same W/CM ratio (BB16, BB15) demonstrates that SNF performs better than mid-range admixture in terms of increased slump. The mixture with PCE admixture (BB14) had superior performance considering 0.05 reduction of W/CM compared to other two mixtures (BB16, BB15); only this mixture performs better than the reference (BB04) in terms of workability.

Comparing mixtures BB13, BB17, and BB14 containing the same type of admixtures reveals that some cements require higher water content to achieve the same workability; however the air content (which can have significant contribution) varies between the three mixtures by about 2%.

As represented in *Table 29* and *Table 30*, for concrete with reduced cement content level of 249.2 kg/m^3 [420 lb/yd^3], the workability was evaluated right after mixing and at 30 minute period after mixing water and cement. This experimental matrix was conducted with one type of WRA and PCE type of HRWRA. Comparing mixtures based on with Lafarge cement proves that the mixtures with PCE admixture (BB21) provide 100 mm higher slump that the mixture with

mid-range admixture (BB20) when tested at about the same W/CM ratio of 0.45; however, at higher air content. Increase in W/CM ratio or air content may be required for concrete mixtures with reduced cement content 249.2 kg/m^3 [420 lb/yd^3] (BB20) to achieve the required workability as that of the concrete with 279 kg/m^3 [470 lb/yd^3] cement content (BB04).

For SCM concrete with reduced cementitious materials content mixtures at about the same W/CM ratio of 0.4 (BB22, BB23, BB24) the mixture containing slag provides an improved slump, even at slightly lower air contents (versus other two mixtures and the reference mixture BB04). In case of mixtures with reduced cement content based on Holcim (BB29, BB27) and St Marys (BB28, BB26) cements at the same W/CM ratio of about 0.4, the mixtures had the same fresh performance depending on the air content. It must be noted that the contribution of additional air in mixtures with reduced cement content is essential to maintain the required volume of cement paste and compensate for the reduced amount of the cementitious materials.

4.2.4. Optimized Mixture: Hardened Properties

Table 29 and *Table 29* report on the hardened properties including the compressive strength and modulus of rupture for concrete with cementitious content of 279 kg/m^3 [470 lb/yd^3] and 249.2 kg/m^3 [420 lb/yd^3] respectively. The mechanical performance was evaluated for early and long-term (up to 1 year) ages. Similar to fresh properties, the effect of air content on mechanical performance is obviously crucial.

As reported by *Table 29*, concrete based on Lafarge cement at the same W/CM ratio of 0.42 reference mixture (BB09, reference BB04) demonstrated better strength at the ages of 1, 3, and 7 days compared to mixtures with SCMs (BB02, BB08, BB05, BB03). In 28-day age and

afterwards, concrete containing slag (BB02, BB08) exceeded the strength of plain concrete. The compressive strength of class F fly ash (BB05, BB03) was lower than the reference (including 1-year strength).

In the case of W/CM ratio of 0.38, the plain concrete (BB13) performed better than the slag concrete with PCE (BB11) and class C fly ash concrete with mid-range and SNF (BB06, BB07) at early ages, but after 7 days class C fly ash concrete exceeds the strength of plain concrete (BB13) and, after 28 days, slag concrete (BB11) reached the same strength as the reference (BB13). All the mixtures at such W/CM ratio achieved early and long-term strength higher than that of the reference (BB04) as reported in *Table 29*. Concrete containing class C fly ash reached the highest compressive strength versus all other mixtures at the age of 1 year. However, the PCE concrete however had the highest strength when compared to other admixtures, mainly due to its ability to lower W/CM ratio and also due to very good compatibility between the PCE and cementitious materials.

In case of W/CM ratio of 0.33 two mixtures containing class C and Class F fly ash (BB10, BB12) with PCE admixture both exceed in early and long-term strength compared to that of the reference as represented in *Table 29*.

Concrete based on Holcim cement produced at the same W/CM ratio (BB19, BB18, BB17) achieved extremely high early strength which is about three times as high as the reference and achieves the minimum specified compressive strength (20MPa, 3000 psi for traffic opening) at 1 day as shown in *Table 29*. The long-term strength of this concrete is similar to performance of concrete based on Lafarge cement and class C fly ash. The concrete with PCE admixtures

performed the best at the age of up to 28 days and SNF type admixture performed the best at later ages.

Concrete based on St Marys cement (BB16, BB15, BB14) revealed that these performed slightly better or at the same level as the reference concrete (BB04) for all the ages, as shown in *Table 29*.

Comparing plain concrete based on St Marys cement to Holcim and Lafarge cement based concrete demonstrated that St Marys performed better compared to Lafarge cement in terms of 1-day strength. Holcim cement performed better than Lafarge in all the ages, all types of admixture, and most of the SCMs (except for class C and PCE admixture). However, these cements were comparable in long-term behavior in combination with slag concrete with Lafarge.

As represented in *Table 29* and *Table 30*, the fresh properties evaluated right after mixing and at 30 minute (after mixing water and cement) for concrete with reduced cement content level of 249.2 kg/m^3 [420 lb/yd^3]. This experimental matrix was conducted with one type of WRA (mid-range) and one type of HRWRA (PCE). Comparing concrete mixtures based on Lafarge cement reveals that the PCE admixture (BB21) provides about 100 mm higher slump than the mixture with mid-range admixture (BB20) at about the same W/CM ratio of 0.45; however, at higher air content. Slightly higher W/CM ratio or elevated air content can be required for concrete mixtures with lowered cement content to achieve the same workability as that of the reference concrete with 279 kg/m^3 [470 lb/yd^3] cement content (BB04).

For concrete mixtures with reduced cementitious content containing SCMs and produced at about the same W/CM ratio 0.4 (BB22, BB23, BB24) the mixture containing slag cement

provides enhanced slump even at slightly lower air contents versus the other two mixtures (and the reference mixture, BB04). In case of reduced cementitious content mixtures based on Holcim (BB29, BB27) and St Marys (BB28, BB26) cements is produced at the at the same W/CM ratio of about 0.4, all the had similar performance with little variation depending on the air content demonstrating lower slump versus reference BB04 (and also BB20). It must be noted that the additional air is essential for concrete with reduced cement content to compensate for reduced volume of cement paste.

The relationship between the modulus of rupture and compressive strength is represented in *Figure 32* combining all corresponding ages. As illustrated in this figure, *Table 31* and *Table 34* the modulus of rupture (MOR) obtained from flexural center-point (3-point) loading of the beams has a good correlation with corresponding compressive strength for various mixtures and ages. The variation depends on the type of SCMs, W/CM ratio, and cement type. Therefore, the modulus of rupture can be evaluated and predicted based on compressive strength as illustrated in *Figure 32*.

Table 29. Mixture proportioning of final optimized concrete mixtures at cementitious materials of 279 kg/m³ [470 lb/yd³]

	Labels		Chemical Admixture (%)				Cement Content	SCM	Aggregate (SSD) (Kg/m ³)			Total Agg.	WRA / HRARA	Air Entrainer	Total Water
			PCE	SNF	Mid-Range	AE	kg/m ³	kg/m ³	CA	IA	FA	kg/m ³	kg/m ³	kg/m ³	kg/m ³
279 kg/ m ³ (470 lb/ yd ³)	L-S-M	BB04			0.15	0.01	278.9	0.0	750	185	894	1829	1.038	0.227	118.0
	L-S-N	BB09		0.4		0.015	278.9	0.0	747	185	891	1823	2.768	0.340	119.3
	L-S-P	BB13	0.15			0.02	278.9	0.0	765	189	912	1866	1.230	0.453	103.8
	L-S-M-S	BB02			0.15	0.005	139.5	139.5	747	185	890	1822	1.038	0.227	118.2
	L-S-N-S	BB08		0.4		0.015	139.5	139.5	744	184	887	1816	2.768	0.340	119.4
	L-S-P-S	BB11	0.15			0.025	139.5	139.5	762	188	908	1858	1.230	0.567	104.0
	L-S-M-C	BB06			0.15	0.005	195.2	83.7	761	188	907	1857	1.038	0.567	103.8
	L-S-N-C	BB07		0.4		0.01	195.2	83.7	759	188	905	1852	2.768	0.227	104.7
	L-S-P-C	BB10	0.15			0.01	195.2	83.7	777	192	926	1895	1.230	0.227	89.0
	L-S-M-F	BB05			0.15	0.02	195.2	83.7	742	183	884	1809	1.038	0.340	118.5
	L-S-N-F	BB03		0.4		0.025	195.2	83.7	739	183	881	1803	2.768	0.567	119.9
	L-S-P-F	BB12	0.15			0.015	195.2	83.7	772	191	921	1884	1.230	0.340	89.3
	H-S-M	BB19			0.15	0.005	278.9	0.0	765	189	912	1867	1.038	0.113	103.2
	H-S-N	BB18		0.4		0.015	278.9	0.0	763	189	909	1861	2.768	0.340	104.6
	H-S-P	BB17	0.15			0.020	278.9	0.0	765	189	912	1866	1.230	0.453	103.8
	S-S-M	BB16			0.15	0.010	278.9	0.0	750	185	894	1829	1.038	0.227	118.0
S-S-N	BB15		0.4		0.025	278.9	0.0	747	185	891	1823	2.768	0.567	119.5	
S-S-P	BB14	0.15			0.045	278.9	0.0	764	189	911	1864	1.230	1.020	104.3	

Table 30. The fresh properties of final optimized concrete mixtures at cementitious materials of 279 kg/m³ [470 lb/yd³]

	Labels		W/CM	Yield	Aggregate Proportions			Slump (mm)		Air %	Bulk Density kg/m ³	Temp. °F	Vol. of Agg. kg/m ³
					C1, %	I1, %	F1, %	0 min	30 mins				
279 kg/ m ³ (470 lb/yd ³)	L-S-M	BB04	0.42	0.94	40	10	50	49	30	6.5	2358	71	0.678
	L-S-N	BB09	0.43	0.93	40	10	50	51	20	5.0	2399	69	0.676
	L-S-P	BB13	0.37	0.96	40	10	50	43	30	7.1	2344	69	0.692
	L-S-M-S	BB02	0.42	0.95	40	10	50	100	55	8.0	2324	68	0.675
	L-S-N-S	BB08	0.43	0.94	40	10	50	100	50	7.1	2355	69	0.673
	L-S-P-S	BB11	0.37	0.92	40	10	50	188	160	4.7	2424	68	0.689
	L-S-M-C	BB06	0.37	0.93	40	10	50	30	15	5.4	2409	73	0.689
	L-S-N-C	BB07	0.38	0.92	40	10	50	65	35	5.9	2429	69	0.686
	L-S-P-C	BB10	0.32	0.94	40	10	50	45	10	4.8	2410	69	0.702
	L-S-M-F	BB05	0.42	0.96	40	10	50	95	65	9.0	2299	69	0.671
	L-S-N-F	BB03	0.43	0.97	40	10	50	130	92	9.5	2265	69	0.668
	L-S-P-F	BB12	0.32	1.01	40	10	50	32	25	6.9	2224	71	0.698
	H-S-M	BB19	0.37	0.92	40	10	50	7	0	4.5	2442	68.8	0.692
	H-S-N	BB18	0.38	0.91	40	10	50	10	8	4.0	2467	67.3	0.690
	H-S-P	BB17	0.37	0.97	40	10	50	92	39	8.5	2324	73.5	0.692
	S-S-M	BB16	0.42	0.93	40	10	50	35	20	6.6	2381	68	0.678
S-S-N	BB15	0.43	0.94	40	10	50	56	42	6.6	2363	71.7	0.676	
S-S-P	BB14	0.37	0.94	40	10	50	30	20	6.2	2394	71.4	0.691	

Table 31. The mechanical performance of final optimized concrete at cementitious materials of 279 kg/m³ [470 lb/yd³]

Labels	W/CM	Compressive Strength at Various Ages, MPa							Modulus or Rupture, MPa			
		1	3	7	28	90	360	3	7	28	90	
L-S-M	BB04	0.42	6.8	17.7	25.2	31.7	35.0	38.8	6.6	7.3	8.8	8.6
L-S-N	BB09	0.43	13.9	22.6	27.2	33.6	39.2	40.9	6.4	7.2	8.6	9.5
L-S-P	BB13	0.37	13.6	27.7	32.5	38.1	43.6	47.4	7.1	7.7	9.3	7.3
L-S-M-S	BB02	0.42	2.9	13.2	19.8	33.3	41.6	45.1	0.0	6.7	8.9	9.6
L-S-N-S	BB08	0.43	4.9	14.7	24.2	35.2	41.0	43.5	5.2	7.5	9.9	9.7
L-S-P-S	BB11	0.37	8.9	20.2	30.3	38.0	40.3	48.0	5.9	7.3	9.2	8.4
L-S-M-C	BB06	0.37	6.0	23.3	35.0	48.3	56.4	59.4	6.1	8.1	9.6	11.4
L-S-N-C	BB07	0.38	5.1	22.0	30.0	41.9	50.4	50.7	6.6	6.6	9.1	10.9
L-S-P-C	BB10	0.32	10.1	25.7	38.1	49.3	56.6	63.2	7.0	8.6	10.4	11.6
L-S-M-F	BB05	0.42	3.5	9.6	13.3	19.1	27.0	31.3	3.7	4.6	5.9	7.5
L-S-N-F	BB03	0.43	4.0	8.8	12.6	18.6	25.2	29.4	3.8	4.7	6.0	7.5
L-S-P-F	BB12	0.32	10.0	20.3	25.0	32.7	42.6	48.4	6.2	6.3	8.0	7.5
H-S-M	BB19	0.37	20.4	31.0	34.9	41.7	49.2	46.6	5.8	6.7	7.3	8.3
H-S-N	BB18	0.38	22.8	33.4	40.2	43.8	51.0	55.3	6.2	6.9	7.3	8.8
H-S-P	BB17	0.37	25.1	25.6	29.3	32.9	38.0	43.4	5.5	5.6	6.1	8.8
S-S-M	BB16	0.42	11.1	17.7	22.8	29.9	35.6	38.7	6.4	6.1	7.0	8.2
S-S-N	BB15	0.43	13.0	18.8	23.1	28.2	34.0	37.3	6.3	7.3	6.6	6.8
S-S-P	BB14	0.37	16.3	24.0	27.4	34.6	42.8	48.1	6.8	7.6	7.1	7.8

279 kg/ m³ (470 lb/yd³)

Table 32. Mixture proportioning of final optimized concrete mixtures at cementitious materials of 250 kg/m³ [420 lb/yd³]

	Labels		Chemical Admixture (%)				Cement Content	SCM	Aggregate (SSD) (Kg/m ³)			Total Agg.	WRA / HRAR A	Air Entrainer	Total Water
			PCE	SNF	Mid-Range	AE	kg/m ³	kg/m ³	CA	IA	FA	kg/m ³	kg/m ³	kg/m ³	kg/m ³
249 kg/ m ³ (420 lb/yd ³)	L-S-M-R	BB20			0.15	0.010	249.2	0.0	750	185	929	1864	0.928	0.203	113.1
	L-S-P-R	BB21	0.15			0.030	249.2	0.0	776	192	914	1881	1.099	0.608	107.7
	L-S-P-C-R	BB22	0.15			0.015	174.4	74.8	780	193	934	1907	1.099	0.304	94.4
	L-S-P-S-R	BB23	0.15			0.03	124.6	124.6	762	188	940	1890	1.099	0.608	100.7
	L-S-P-F-R	BB24	0.15			0.05	174.4	74.8	757	187	934	1878	1.099	1.013	101.3
	H-S-M-R	BB29			0.15	0.015	249.2	0.0	771	191	920	1882	0.928	0.304	103.3
	H-S-P-R	BB27	0.15			0.020	249.2	0.0	778	192	928	1898	1.099	0.405	96.2
	S-S-M-R	BB28			0.15	0.005	249.2	0.0	772	191	920	1882	0.928	0.101	103.5
	S-S-P-R	BB26	0.15			0.025	249.2	0.0	771	191	919	1881	1.099	0.507	102.3

Table 33. The fresh properties of final optimized concrete mixtures at cementitious materials of 250 kg/m³ [420 lb/yc³]

	Labels		W/CM	Yield	Aggregate Proportions			Slump (mm)		Air %	Bulk Density kg/m ³	Temp. °F	Vol. of Agg. kg/m ³
					C1, %	I1, %	F1, %	0 min	30 mins				
249 kg/ m ³ (420 lb/yc ³)	L-S-M-R	BB20	0.45	0.96	40	10	50	35	11	8.4	2320	73.5	0.691
	L-S-P-R	BB21	0.43	0.97	40	10	50	133	113	9.4	2302	68.3	0.697
	L-S-P-C-R	BB22	0.38	0.94	40	10	50	37	30	6.6	2389	71.1	0.707
	L-S-P-S-R	BB23	0.40	0.94	39	10	51	110	45	5.9	2380	70.7	0.701
	L-S-P-F-R	BB24	0.41	1.00	39	10	51	68	30	9.8	2218	67.8	0.696
	H-S-M-R	BB29	0.41	0.93	40	10	50	13	0	5.0	2397	67	0.697
	H-S-P-R	BB27	0.41	0.96	40	10	50	40	7	8.0	2338	72.4	0.703
	S-S-M-R	BB28	0.42	0.94	40	10	50	22	12	7.4	2375	67.2	0.698
	S-S-P-R	BB26	0.41	0.98	40	10	50	38	28	9.9	2284	71.6	0.697

Table 34. The mechanical performance of final optimized concrete at cementitious materials of 250 kg/m³ [420 lb/yd³]

	Labels		W/CM	Compressive Strength, MPa						Modulus or Rupture, MPa			
				1	3	7	28	90	360	3	7	28	90
249 kg/ m ³ (420 lb/yd ³)	L-S-M-R	BB20	0.45	3.9	14.0	19.5	23.4	28.7	29.8	3.8	4.3	5.3	5.5
	L-S-P-R	BB21	0.43	8.4	18.3	21.1	26.6	29.3	30.9	4.3	5.2	5.4	5.6
	L-S-P-C-R	BB22	0.38	7.1	19.6	28.2	39.7	44.1	49.8	4.5	5.5	7.1	8.3
	L-S-P-S-R	BB23	0.40	7.8	18.5	28.3	38.0	39.8	44.3	4.7	5.9	7.8	8.1
	L-S-P-F-R	BB24	0.41	6.1	10.0	12.5	16.9	22.7	26.7	3.1	3.2	4.0	4.4
	H-S-M-R	BB29	0.41	12.3	20.7	23.1	30.1	37.2	38.6	4.2	5.7	6.9	7.1
	H-S-P-R	BB27	0.41	17.9	23.9	26.6	32.1	35.2	37.2	5.2	5.2	6.1	6.9
	S-S-M-R	BB28	0.42	14.1	22.6	26.4	31.2	35.3	37.5	5.2	5.7	6.3	7.2
	S-S-P-R	BB26	0.41	11.1	15.7	18.8	25.1	29.0	31.9	3.9	4.3	5.7	5.7

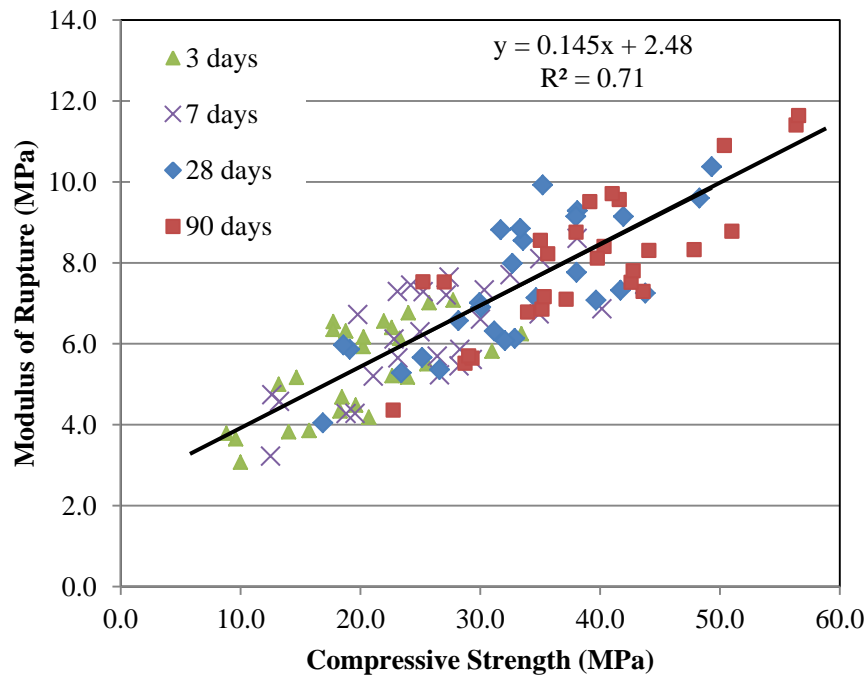


Figure 32. The relationship between the compressive strength and modulus of rupture

4.2.5. Optimized Mixtures: Strength Development

As discussed (in section 4.2.4) various mixtures illustrate different strength development depending on whether the SCMs were used and also the type of SCMs, WRA/HRWRA, W/CM ratio, and cement type. *Figure 33 to Figure 36* represent the strength development of all the mixtures plotted using logarithmic scale and evaluated for the period of up to 1 year as compared to reference concrete (L-S-M, BB04) based on Lafarge cement, southern aggregates and mid-range WRA.

Figure 34 illustrated the compressive strength behavior of the mixtures produced at W/CM ratio of 0.42. The concrete mixtures containing slag and mid-range / SNF admixtures gain strength at a higher rate than other mixtures, especially at later stages of hardening at this W/CM ratio. The plain concrete based on Lafarge mixtures compared to

St Marys also achieved enhanced strength at higher rates for similar types of admixtures (Mid-range / SNF) and same W/C ratio. However, the strength gain for mixtures containing class F fly ash was not sufficient.

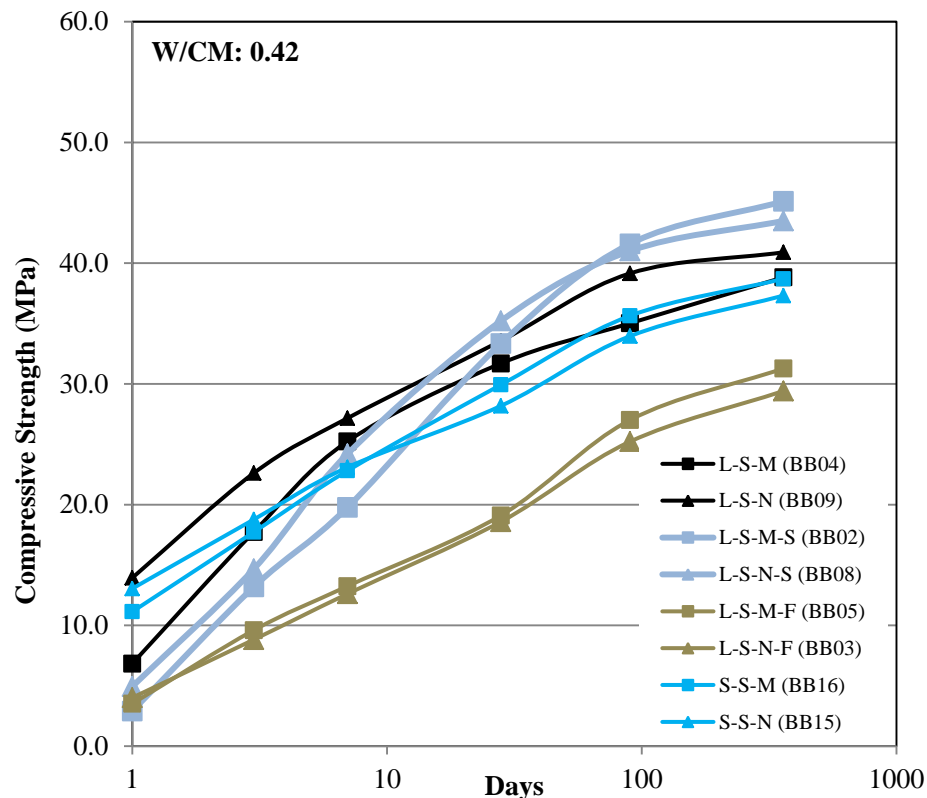


Figure 33. Strength development of the concrete produced at W/CM of 0.42 and 279 kg/m³ [470 lb/yd³] cementitious materials content

As illustrated in Figure 33, the concrete based on Lafarge cement containing fly ash with mid-range and SNF admixtures gain additional strength and develop strength at a higher rate compared to other mixtures produced at this W/CM ratio. The same behavior can be observed for mixture containing slag with PCE admixtures. The Holcim concrete had the same strength gain as the reference mixture, but with enhanced early strength up

to 8 MPa depending on the admixture type. Concrete based on St Marys cement and PCE admixtures was able to provide higher strength versus reference.

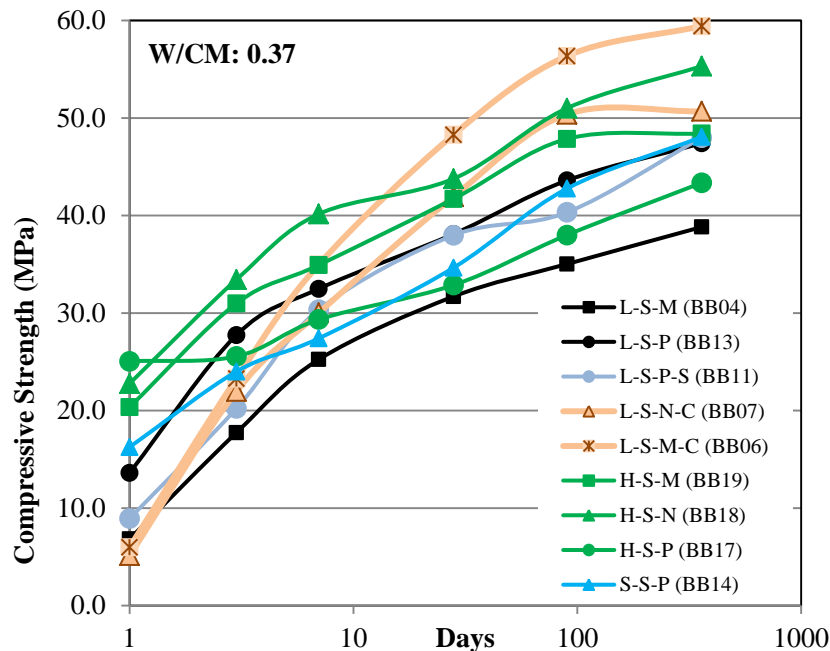


Figure 34. Strength development of the concrete produced at W/CM of 0.37 and 279 kg/m³ [470 lb/yd³] cementitious materials content

As illustrated in Figure 33, the mixtures with Lafarge cement containing class C and F fly ash with PCE admixtures provided the suitable performance at low W/CM ratio. Compared to the reference mixtures, these mixtures developed strength at accelerated rates, especially mixtures with class C fly ash. While concrete with class F fly ash and other types of admixtures were not achieve satisfactory in terms of strength development, concrete with PCE achieved 20 MPa (3000 psi) in 3 days. The water-reducing effect of PCE resulted in excellent strength gain especially in combination with class C fly ash; this concrete (BB10) reached outstanding by reaching 63 MPa in 1 year.

Figure 33 represents the strength development of concrete with reduced cementitious content of 250 kg/m³ [420 lb/yd³] and compares the performance to reference concrete with 279 kg/m³ [470 lb/yd³] cement content (BB04). Only mid-range and PCE admixtures were tested at such cement content. The mixtures were produced at target W/CM ratio of 0.41 except for BB22 and BB20 which were produced at 0.38 and 0.45, respectively due to water reduction. The concrete strength development appeared to have the same trend regarding the type of SCMs and chemical admixtures. Concrete containing slag and class C fly ash gained additional strength versus concrete with class F fly ash. The reduced concrete based Holcim cement had similar performance as the reference. However due to significant reduction of cement content 250 kg/m³ [420 lb/yd³] concrete based on St Marys, and plain Lafarge cements as well as Lafarge cement with class F fly ash did not achieve similar strength as reference concrete, even at later ages.

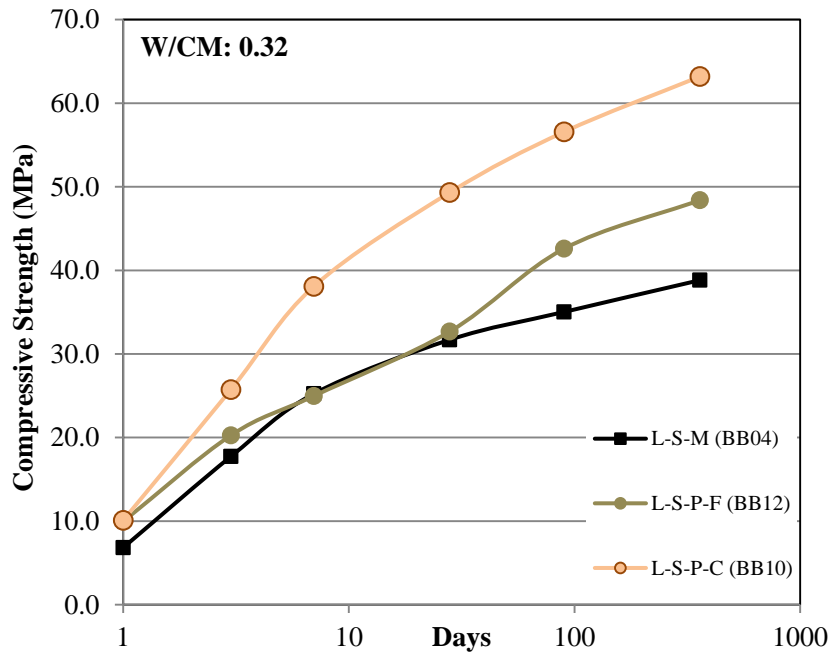


Figure 35. Strength development of concrete produced at W/CM of 0.32 at 279 kg/m³ [470 lb/yd³] cementitious materials content

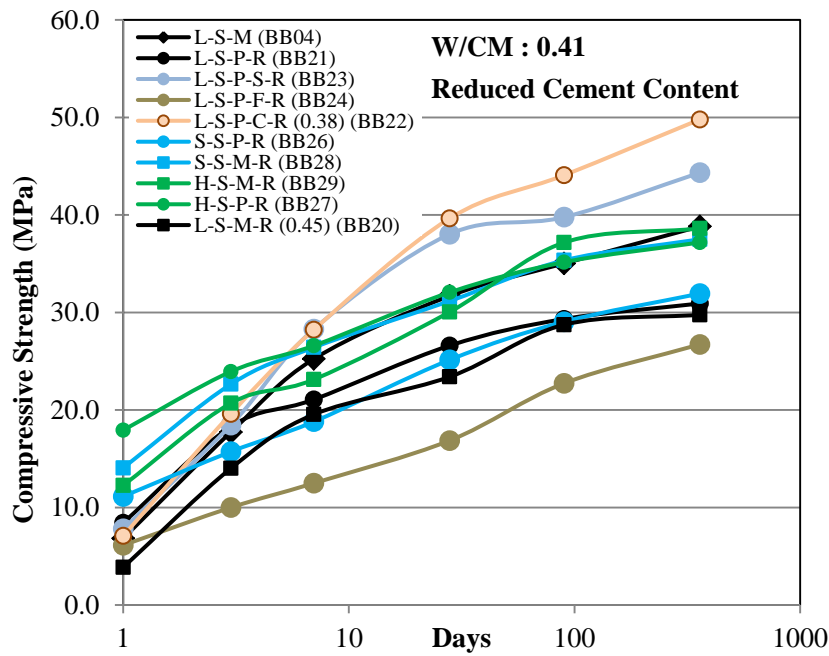


Figure 36. Strength development of concrete produced at W/CM of 0.41 at 250 kg/m³ [420 lb/yd³] cementitious materials content

It must be noted that the strength development of three different cements was different for early and later ages as illustrated in *Figure 37*. Plotting the strength development in logarithmic scale it was found that the plain Lafarge concrete obtained lower strength at early ages compared to other two cements, but developed strength at a higher rate after until 3 days, while Holcim and St Marys cements development strength in a linear manner throughout. However, the rate also depends on the type of admixture combination used, and becomes similar after 28 days.

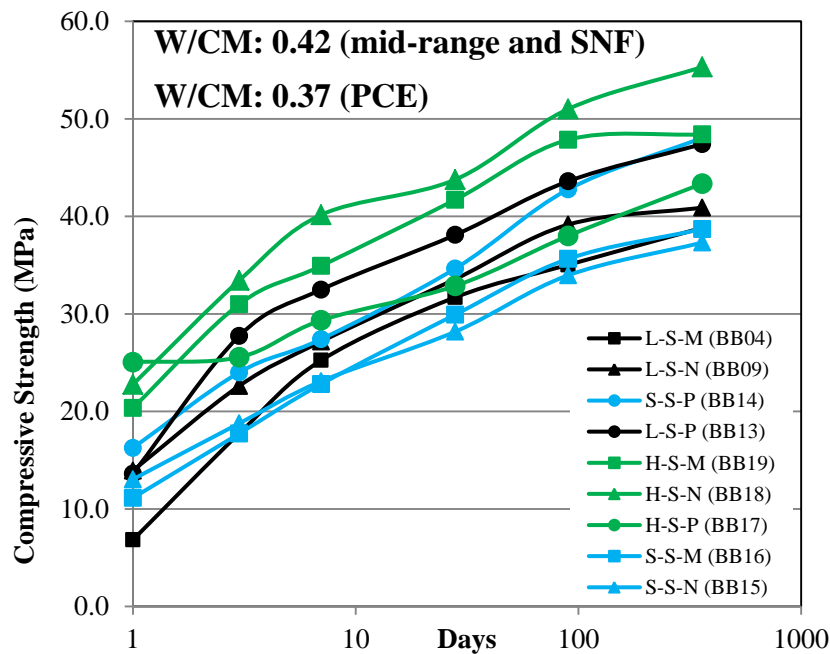


Figure 37. Strength development of concrete based on different cements produced at W/CM of 0.42 and 279 kg/m³ [470 lb/yd³] cementitious materials content

4.2.6. Optimized Mixture: Durability

All the optimized mixtures were evaluated for durability using freezing-thawing (F/T) and rapid-chloride permeability (RCP) testing at various ages as illustrated in *Table 35*, *Table 36*, *Figures 38* and *39*.. It can be observed that for all concrete the permeability drops at later ages. It must be considered that the mixtures were produced a three different W/CM ratios ranging from 0.42 to 0.32. Except for a few mixtures which demonstrated moderate permeability in 30 days, all other optimized concrete achieved a low and a very low permeability benchmark. Reduced cement content concrete as compared to the corresponding specimen at 279 kg/m³ [470 lb/yd³] achieved lowered permeability, even at higher W/CM ratio except for mixtures with class F fly ash and slag which achieve slightly lower permeability at 279 kg/m³ [470 lb/yd³] cement content and also the mixtures with mid-range WRA for Holcim and St Mary cement. The lower permeability for reduced cement content produced at the same W/CM ratio is due to the reduced volume of cementitious phase and lower permeability of aggregates. The higher porosity in cementitious materials associated with higher W/CM causes higher transport properties of the matrix; however, lowering cement content would lower the volume of the cement phase in the concrete. Therefore, the mixtures produced at lower cement content have a higher aggregate content. The total permeability, therefore, drops even though the cement paste produced at lower W/CM ratio is more permeable than the cement paste produced at higher W/CM ratio. This indicates that the effect of the volume of cement and aggregate in the mix is more significant than the permeability of the materials with higher transport properties.

Table 35. The durability of concrete with cementitious materials content of 279 kg/m³ [470 lb/yd³]

	Labels		W/CM	Air	RCP Charge Passed, Coulomb			F/T Durability Factor	F/T Mass Loss
			%	%	30 days	90 days	Drop %	%	%
279 kg/ m ³ (470 lb/yd ³)	L-S-M	BB04	0.42	6.5	3220	2299	29	99.2	-0.10
	L-S-N	BB09	0.43	5.0	3416	2192	36	94.7	1.19
	L-S-P	BB13	0.37	7.1	2446	1897	22	100.0	-0.54
	L-S-M-S	BB02	0.42	8.0	1165	731	37	93.5	3.68
	L-S-N-S	BB08	0.43	7.1	1368	706	48	93.5	3.54
	L-S-P-S	BB11	0.37	4.7	1278	900	30	92.4	4.49
	L-S-M-C	BB06	0.37	5.4	1988	1045	47	92.9	3.82
	L-S-N-C	BB07	0.38	5.9	2263	1110	51	93.9	4.10
	L-S-P-C	BB10	0.32	4.8	1653	695	58	98.0	0.61
	L-S-M-F	BB05	0.42	9.0	3321	944	72	99.2	1.05
	L-S-N-F	BB03	0.43	9.5	2306	853	63	98.5	1.05
	L-S-P-F	BB12	0.32	6.9	1606	670	58	99.8	0.08
	H-S-M	BB19	0.37	4.5	2058	1333	35	97.0	0.99
	H-S-N	BB18	0.38	4.0	1939	1409	27	95.0	2.06
	H-S-P	BB17	0.37	8.5	2151	1647	23	100.0	-0.73
	S-S-M	BB16	0.42	6.6	2416	1503	38	100.0	0.22
	S-S-N	BB15	0.43	6.6	2344	1474	37	98.0	0.36
S-S-P	BB14	0.37	6.2	1775	1308	26	98.0	0.64	

Table 36. The durability of concrete with cementitious materials content of 250 kg/m^3 [420 lb/yd^3]

	Labels		W/CM	Air	RCP Charge Passed, Coulomb			F/T Durability Factor	F/T Mass Loss
			%	%	30 days	90 days	Drop %	%	%
249 kg/m ³ (420 lb/yd ³)	L-S-M-R	BB20	0.45	8.4	3058	2126	30	100.0	-0.07
	L-S-P-R	BB21	0.43	9.4	2768	2129	23	99.0	-0.53
	L-S-P-C-R	BB22	0.38	6.6	2119	1035	51	100.0	1.2
	L-S-P-S-R	BB23	0.40	5.9	934	577	38	98.0	1.76
	L-S-P-F-R	BB24	0.41	9.8	1964	949	52	97.0	1.54
	H-S-M-R	BB29	0.41	5.0	2050	1244	39	100.0	0.24
	H-S-P-R	BB27	0.41	8.0	2283	1936	15	100.0	-0.99
	S-S-M-R	BB28	0.42	7.4	2569	1768	31	100.0	-0.35
	S-S-P-R	BB26	0.41	9.9	1997	1107	45	100.0	0.11

Almost all the concrete with cementitious materials content of 279 kg/m^3 [470 lb/yd^3] obtained lower permeability compared to the reference mixture (L-S-M) at both 30 days and 90 days. In 90 days, concrete based on Lafarge with SCMs obtained almost 50% lower permeability than plain concrete (less than 1000 coulombs) and the class F fly ash concrete obtained the highest drop when compared to other mixtures. Concrete based on Holcim and St Marys cements performed better than Lafarge concrete in terms of RCP by about 500 coulombs. The concrete based on class F fly ash performed better than Class C concrete in 30 days permeability and concrete with slag performed superior to other material at both ages of 90 days and 30 days. Except for slag and Holcim concrete mixtures, the use of PCE admixture enabled lower permeability versus concrete with SNF and mid-range admixtures. The highest drop in permeability was demonstrated by concrete with SCMs especially, in concrete with class F fly ash.

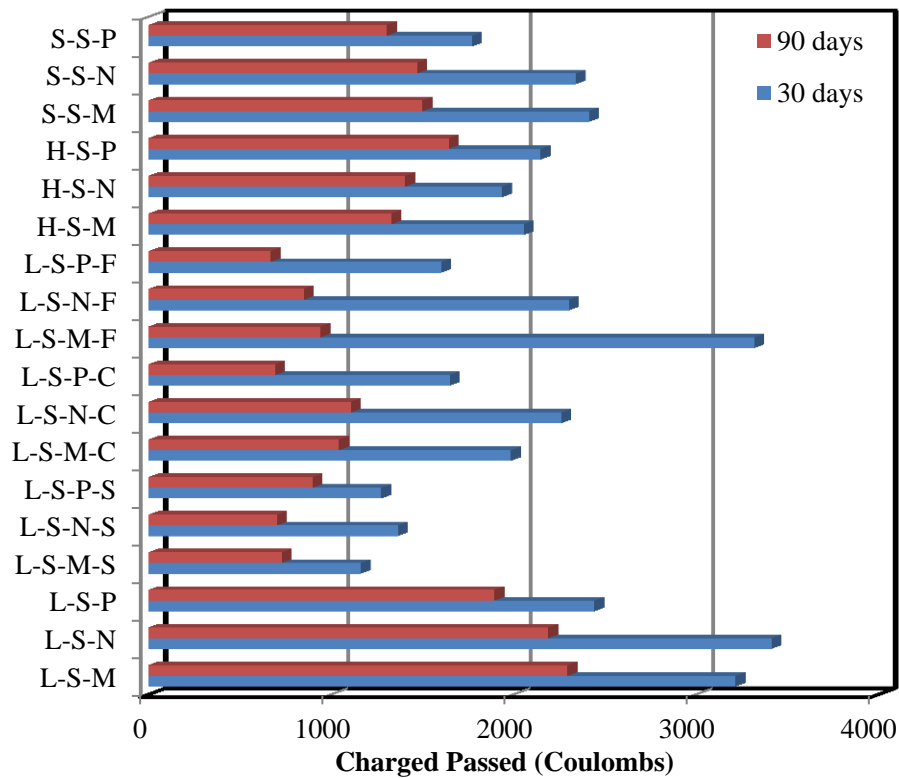


Figure 38. The RCP of concrete with cementitious materials content of 279 kg/m^3 [470 lb/yd^3]

Almost all the concrete with cementitious materials of 250 kg/m^3 [420 lb/yd^3], obtained lower permeability than the reference mixture (L-S-M) at both 30 days and 90 days. At 90 days, concrete with SCMs had up to 50% lower permeability than plain mixtures (less than 1000 coulombs) and the concrete with class F and C fly ash had the highest drop at 90 days compared to other mixtures. Concrete based on Holcim and St Marys cements performed better than Lafarge at this cement content level in terms of RCP. Concrete with slag performed better than Class F and C fly ash concrete in both testing ages and achieved the lowest permeability as compared to all other mixtures at any cement content. Except for plain Lafarge and Holcim cement concrete, the mixtures

with PCE achieved lowest permeability versus corresponding concrete mixtures with SNF and mid-range at reduced cement content.

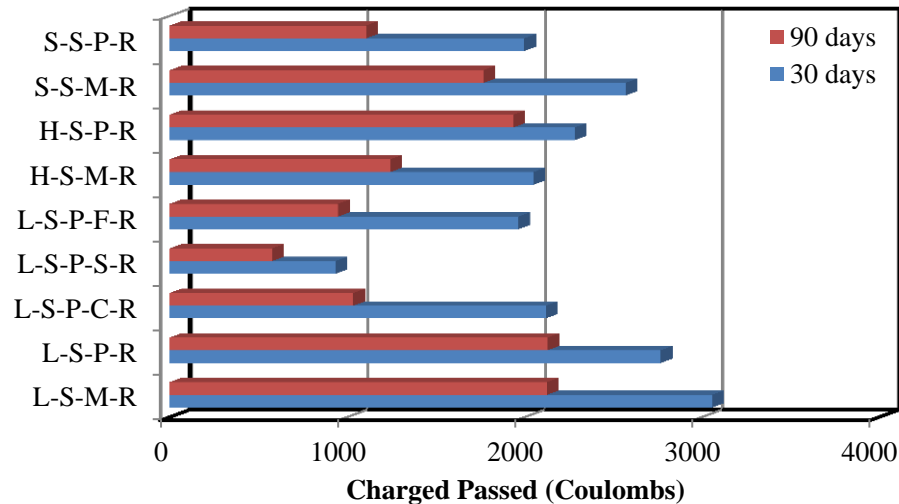


Figure 39. The RCP of concrete with cementitious materials content of 250 kg/m^3 [420 lb/yd^3]

The freezing and thawing resistance of investigated concrete is summarized in Table 355 and Table 366. All concrete at both cement content levels achieved durability factor above 90% and so passed the ASTM C666 requirement for 60% durability factor after 300 cycles. However, maintaining 60% DF does not necessarily represent durable concrete. In many regions in North America which typically have 30-50 cycles per year, 300 cycles guarantee adequate performance for only 6 years. Concrete containing slag (BB02, BB08, B11), class C fly ash (BB06, BB07), concrete based on Holcim cement (BB18, BB19) and also plain mixture BB09 had demonstrated obtained lower durability compared to other types. For these concrete types, the durability factor up until 300 cycles was also reduced at an accelerated rate when compared to other types. Therefore it can be anticipated that these concrete mixtures fail earlier than others beyond 300 freezing-thawing cycles. A few concrete mixtures had small expansion or mass gain

throughout the 300 cycles. Table 35 and Table 36 report on the mass loss at 300 cycles for all the concrete mixtures.

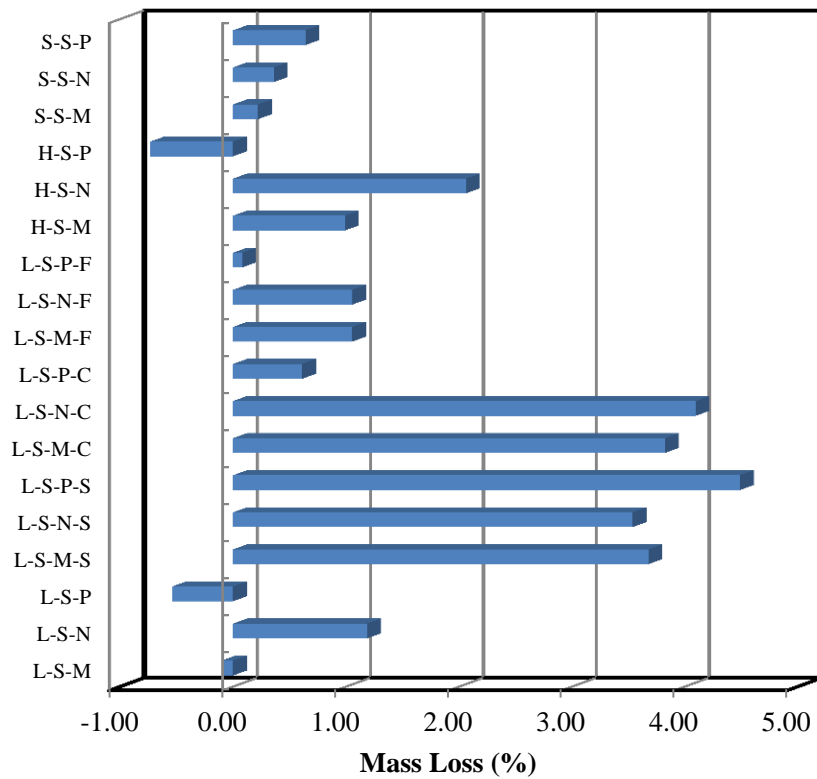


Figure 40. The mass loss of concrete with cementitious material content of 279 kg/m³ [470 lb/yd³] at 300 freezing-thawing cycles

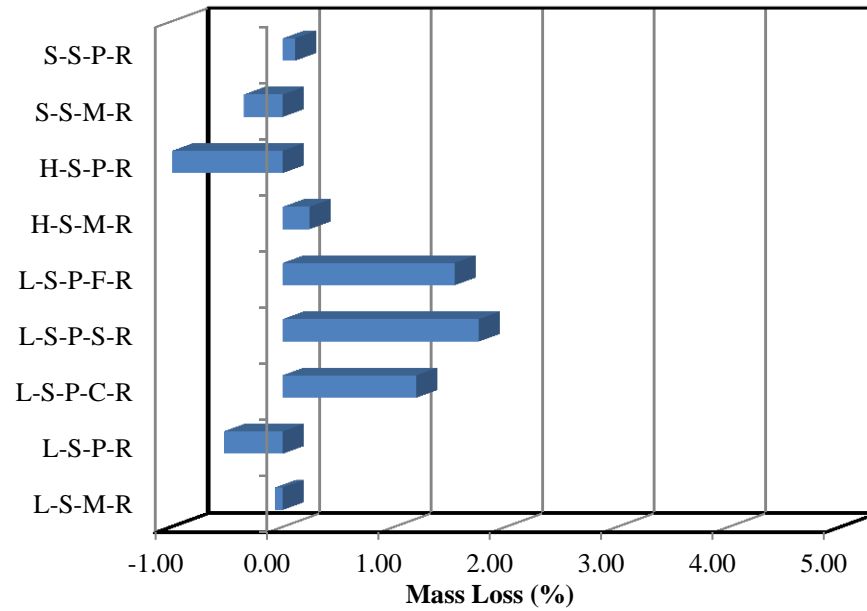


Figure 41. The mass loss of concrete with cementitious material content of 250 kg/m^3 [420 lb/yd^3] at 300 freezing-thawing cycles

As illustrated in Figures 41 and 42 two mixtures containing slag and PCE admixtures at both cement content levels (BB17, BB27) gained about 1% mass.

The RCP behavior of developed concrete compositions with slag obtained the lowest overall permeability which may be due to significant 50% reduction of cement compared to the concrete with 30% fly ash replacement.

5. CONCLUSIONS

Concrete mixture can be effectively designed by optimizing two essential phases i.e. the aggregates, and cement paste. The theoretical and experimental optimization of aggregate and cement paste was realized with extensive concrete testing. As a result of optimization cement content was reduced by up to 35% versus current WisDOT specifications for concrete mixtures that satisfy all other requirements.

Aggregate optimization can enhance the compressive strength by identification of the best blend through multiple criteria. Aggregate optimization criteria used in this research showed consistency. Multiple criteria can be used to evaluate the effect of packing density on concrete performance. The aggregate packing alone can be used as an effective tool to optimize the aggregate blends of concrete designed for different applications. The continuous power curves can serve as another criterion. The coarseness chart can assist in elaborating the level of workability of concrete and coarseness of the blends with binary, ternary or multi-class aggregates. The chart can also be used as a tool to tune the aggregate blends for the mixtures with various cement contents and aggregate combinations.

The 3D packing models that are able to imitate particulate packing and to connect the packing with particle size distribution (PSD) can provide a quick feedback and 3D visualization of optimal blends. The realistic combined grading curves (PSD) can deliver better packing arrangements achievable in concrete; and developed realistic gradings have a low deviation from the power curves. Furthermore, the results of simulation can

be used as a reference PSD to match with the experimental blends using various aggregates available.

The experimental results on packing degree and performance of concrete mixtures can provide useful relationships for the selection of the best aggregate blends and evaluate the differences between the simulation and experimental packing due to shape and packing methods. The high density mixtures are achievable using power curves as proved by the simulation and experimental packings. As demonstrated by experimental and simulations the 0.35-0.45 power curves can provide a better packing versus 0.7 power curve for the concrete mixtures with maximum aggregate size (D_{max}) typical in construction industry.

In concrete with cementitious material content of less than 300 kg/m^3 the aggregate optimization may require using higher proportions of sand, up to 50% in the aggregates blend. Due to improved grading and packing the use of intermediate aggregates is beneficial for concrete performance. The intermediate aggregates fractions can be used in the blends, replacing up to 30% of the coarse aggregates depending on the type of the aggregates.

Power curves (PC) can be used as an effective tool for aggregate optimization. The mixtures with higher fine aggregates content can be fitted to smaller PC exponents such as 0.35-0.45, while binary mixtures and mixtures with lower volume of fine aggregates are closer to power 0.5-0.7 gradings. The combined packing and grading methods enhance the optimization procedure and can be used as a tool for comparison of various aggregate blends and mixture proportioning. Also, the use of aggregate packing

as a tool to optimize concrete mixtures provides a good prediction for the compressive strength and explains the difference in concrete performance.

The compressive strength of concrete can be correlated with the packing degree of aggregates. This correlation is more pronounced for Southern aggregates and is more clear at the age of 7 days. As a result of aggregate optimization, the concrete compressive strength can be increased by up to 37% (31.3 vs. 22.8 MPa for S9 and S1 mixtures based on Southern aggregates, accordingly) and, consequently, enhanced performance can be used to further reduce the volume of cementitious materials. The optimization of the aggregate's grading with ternary aggregate blends can greatly assist in this process. However, no strength correlation was observed for Northern aggregates which may be due to the difference in shape (round) and texture of aggregates.

The heat of hydration of the cement paste or mortar can be used for optimization of dosage of HRWRA/WRA chemical admixtures prior to application in concrete mixtures. The optimization of chemical admixtures is essential when various cements, SCMs, and other chemical admixtures are used.

The optimized concrete mixtures with PCE admixtures enable up to 10 % reduction of W/C ratio and also can provide an excellent compatibility with AE and various SCMs. As a result of an additional strength gain due to reduced W/C ratio, the cement content can be reduced by 12% and 35% to 279 kg/m³ [470 lb/yd³] and 249.2 kg/m³ [420 lb/yd³], respectively versus current WisDOT specification requirement.

The use of PCE admixtures and class C fly ash enables to reduce in W/C and enhance the workability. The combination of the two materials works perfect in terms of

mechanical performance to achieve strength as high as 40 MPa at 28 days and above 60 MPa at 90 days.

The use of class F fly ash requires the application of PCE and adjustment of air content that enables the reduction of W/CM ratio and resulting in a higher strength above acceptable ranges.

The use of aggregate optimization and incorporation of additional air (by using higher dosage of AE admixture) beyond conventional specifications may be essential in low cement mixtures (249.2 kg/m^3 [420 lb/yd^3]) are designed.

The fresh density and air content of concrete mixtures have a strong relationship and the air content can be estimated from the fresh density-air content graph as illustrated in *Figure 31*. The relationship between air content and fresh density of tested final mixtures

The modulus of rupture (MOR) obtained from the flexural center-point (3-point) loading of the beams has a good correlation with corresponding compressive strength as demonstrated for various mixtures and ages.

The permeability for low cement content concrete produced at the same W/CM ratio is reduced due to the reduced volume of cementitious phase and lower permeability of predominant aggregate fraction. However, the higher porosity in cementitious materials associated with higher W/CM causes higher transport properties of the matrix.

Various mixtures performed differently in RCP performance, but had very similar response in freeze-thaw tests. All investigated concrete mixtures had selectively higher air content (achieved by application of AE admixture) and excellent freeze-thaw

resistance. The use of SCMs and various W/CM ratios can lead to variations and differences in microstructure of cementitious system in different durability tests. The differences in air content, saturation degree, as well as volume of cement paste and aggregates also affect the transport properties and freeze-thaw resistance.

The developed approaches and test results can serve as a solid foundation for specification of sustainable concrete with reduced use of cementitious materials and enhanced performance as required for WisDOT applications.

6. FUTURE RESEARCH

The various aspects of reported research can be further extended. A comprehensive multi-scale model of concrete can be developed based on extensive test results of this research; and furthermore, this model can be used for development of a new concrete mix design procedure that targets the low cement contents minimizes the experiments, and serves the applications for WisDOT. This procedure can involve the use of different components of paste, mortar and concrete into consistent design routine for the mixtures with required performance level.

The development of a software package for aggregate optimization as a tool based on the results of packing simulations, theoretical models, and experimental approaches can be useful for the implementation of reported research effort.

REFERENCES

1. *Report Card for America's Infrastructure*, 2013, ASCE.
2. Van Dam, T., et al., *Sustainable concrete pavements: A manual of practice*. 2012.
3. Abrams, D., *A tribute to Proportioning Concrete Mixtures*. ACI Special Publication, 2008. **249**.
4. Abrams, D., *Proportioning of concrete mixtures* Structural Materials Research Laboratory December 1918. **Bulletin No.1**.(Lewis Institute Chicago).
5. Gilkey, J.H., *Water-Cement Ratio versus Strength – Another Look* ACI Journal Proceeding April 1961. **(4)**: p. 57.
6. Neville, A.M., *Proportioning of concrete mixtures*. 1995: p. 269-272.
7. Neville, A., *Properties of concrete. Fourth and final edition standards*, 1996, Pearson, Prentice Hall. ISBN 0-582-23070-5. OCLC.
8. Goltermann, P. and V. Johansen, *Packing of aggregates: an alternative tool to determine the optimal aggregate mix*. ACI Materials Journal, 1997. **94**(5).
9. de Larrard, F. and T. Sedran, *Optimization of ultra-high-performance concrete by the use of a packing model*. Cement and Concrete Research, 1994. **24**(6): p. 997-1009.
10. Vorobiev, V., *Application of physical and mathematical methods in concrete research*. Visshaya Shkola, Moscow, 1977.
11. Fuller, W.B. and S.E. Thompson, *The laws of proportioning concrete*. Transactions of the American Society of Civil Engineers, 1906. **57**(2): p. 67-143.
12. *American Concrete Institute, Aggregates for Concrete Bulletin E1-07, First Print*, 2007.
13. Sobolev, K. and A. Amirjanov, *Application of genetic algorithm for modeling of dense packing of concrete aggregates*. Construction and Building Materials, 2010. **24**(8): p. 1449-1455.
14. de Larrard, F., *A method for proportioning high-strength concrete mixtures*. Cement, concrete and aggregates, 1990. **12**(1): p. 47-52.
15. de Larrard, F. and A. Belloc, *The influence of aggregate on the compressive strength of normal and high-strength concrete*. ACI Materials Journal, 1997. **94**(5).
16. Hansen, T.C. *Influence of aggregate and voids on modulus of elasticity of concrete, cement mortar, and cement paste*. in *ACI Journal Proceedings*. 1965. ACI.
17. Li, S.-t.i. *Proposed Synthesis of Gap-Graded Shrinkage-Compensating Concrete*. in *ACI Journal Proceedings*. 1967. ACI.
18. Richardson, D.N., *Aggregate gradation optimization: literature search*. 2005.
19. Sobolev, K., et al. *Packing of aggregates as an approach to optimizing the proportioning of concrete mixtures aggregates: asphalt concrete, portland cement concrete, bases, and fines, presented at*. 2004. ICAR/AFTRE/NSSGA Symp.
20. Fennis, S., *Design of ecological concrete by particle packing optimization* 2011: TU Delft, Delft University of Technology.
21. Roy, D., et al., *Concrete components packing handbook*, 1993.

22. Powers, T., *Properties of Fresh Concrete*, John Wiley and Sons. Inc., New York, 1968: p. 301.
23. Andersen P.J., J.V., *Particle packing and concrete properties*. Material Science of Concrete, The American Ceramic Society, Inc., 1991(II).
24. Aim, R.B. and P. Le Goff, *Effet de paroi dans les empilements désordonnés de sphères et application à la porosité de mélanges binaires*. Powder Technology, 1968. **1**(5): p. 281-290.
25. Toufar, W., M. Born, and E. Klose, *Beitrag zur Optimierung der Packungsdichte polydispenser körniger Systeme*. Freiburger Forschungsheft, 1976. **558**(29-44): p. 201.
26. De Larrard, F., *Concrete mixture proportioning: a scientific approach* 1999: CRC Press.
27. Dewar, J., *Computer modelling of concrete mixtures* 2002: CRC Press.
28. Brouwers, H. and H. Radix, *Self-compacting concrete: theoretical and experimental study*. Cement and Concrete Research, 2005. **35**(11): p. 2116-2136.
29. Vogt, C. *Ultrafine particles to save cement and improve concrete properties*. in *Nordic Concrete Research, Sandefjord, Norway, June 13-15, 2005*. 2005. The Nordic Concrete Federation.
30. Feret, R., *Sur la compactie des mortiershydrauliques*, *Ann.Ponts Chaussée, mémoires et documents*. Série 7, 1892. **no. IV**: p. 5-164.
31. Fu, G. and W. Dekelbab, *3-D random packing of polydisperse particles and concrete aggregate grading*. Powder Technology, 2003. **133**(1): p. 147-155.
32. Kolonko, M., S. Raschdorf, and D. Wäsch, *A hierarchical approach to estimate the space filling of particle mixtures with broad size distributions*. submitted to Powder Technology, 2008.
33. Sobolev, K. and A. Amirjanov, *The development of a simulation model of the dense packing of large particulate assemblies*. Powder Technology, 2004. **141**(1): p. 155-160.
34. Yurdakul, E., et al., *A paper to be submitted to Journal of Materials in Civil Engineering (ASCE)*. Proportioning for performance-based concrete pavement mixtures, 2013: p. 65.
35. Ashraf, W. and M. Noor, *Performance-evaluation of concrete properties for different combined aggregate gradation approaches*. Procedia engineering, 2011. **14**: p. 2627-2634.
36. Zhao, H., et al., *The effect of coarse aggregate gradation on the properties of self-compacting concrete*. Materials & Design, 2012. **40**: p. 109-116.
37. Moini Mohamadreza, Muzenski Scott, Ismael Flores-Vivian, Sobolev Konstantin. "Aggregate optimization for concrete mixtures with low cement factor", (2nd international) conference on concrete and reinforced concrete: glance at future. Vol. 4, Moscow, May 12, 2014, pp. 349–59.
38. Torquato, S., T.M. Truskett, and P.G. Debenedetti, *Is random close packing of spheres well defined?* Physical review letters, 2000. **84**(10): p. 2064.
39. Kwan, A. and C. Mora, *Effects of various, shape parameters on packing of aggregate particles*. Magazine of concrete Research, 2002. **53**(2): p. 91-100.
40. Stroeven, P. and M. Stroeven, *Assessment of packing characteristics by computer simulation*. Cement and Concrete Research, 1999. **29**(8): p. 1201-1206.

41. Mostofinejad, D. and M. Reisi, *A new DEM-based method to predict packing density of coarse aggregates considering their grading and shapes*. Construction and Building Materials, 2012. **35**: p. 414-420.
42. Moini, M. and A. Lakizadeh, *Concrete Workability: An Investigation on Temperature effects Using Artificial Neural Networks*. AuthorHouse, 2011.
43. Sobolev, K. and A. Amirjanov, *A simulation model of the dense packing of particulate materials*. Advanced Powder Technology, 2004. **15**(3): p. 365-376.
44. Sobolev, K., *The development of a new method for the proportioning of high-performance concrete mixtures*. Cement and Concrete Composites, 2004. **26**(7): p. 901-907.
45. https://pantherfile.uwm.edu/sobolev/www/V_LAB/.
46. Moini, M. R., A. Lakizadeh, and M. Mohaqeqi. "Effect of mixture temperature on slump flow prediction of conventional concretes using artificial neural networks." *Australian Journal of Civil Engineering* 10, no. 1 (2012).
47. Colleparidi, S., et al., *Mechanisms of Actions of Different Superplasticizers For High Performance Concrete*. ACI Special Publication, 1999. **186**.
48. Ramseyer, C.C. and R. Kiamanesh, *Optimizing Concrete Mix Designs to Produce Cost Effective Paving Mixes*, 2009, Civil Engineering and Environmental Science, University of Oklahoma.
49. Rached, M., M. De Moya, and D.W. Fowler, *Utilizing aggregates characteristics to minimize cement content in portland cement concrete*. International Center for Aggregates Research (ICAR 401), University of Texas, Austin, USA, 2009.
50. Quiroga, P.N. and D.W. Fowler, *The effects of aggregates characteristics on the performance of Portland cement concrete*, 2004, International Center for Aggregates Research, University of Texas at Austin.
51. De Larrard, F. and T. Sedran, *Mixture-proportioning of high-performance concrete*. Cement and Concrete Research, 2002. **32**(11): p. 1699-1704.
52. Sobolev, K. and S. Soboleva, *High-Performance Concrete Mixture Proportioning*. ACI Special Publication, 1998. **179**.
53. Peterson, K., L.L. Sutter, and G. Anzalone, *Reduction of Minimum Required Weight of Cementitious Materials in WisDOT Concrete Mixes*, 2011.
54. Ji, T., et al., *A mix proportion design method of manufactured sand concrete based on minimum paste theory*. Construction and Building Materials, 2013. **44**: p. 422-426.
55. Moini M., Flores-Vivian I., Amirjanov A., Sobolev K., *The Optimization of Aggregate Blends for Sustainable Low Cement Concrete*. Construction & Building Materials Journal, 2015.
56. Noguchi, T., I. Maruyama, and M. Kanematsu. *Performance based design system for concrete mixture with multi-optimizing genetic algorithm*. in *Proceedings of the 11th International Congress on the Chemistry of Cement "Cements Contribution to the Development in the 21st Century"*, Durban. 2003.
57. Yeh, I.-C., *Computer-aided design for optimum concrete mixtures*. Cement and Concrete Composites, 2007. **29**(3): p. 193-202.
58. Cheng, M.-Y., D. Prayogo, and Y.-W. Wu, *Novel Genetic Algorithm-Based Evolutionary Support Vector Machine for Optimizing High-Performance Concrete Mixture*. Journal of Computing in Civil Engineering, 2013. **28**(4).

59. Fennis, S.A. and J.C. Walraven, *Using particle packing technology for sustainable concrete mixture design*. Heron, 57 (2012) 2, 2012.
60. Liu, R., et al., *Optimization of cementitious material content for sustainable concrete mixtures*. Journal of Materials in Civil Engineering, 2011. **24**(6): p. 745-753.
61. Easa, S.M. and E.K. Can, *Optimization model for aggregate blending*. Journal of construction engineering and management, 1985. **111**(3): p. 216-230.
62. Cordon, W.A. and H.A. Gillespie. *Variables in concrete aggregates and Portland cement paste which influence the strength of concrete*. in *ACI Journal Proceedings*. 1963. ACI.
63. Koehler, E.P., *Aggregates in self-consolidating concrete*2007: ProQuest.
64. Simon, M.J., E.S. Lagergren, and K.A. Snyder. *Concrete mixture optimization using statistical mixture design methods*. in *Proceedings of the PCI/FHWA international symposium on high performance concrete*. 1997.
65. Kwan, A. and H. Wong, *Packing density of cementitious materials: part 2—packing and flow of OPC+ PFA+ CSF*. Materials and structures, 2008. **41**(4): p. 773-784.
66. Bergman, L.A. *Optimization of Portland-Pozzolan Concrete, Airport Runways*. in *Construction and Materials Issues 2001*. 1962. ASCE.
67. Aydın, S., *A ternary optimisation of mineral additives of alkali activated cement mortars*. Construction and Building Materials, 2013. **43**: p. 131-138.
68. *Aggregate suspension mixture proportioning method*. TechNote, ACI 211.6T-14. 68.
69. Andersen, P.J. and V. Johansen, *A guide to determining the optimal gradation of concrete aggregates*. Contract, 1993. **100**: p. 206.
70. *EUROPACK: User Manual*, G. M. Idorn Consult A/S, Bredevej 2, 2830 Virum, Denmark. Jan. 1996.
71. Mangulkar, M. and S. Jamkar, *Review of Particle Packing Theories Used For Concrete Mix Proportioning*. International Journal Of Scientific & Engineering Research, 2013. **4**(5): p. 143-148.
72. Andersen, P.J., *Control and Monitoring of Concrete Production: A Study of Particle Packing and Rheology: a Thesis in Concrete Technology*1990: Danish Academy of Technical Sciences.
73. Andersen, P.J. and V. Johansen, *Particle packing and concrete properties*1993.
74. Joisel, A., *Composition des Betons Hydrauliques*, Ann. l'ITBTP,58,992-1065, . 1952.
75. Poulsen, A., *Cement in seawater: report on the trials, commenced in 1896 on the recommendation of the society of Scaninavian Portland cement manufacturers*. 1909.
76. Furnas, C.C., *Flow of gases through beds of broken solids*. Vol. 300. 1929: US Govt. print. off.
77. Westman, A.R. and H. Hugill, *THE PACKING OF PARTICLES I*. Journal of the American Ceramic Society, 1930. **13**(10): p. 767-779.
78. Petersen, I.F., *Report on Packing Models*, F. L. Schmidt & Co. 1981.
79. Toufar, W., E. Klose, and M. Born, *Berechnung der packungsdichte von korngemischen*. Aufbereitung-Technik, 1977. **11**: p. 603-608.

80. Furnas, C., *Grading aggregates-I-Mathematical relations for beds of broken solids of maximum density*. Industrial & Engineering Chemistry, 1931. **23**(9): p. 1052-1058.
81. Schwanda, F., *Das rechnerische Verfahren zur Bestimmung des Hohlraumes und Zementleimanspruches von Zuschlägen und seine Bedeutung für den Spannbetonbau*. Zement und Beton, 1966. **37**(8-17): p. 13.
82. Reschke, T., *Der Einfluss der Granulometrie der Feinstoffe auf die Gefügeentwicklung und die Festigkeit von Beton* 2001.
83. Stovall, T., F. De Larrard, and M. Buil, *Linear packing density model of grain mixtures*. Powder Technology, 1986. **48**(1): p. 1-12.
84. Yu, A. and N. Standish, *Porosity calculations of multi-component mixtures of spherical particles*. Powder Technology, 1987. **52**(3): p. 233-241.
85. Talbot, A.N. and F.E. Richart, *THE STRENGTH OF CONCRETE-ITS RELATION TO THE CEMENT, AGGREGATES AND WATER*. Illinois Univ Eng Exp Sta Bulletin, 1923.
86. KUMAR, S. and M. Santhanam, *Particle packing theories and their application in concrete mixture proportioning: A review*. Indian concrete journal, 2003. **77**(9): p. 1324-1331.
87. Funk, J., D. Dinger, and J. Funk Jr, *Coal Grinding and Particle Size Distribution Studies for Coal-Water Slurries at High Solids Content*. Final Report, Empire State Electric Energy Research Corporation (ESEERCO), New York, NY, 1980.
88. Funk, J.E. and D. Dinger, *Predictive process control of crowded particulate suspensions: applied to ceramic manufacturing* 1994: Springer Science & Business Media.
89. Walker, W., *Persistence of Granular Structure during Compaction Processes*. Kona, 2003. **21**: p. 133-142.
90. Zheng, J., P.F. Johnson, and J.S. Reed, *Improved equation of the continuous particle size distribution for dense packing*. Journal of the American Ceramic Society, 1990. **73**(5): p. 1392-1398.
91. Peronius, N. and T. Sweeting, *On the correlation of minimum porosity with particle size distribution*. Powder Technology, 1985. **42**(2): p. 113-121.
92. Garas, V. and K. Kurtis, *Assessment of methods for optimising ternary blended concrete containing metakaolin*. Magazine of concrete Research, 2008. **60**(7): p. 499-510.
93. Hunger, M., *An integral design concept for ecological self-compacting concrete*, 2010, Technische Universiteit Eindhoven.
94. Toufar, W., M. Born, and E. Klose, *Freiberger Forschungsheft A 559*. VEB Deutscher Verlag Fuer Grundstoffindustrie, 1967.
95. Zheng, J. and P. Stroeven. *Computer Simulation of Particle Section Patterns from Sieve Curves for Spherical Aggregate*. in *Modern concrete materials: binders, additions and admixtures: proceedings of the international Conference held at the University of Dundee, Scotland, UK on*. 1999.
96. Snoeijer, J.H., et al., *Packing geometry and statistics of force networks in granular media*. Physical Review E, 2004. **70**(1): p. 011301.
97. Gram, A. and J. Silfwerbrand, *Computer simulation of SCC flow*. Betonwerk und Fertigteil-Technik, 2007. **73**(8).

98. Roussel, N., et al., *Computational modeling of concrete flow: General overview*. Cement and Concrete Research, 2007. **37**(9): p. 1298-1307.
99. Stroeven, P., J. Hu, and Z. Guo, *Shape assessment of particles in concrete technology: 2D image analysis and 3D stereological extrapolation*. Cement and Concrete Composites, 2009. **31**(1): p. 84-91.
100. Kwan, A., C. Mora, and H. Chan, *Particle shape analysis of coarse aggregate using digital image processing*. Cement and Concrete Research, 1999. **29**(9): p. 1403-1410.
101. Mora, C. and A. Kwan, *Sphericity, shape factor, and convexity measurement of coarse aggregate for concrete using digital image processing*. Cement and Concrete Research, 2000. **30**(3): p. 351-358.
102. Kwan, A. and W. Fung, *Packing density measurement and modelling of fine aggregate and mortar*. Cement and Concrete Composites, 2009. **31**(6): p. 349-357.
103. Flores-Vivian, Ismael, R. Pradoto, Mohamadreza Moini, and Konstantin Sobolev. "The use of nanoparticles to improve the performance of concrete." In *Nano Conference*. 2013.
104. Konstantin Sobolev, Mohamadreza Moini, Steve Cramer, Ismael Flores-Vivian, Scott Muzenski, Rani Pradoto, Ahmed Fahim, Le Pham, Marina Kozhukhova, "Laboratory Study of Optimized Concrete Pavement Mixtures", No. 0092-13-04. 2016.
105. Shilstone Sr, J.M., *Concrete mixture optimization*. Concrete International, 1990. **12**(6).